Dissecting Fusarium head blight resistance on wheat chromosome 4D

Benjamin Hales

Doctor of Philosophy (PhD)

University of East Anglia (UEA)

Department of Crop Genetics, John Innes Centre

September 2019

Abstract

Fusarium head blight (FHB) is a fungal disease of wheat and other cereal crops. It is responsible for grain yield and quality reductions, in addition to the accumulation of predominantly trichothecene mycotoxins in grain. The most important of these mycotoxins is deoxynivalenol (DON), which is harmful to human and animal consumers, in addition to acting as a virulence factor in wheat by promoting the spread of infection.

It has been shown previously that the short arm of chromosome 4D carries an FHB susceptibility factor. Chinese Spring cytogenetic material confirmed that the FHB susceptibility factor promotes the spread of the fungus independently of DON. Two resistance factors were also identified on 4D: a 4DS DON resistance factor and a 4DL Type I resistance factor. Genotyping and phenotyping of Chinese Spring terminal deletion lines refined the FHB susceptibility factor to a 31.7 Mbp interval containing 274 genes and the DON resistance interval was refined to 4.2 Mbp, containing 49 genes.

A deletion mapping approach, using a gamma-irradiated Paragon population, was used to further refine the position of the FHB susceptibility factor. Lines containing deletions across the remaining interval were identified using two successive markers screens, in addition to skim sequencing of a subset of the population. Disease phenotyping eliminated most of the FHB susceptibility interval, leaving three small intervals containing a total of 66 genes.

Functional annotation and gene expression data were used to interrogate the 4DS DON resistance interval, to identify potential candidates responsible for the DON resistance. DON application experiments were conducted on Cadenza TILLING mutants of two genes encoding aldo-keto reductases and on gamma-irradiated Paragon lines to refine the DON resistance interval. However, no change in DON susceptibility was observed in the lines, which prevented interval refinement.

Acknowledgements

This PhD project was funded by the Biotechnology and Biological Sciences Research Council (BBSRC) and RAGT Seeds Ltd. Thank you to both organisations for making this research possible.

I would like to thank my primary supervisor, Prof. Paul Nicholson, for the guidance, encouragement and support provided throughout this PhD project. I would also like to thank my secondary and industrial supervisors, Dr Simon Griffiths and Dr Christopher Burt (RAGT Seeds), for their constructive comments and feedback throughout the project.

Thank you to everyone who has worked in the Nicholson group over the course of this PhD project, for your help and for making work so enjoyable! Particular thanks go to Andy Steed for the assistance and wisdom in conducting the genotyping and phenotyping work.

I am very grateful to my family and friends for the love and support they have provided over the last four years.

Abbreviations

ABA	abscisic acid
add	addition line
AKR	aldo-keto reductase
BLAST	basic local alignment search tool
bp	base pair
CER	controlled environment room
cm	centimetre
CRISPR	clustered regularly interspaced short palindromic repeats
CS	Chinese Spring
CZ	Cadenza
dH_2O	deionised water
DON	deoxynivalenol
dpi	days post inoculation
DT	ditelosomic
EDTA	ethylenediaminetetraacetic acid
EMS	ethyl methanesulfonate
FHB	Fusarium head blight
FL	fraction length
Gbp	giga base pair
GLM	general linear model
h	hour
hpi	hours post inoculation
Hz	Hertz
indel	insertion and deletion
JA	jasmonic acid
KASP	kompetitive allele specific PCR
kb	kilo base pair
L	litre
LRR-RK	leucine rich repeat receptor kinase

M	molar
Mbp	mega base pair
mg	milligram
min	minutes
mL	millilitre
Mlo	*Mildew resistance locus o*
MUSCLE	multiple sequence comparison by log-expectation
Mv9kr1	Martonvasari9 *kr1*
NBS-LRR	nucleotide binding site-leucine rich repeat
NHEJ	non-homologous end-joining
NIV	nivalenol
PCR	polymerase chain reaction
PFT	*pore-forming toxin-like*
PG	Paragon
ppm	parts per million
QTL	quantitative trait locus
R	resistant
REML	linear mixed model
ROS	reactive oxygen species
s	seconds
S	susceptible
SA	salicylic acid
SDS	sodium dodecyl sulfate
s.e.	standard error
SNB	Stagonospora nodorum blotch
SNP	single nucleotide polymorphism
sub	substitution line
TALENs	transcription activator-like effector nucleases
TILLING	targeted induced local lesions in genomes
tpm	transcripts per kilobase million
trans	translocation line

Tris-HCl	trisaminomethane hydrochloride
x g	times gravity
ya	years ago
WT	wild type
°C	degrees centigrade
µL	microlitre
µM	micromolar

Contents

List of Tables

List of Figures

Chapter 1: General Introduction

1.1 Wheat

1.1.1 Importance of wheat

Wheat (*Triticum* spp.) constitutes the world's third largest food source after maize (*Zea mays*) and rice (*Oryza* spp.) with 2017/18 global wheat production estimated at 759.9 million metric tonnes (Food and Agricultural Organisation, 2019, United States Department of Agriculture, 2019). In the UK, wheat is the primary crop, with 14.1 million tonnes of wheat being produced from approximately 1.8 million hectares of land in 2018 (Department for Environment Food and Rural Affairs, 2018a, Department for Environment Food and Rural Affairs, 2018b).

Bread wheat (*Triticum aestivum*), also known as common wheat, is the most widely grown form of wheat and is generally used to make bread and biscuits, as well as for animal feed. Durum wheat (*Triticum turgidum* ssp. *durum*) is commonly grown in Mediterranean countries, due to its ability to tolerate the warm and dry climate. Durum wheat is most widely used for making pasta. Wheat provides approximately 19 % of calories consumed by humans and, as a result, is of significant economic and social importance (Food and Agricultural Organisation, 2014). Humanity must continue to meet the demands of a growing population, by further increasing wheat yields and protecting wheat from pests and pathogens.

1.1.2 Evolution and genetics of wheat

Bread wheat (*Triticum aestivum*) possesses a large and complex allohexaploid genome resulting from two hybridisation events (Petersen *et al.*, 2006) (**Figure 1.1**). The 17 Gbp bread wheat genome (Brenchley *et al.*, 2012) consists of 21 chromosome pairs, donated by three diploid donor species, each possessing 7 chromosome pairs. The first hybridisation event occurred approximately half a million years ago between *Triticum urartu* (AA) and a species believed to be an extinct

ancestor of *Aegilops speltoides* (BB) to form the tetraploid *Triticum turgidum* (AABB). The resulting tetraploid hybrid was later domesticated to form the tetraploid emmer wheat (*Triticum turgidum* ssp. *dicoccoides*). The second hybridisation event is estimated to have taken place 8,000-10,000 years ago, between *Triticum turgidum* ssp. *dicoccoides* (AABB) and *Aegilops tauschii* (DD), resulting in hexaploid *Triticum aestivum* (AABBDD). Further domestication of tetraploid wheat resulted in modern durum wheat (*Triticum turgidum* ssp. *durum*). Correct pairing of homologous chromosomes is maintained by the *Ph1* locus, present on chromosome 5B (Riley and Chapman, 1958, Griffiths *et al.*, 2006).

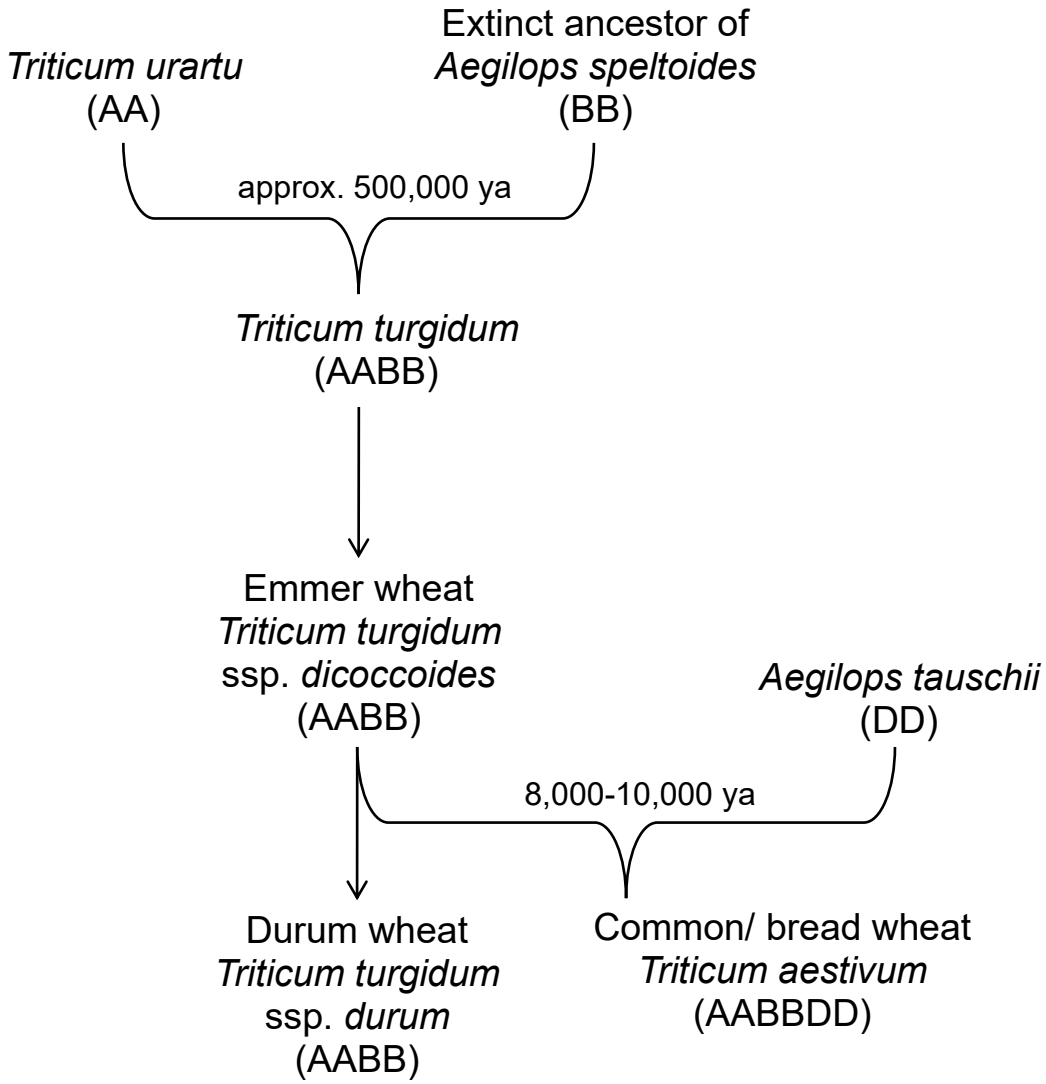

Figure 1.1 The evolution of common/ bread wheat (*Triticum aestivum*). Two hybridisation events (arrow braces), firstly between *Triticum urartu* and what is believed to be an extinct ancestor of *Aegilops speltoides*, resulting in the tetraploid *Triticum turgidum*. The second hybridisation occurred between the domesticated *Triticum turgidum* ssp. *dicoccoides* and *Aegilops tauschii*, giving rise to hexaploid bread wheat (*Triticum aestivum*). Further domestication of tetraploid wheat resulted in durum wheat (*Triticum turgidum* ssp. *durum*).

The large genome size, combined with the close similarity of homoeologous genome sequences, of as much as 95-99 % in coding regions, and a large proportion of repetitive DNA in excess of 80 %, have made the production of a high-quality wheat genome sequence a major challenge (Borrill *et al.*, 2015, IWGSC, 2018). However, improved drafts of the genome sequence have been rapidly emerging in recent years. A reference sequence was generated for the 1 Gbp chromosome 3B by sequencing a bacterial artificial chromosome (BAC) assembly (Choulet *et al.*, 2014) but the remaining chromosomes remained highly fragmented (Chapman *et al.*, 2015). A draft genome assembly of the variety Chinese Spring was produced by the Earlham Institute (formerly called The Genome Analysis Centre [TGAC]) and released in January 2016 (Clavijo *et al.*, 2017). Up to this point, most genes were annotated but the assembly remained fragmented, and hence there was limited information regarding the physical distances between genes. This changed upon the release of the first draft of the Chinese Spring reference sequence assembly (IWGSC RefSeq v1.0), which was made available in May 2016 (IWGSC, 2018). The genome was successfully assembled into pseudomolecules, corresponding to the 21 wheat chromosomes. An updated version of the assembly (IWGSC RefSeq v1.1) has since been released, which has been made available on Ensembl Plants. In this thesis, IWGSC RefSeq v1.1 gene codes are used throughout. The unannotated IWGSC RefSeq v2.0 has recently been made available for BLAST searches under the terms of the Toronto agreement (Toronto International Data Release Workshop Authors, 2009) and is the most complete wheat genome assembly at the time of writing.

Now that a high-quality wheat genome assembly for Chinese Spring has been realised, the effort to assemble a wheat pangenome has gained momentum. A number of cultivars, mostly from Europe, North America and Australia, have been selected to best represent the genetic diversity present from these regions (10+ Wheat Genomes Project, 2019). Sequence data is available to perform BLAST

searches to UK varieties such as Cadenza, Paragon, Robigus, Claire and tetraploid Kronos. This enables variation between varieties to be identified.

1.2 Fusarium head blight

1.2.1 Economic importance

Wheat yields are threatened by a range of pathogens and pests. However, the most serious diseases of wheat are caused by fungi, including *Fusarium* spp., *Zymoseptoria tritici* and *Puccinia* spp. (Dean *et al.*, 2012). With the human population expected to reach 9.7 billion by 2050 (United Nations, 2013), it is essential to be capable of protecting the crop yields already achievable from available arable land. To achieve this will require the development of more effective methods of controlling crop pests and diseases.

Fusarium head blight (FHB), also known as Fusarium ear blight (FEB) or wheat scab, is an economically significant fungal disease of small grain cereal crops, including wheat (*Triticum* spp.), barley (*Hordeum vulgare*), rye (*Secale cereale*) and oats (*Avena sativa*). The disease was first described by Smith (1884) in England, who associated the disease with the fungus *Fusisporium culmorum*. Between 1890 and 1892, several reports across the USA also described the disease (Parry *et al.*, 1995). Fusarium head blight (FHB) is caused by a number of species from the genera *Fusarium* and *Microdochium*; the most important species in Europe and North America being *F. graminearum* and *F. culmorum*. FHB not only results in reductions in yield and grain quality, but also the accumulation of mycotoxins in grain, most notably deoxynivalenol (DON), which are harmful to both humans and animals (Fung and Clark, 2004). Whilst *Microdochium nivale* and *M. majus* cause FHB, they are not known to produce mycotoxins (Xu *et al.*, 2008). FHB has a significant economic impact as a result of direct yield losses, costs of fungicide application, the need to screen for DON contamination of grain and the devalued or unusable yields due to DON contamination. In the USA, combined direct and

secondary losses as a result of FHB, affecting all susceptible crops, was estimated to be $7.7 billion between 1993 and 2001 (Nganje *et al.*, 2004). More recent figures estimate total losses due to FHB in the USA at $1.176 billion in 2015 and 2016 (Wilson *et al.*, 2018).

1.2.2 Geographic distribution of *Fusarium* spp.

FHB is found in almost all cereal-growing regions worldwide. *F. graminearum* is more common in warm and humid climates, such as regions of the USA, Canada, Australia and central Europe, whilst *F. culmorum* is typically associated with cooler climates, such as Northwest Europe (Parry *et al.*, 1995). However, recent reports suggest a shift from *F. culmorum* being the predominant species to *F. graminearum* in western European countries such as the Netherlands, Luxembourg, France, Germany and Denmark (van der Lee *et al.*, 2015). This may be the result increased growth of maize crops in these areas, the effect of changing climate favouring *F. graminearum*, or the ability of *F. graminearum* to produce sexual ascospores, which can be wind-borne (van der Lee *et al.*, 2015).

There are a number of other *Fusarium* spp. that are responsible for FHB, the most important being *F. poae*, *F. langsethiae* and *F. avenaceum*. These species are unable to synthesise DON and hence are typically less virulent than *F. graminearum* and *F. culmorum*. *F. poae* is believed to have a wide geographic distribution and primarily results in grain contamination with nivalenol (NIV) (Nazari *et al.*, 2018). *F. langsethiae* and *F. avenaceum* both predominate in cooler climates, such as Scandinavia and Canada. *F. langsethiae* commonly affects oats (*Avena sativa*), in which it does not exhibit FHB symptoms but nevertheless results in accumulation of T-2/ HT-2 mycotoxins in grain (Schoneberg *et al.*, 2019).

1.2.3 Lifecycle of F. graminearum

The fungus overwinters on crop debris in the form of saprophytic mycelia (Goswami and Kistler, 2004), from which asexual macroconidia are produced and transmitted

to plants predominantly through rain splash (Schmale and Bergstrom, 2003) (**Figure 1.2**). Warm, damp and humid conditions promote the sexual lifecycle stage (*Gibberella zeae*), resulting in production of sexual ascospores of *F. graminearum*, which can be transmitted to plants by wind (Parry *et al.*, 1995, Schmale and Bergstrom, 2003). Wheat plants are most vulnerable to infection during mid-anthesis (Goswami and Kistler, 2004), immediately following the extrusion of anthers (Schmale and Bergstrom, 2003). Conidia germinate 6-12 hours post-infection (hpi) and a germ tube grows over the surface of the glumes and florets, entering the host through stomata or by direct penetration (Kang and Buchenauer, 2000, Zhuang *et al.*, 2013). The presence of anthers and pollen is also believed to promote fungal growth (Kang and Buchenauer, 2000). The fungus has a brief biotrophic phase before switching to necrotrophy at around 72 hpi (Zhuang *et al.*, 2013). Initial infection is indicated by small water-soaked spots at the base or middle of the glumes or on the rachis, which rapidly spreads in all directions (Parry *et al.*, 1995). Later in infection, salmon pink growth can be observed along the edge of glumes and at the base of spikelets (Parry *et al.*, 1995). Infected grains become shrivelled and discoloured (commonly described as tombstone grains), and the characteristic premature bleaching of spikelets can typically be observed (**Figure 1.3**) (Parry *et al.*, 1995). Infection spreads to adjacent spikelets through the vascular bundles of the rachilla and rachis (Ribichich *et al.*, 2000).

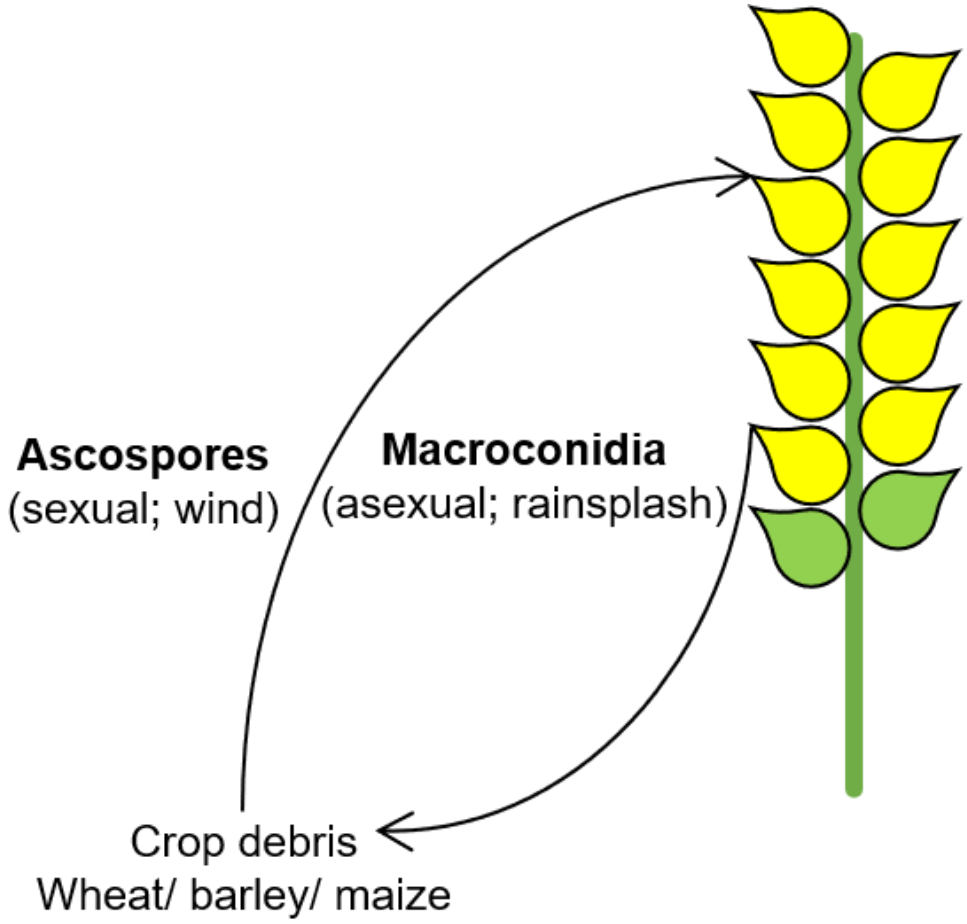

Figure 1.2 Diagram illustrating the life cycle of *Fusarium graminearum*.

Figure 1.3 Wheat head (centre foreground) infected with *Fusarium* sp. in the field, displaying the characteristic premature bleached spikelets, which has spread throughout the aerial part of the head. Photograph was taken in summer 2017.

1.3.1 Mycotoxins

Fusarium spp. produce a diverse range of mycotoxins, which accumulate in grain following infection. Furthermore, incorrect storage of grain post-harvest can promote the growth of *Fusarium* spp. and increased mycotoxin concentrations in grain (Magan *et al.*, 2010). This is a major problem in agriculture and food production, as these mycotoxins are harmful to the health of both animal and human consumers (Foroud and Eudes, 2009, Pestka, 2010). Many countries have set maximum legal limits for DON content in cereals and cereal products. European regulations state that unprocessed wheat must contain no more than 1.25 ppm DON, whilst final cereal products in the form of bread and biscuits, etc. must contain below 0.5 ppm DON (Food Standards Agency, 2007).

Trichothecenes are the most economically important class of *Fusarium* mycotoxins, and include deoxynivalenol (DON), nivalenol (NIV), as well as the T-2 and HT-2 toxins. The two most common *Fusarium* species, *F. graminearum* and *F. culmorum*, primarily produce DON, NIV, and their derivatives (Foroud and Eudes, 2009). Despite the lower toxicity of DON compared to T-2 and HT-2, DON is by far the most economically important mycotoxin (Foroud and Eudes, 2009), as it is produced in abundance by both *F. graminearum* and *F. culmorum*.

DON inhibits protein synthesis in eukaryotic cells, and also causes damage to the plasma membrane, ribosomes and chloroplasts, as well as resulting in the production of hydrogen peroxide, ultimately leading to cell death (Walter *et al.*, 2010). DON importantly acts as a virulence factor in wheat and facilitates the spread of the fungus from the site of infection to adjacent spikelets (Desjardins *et al.*, 1996, Langevin *et al.*, 2004, Maier *et al.*, 2006). DON is particularly influential in promoting infection above the point of initial infection.

1.3.2 Types of resistance and susceptibility to Fusarium head blight

Schroeder and Christensen (1963) classified the two most commonly studied forms of resistance to FHB:

- Type I: resistance to initial infection.
- Type II: resistance to spread of infection from an infected spikelet to adjacent spikelets through the rachis.

Type I resistance is typically assessed by spraying flowering wheat plants with a conidial suspension and observing the proportion of spikelets showing symptoms of infection at regular time points post-inoculation (Gosman *et al.*, 2005, Draeger *et al.*, 2007). Type II resistance is analysed by injecting conidia into a single spikelet, approximately central on the wheat spike, and recording the spread of infection to adjacent spikelets above and below the inoculated spikelet regularly post-inoculation (Saville *et al.*, 2012). There have been many reports of Type II and, to a lesser extent, Type I resistance QTL.

Other forms of resistance to FHB have also been described but are considered less frequently in studies and are not typically used to assess disease severity. The definition of Type III, IV and V resistances varies in the literature but categorisation, as used by Boutigny *et al.* (2008) and Gunupuru *et al.* (2017) are used herein:

- Type III: resistance to infection of kernels.
- Type IV: tolerance of FHB infection and / or DON. Tolerance is indicated by a significantly different effect on growth or yield when comparing two varieties showing similar levels of FHB symptoms (Mesterhazy, 1995).
- Type V: resistance to accumulation of DON.
    - Class 1: through processes that chemically modify DON to a less toxic form.
    - Class 2: through processes that reduce the accumulation of DON.

1.3.3 Sources of FHB resistance and QTL studies

FHB has been the focus of numerous QTL studies, which together have identified over 250 FHB resistance QTL, present across all 21 wheat chromosomes (Steiner *et al.*, 2019, Buerstmayr *et al.*, 2009). However, only a small proportion of these FHB resistance QTL have been identified across two or more studies, most likely because of different environmental conditions and differences in the susceptible parents used (Buerstmayr *et al.*, 2009).

Wheat varieties originating from China are by far the best known source of FHB resistance. The three most repeatable FHB QTL, *Fhb1*, *Fhb2* and *Qfhs.ifa-5A*, on chromosome arms 3BS, 6BS and 5AS, respectively, all originated from, or are at least present in, Chinese cultivars (Buerstmayr *et al.*, 2009). However, varieties from South America (Frontana), and Europe (Arina and F201R) have been identified that possess some degree of FHB resistance and have been used in QTL mapping studies (Draeger *et al.*, 2007, Steiner *et al.*, 2004, Shen *et al.*, 2003).

1.3.4 *Fhb1* QTL

Chinese spring cultivar Sumai 3 possesses the best resistance known in wheat and is commonly used in breeding programmes to confer resistance to FHB in commercial wheat varieties. The quantitative trait locus (QTL) associated with the strongest resistance phenotype in Sumai 3 is present on chromosome 3BS and is referred to as *Fhb1* (Niwa *et al.*, 2014). Two additional resistance factors, *Fhb2* and *Fhb3*, associated with chromosomes 6BS and 7AL respectively, have also been identified in Sumai 3 (Cuthbert *et al.*, 2007, Qi *et al.*, 2008). Furthermore, a Type I resistance QTL has been identified on chromosome 5A in Sumai 3 (Buerstmayr *et al.*, 2003).

Despite its importance in FHB resistance breeding, attempts to clone the gene, or genes, underlying the *Fhb1* QTL have been inconsistent and controversial (Su *et al.*, 2017, Steiner *et al.*, 2017, Rawat *et al.*, 2017, Ma *et al.*, 2017). *Fhb1* was, until

recently, believed to encode, or regulate the expression of, a DON-glucosyltransferase because it appeared to be involved in the detoxification of DON (Lemmens *et al.*, 2005). Schweiger *et al.* (2016) fine-mapped and sequenced the *Fhb1* QTL and identified 28 genes corresponding to the *Fhb1*-containing haplotype. Whilst they did not rule out the possibility that several genes at the *Fhb1* QTL are contributing to FHB resistance, they proposed a GDSL lipase gene as the most promising candidate based on its strong upregulation in response to FHB infection (Schweiger *et al.*, 2016). Soon after, Rawat *et al.* (2016) reported the cloning of a pore-forming toxin-like (*PFT*) gene at the *Fhb1* locus and demonstrated that the gene was responsible for enhanced FHB resistance. Jia *et al.* (2018), however, were unable to find evidence that *PFT* was responsible for improved FHB resistance and found the functional *PFT* gene in highly susceptible wheat varieties.

Su *et al.* (2018) reported that the presence of a deletion at the 5' end of a histidine-rich calcium-binding protein (*TaHRC*) within the *Fhb1* locus was sufficient in identifying varieties carrying *Fhb1*. Su *et al.* (2019) have since reported that a deletion in the *TaHRC* gene results in loss-of-function and this is responsible for the resistance associated with the *Fhb1* QTL. Li *et al.* (2019) also identified the gene encoding the histidine-rich calcium-binding protein as the gene underlying *Fhb1*. However, they report that the deletion in this gene results in a gain-of function, resulting from a different upstream start codon that encodes a protein 14 amino acids larger than the wild type protein (Li *et al.*, 2019).

Lagudah and Krattinger (2019) proposed a model that may explain the conflicting findings of Su *et al.* (2019) and Li *et al.* (2019). They suggest that the protein products of *TaHRC* and its homoeologues on 3A and 3D interact to form heteromultimers, and it is these heteromultimers that the fungus is exploiting to progress infection (Lagudah and Krattinger, 2019). Knocking out *TaHRC* would reduce the number TaHRC proteins available to form multimers, or the absence of

the 3B homoeologue variant may prevent correct heteromultimer function (Lagudah and Krattinger, 2019). The mutant form of TaHRC, proposed by Li *et al.* (2019), may still be capable of forming heteromultimers, but blocks catalytic function of the complex, thereby preventing the fungus from recruiting them (Lagudah and Krattinger, 2019).

Further experiments are necessary to confirm how *TaHRC-R* is functioning to provide resistance and whether there are additional genes in the *Fhb1* QTL that contribute to FHB resistance. Furthermore, recent reports have not explained the link between *Fhb1* and DON detoxification (Lemmens *et al.*, 2005). However, it appears likely that the deletion in the *TaHRC* gene is at least partly responsible for the *Fhb1* resistance.

1.3.5 *Rht* genes and Fusarium head blight

Several FHB susceptibility factors have been identified in wheat. The semi-dwarfing allele *Rht-B1b*, and its homoeologue *Rht-D1b*, were key to the higher yielding wheat cultivars developed during the Green Revolution (Hedden, 2003). *Rht-B1* and *Rht-D1* encode DELLA proteins that function as growth repressors (Peng *et al.*, 1999). DELLA proteins are degraded in response to gibberellin that leads to a de-repression of growth (Peng *et al.*, 1999). The *Rht-B1b* and *Rht-D1b* alleles possess reduced sensitivity to the phytohormone gibberellin compared to the wild type alleles, *Rht-B1a* and *Rht-D1a*, with the effect of reducing stem elongation, resulting in the semi-dwarfing phenotype (Hedden, 2003). However, DELLA proteins have been found to possess pleiotropic effects, resulting in increased resistance to necrotrophic and hemibiotrophic fungi, but increased susceptibility to biotrophic fungi (Saville *et al.*, 2012). Short wheat varieties in possession of these semi-dwarfing alleles show increased susceptibility to FHB (Saville *et al.*, 2012). Both *Rht-B1b* and *Rht-D1b* have been shown to confer higher Type I susceptibility to FHB (Srinivasachary *et al.*, 2009, Saville *et al.*, 2012). *Rht-D1b* is also associated with increased Type II

susceptibility to FHB, which has been proposed to be either due to pleiotropy or the linkage of susceptibility genes and not simply due to the effect of plant height on disease infection and spread (Draeger *et al.*, 2007).

1.3.6 Phytohormones and Fusarium head blight

The phytohormones ethylene, jasmonic acid (JA) and salicylic acid (SA) are important in initiating a defence response to plant pathogens (Robert-Seilaniantz *et al.*, 2007). Impaired ethylene signalling has been found to increase resistance to FHB in *Arabidopsis thaliana*, wheat and barley, suggesting that the fungus is exploiting ethylene signalling during infection (Chen *et al.*, 2009). Chen *et al.* (2009) proposed that the increased susceptibility to FHB associated with ethylene signalling is linked to plant programmed cell death. More recently, Brauer *et al.* (2019) also demonstrated the importance of auxin during FHB infection. They found that higher auxin accumulation following infection was associated with the susceptible variety Roblin, compared to the lower production in resistant varieties Wuhan 1 and Nyubai.

Brassinosteroids are a class of steroid phytohormones possessing functions in regulating a diverse range of physiological and developmental processes, including cell elongation, root growth, senescence and resistance to stress (Kim and Wang, 2010, Zhu *et al.*, 2013). Brassinosteroids also appear to regulate plant defence in response to pathogens (Bari and Jones, 2009). Brassinosteroid signalling was found to act antagonistically with pathogen-associated molecular pattern (PAMP)-triggered immunity in *Arabidopsis thaliana* (Albrecht *et al.*, 2012). As well as effects on plant development, disruption of the brassinosteroid receptor BRI1 in *Brachypodium distachyon* and barley resulted in increased resistance to necrotrophic and hemibiotrophic pathogens, including *Fusarium culmorum*. This evidence would suggest that pathogens exploit the antagonism between brassinosteroids and PAMP-triggered immunity (Goddard *et al.*, 2014).

Oxylipins are signalling molecules involved in responding to plant growth, development and stress. They are derived from the oxidation of fatty acids, which are catalysed by lipoxygenase proteins. Nalam *et al.* (2015) demonstrated that disease caused by *F. graminearum* was limited following the knockdown of 9-lipoxygenases in wheat and *Arabidopsis thaliana*. In Arabidopsis, they demonstrated that this resulted in enhanced accumulation of SA and increased SA signalling, in addition to reduced JA signalling. Hence, the expression of 9-lipoxygenases appear to be manipulated by *F. graminearum* in both bread wheat and *Arabidopsis thaliana* to manipulate phytohormone signalling in its favour (Nalam *et al.*, 2015).

Evidence of susceptibility factors to FHB, including those connected to ethylene, gibberellin and brassinosteroid signalling have been suggested to be the result of fungal exploitation of plant physiological processes (Chen *et al.*, 2009, Goddard *et al.*, 2014). Eliminating susceptibility factors has the potential to increase resistance to FHB. Hence, identifying and locating susceptibility factors may have substantial value to plant breeders and the development of cultivars possessing resistance to the disease.

1.4 Preceding work

1.4.1 Wheat-barley introgression lines provide evidence of a susceptibility factor on the short arm of chromosome 4D

A common means of generating variation in wheat is to introgress parts of chromosomes originating from wheat relatives into a wheat genetic background. Such resources are especially useful for transferring disease resistance from other related species into wheat (Rahmatov *et al.*, 2016, Liu *et al.*, 2016). Wild species from the wheat tertiary gene pool are crossed with wheat and subsequently backcrossed with the wheat parent, in order to introgress chromosomes (Rahmatov *et al.*, 2016). Such efforts have increased in recent years as genomic technologies have increased our ability to track such introgressions (Grewal *et al.*, 2018). Common donor genera include *Aegilops* spp., *Triticum* spp., *Thinopyrum* spp., *Hordeum* spp. and *Secale* spp.

Wheat and barley differ noticeably in Type II resistance. Wheat generally possesses some degree of Type II susceptibility whilst, in contrast, barley is typically highly resistant to fungal spread through the rachis (Langevin *et al.*, 2004). Furthermore, whilst DON has been shown to function as a virulence factor in wheat (Langevin *et al.*, 2004), DON does not appear to possess such a role during infection of barley heads (Maier *et al.*, 2006).

Wheat lines containing introgressions of all or part of barley chromosomes offers an insight into which barley chromosomes contribute most strongly to Type II FHB resistance and whether this resistance can be expressed, and potentially utilised, in a wheat genetic background. Previous unpublished work from the Nicholson group used such lines to establish whether this difference in FHB susceptibility is because barley carries genes conferring resistance, wheat carries genes conferring susceptibility, or whether it is a combination of both factors (Giovannelli, 2012).

FHB point inoculation experiments of the wheat-barley material were conducted twice and are described as experiment 1 (**Figure 1.4A**) and experiment 2 (**Figure 1.4B**). Experiment 1 was conducted by Giovannelli (2012) and experiment 2 was conducted by Steed and Nicholson (unpublished-b). The experiments showed consistent results for most of the lines tested. FHB symptoms were reliably restricted in both barley varieties, Igri and Betzes, and did not spread from the inoculated spikelet. For this reason, Igri and Betzes are presented only for experiment 1 (**Figure 1.4A**). The primary wheat parent, Mv9kr1, was susceptible to the spread of the fungus in both repeats of the experiment.

The addition of chromosomes 1HS (1HS add) and 7H (7H add), in addition to the 5HS-7DS.7DL wheat-barley translocation (7D-5H trans) and the 2DS.2DL-1HS translocation line (2D-1H trans) all showed highly significant increases in FHB resistance compared to Mv9kr1. Hence, the barley chromosomes, or chromosome arms, introgressed into these lines are likely to contain Type II FHB resistance factors.

A particularly strong resistant phenotype was seen with the 4H(4D) substitution (4H(4D) sub), in which disease was almost entirely restricted to the inoculated spikelet in both experiments. In contrast to this, the addition of barley 4H (4H add) showed similar disease levels to Mv9kr1 in experiment 1 (**Figure 1.4A**) and exhibited only a small increase in resistance in experiment 2 (**Figure 1.4B**). The addition of the barley chromosome 4H does not appear to be responsible for the increased FHB resistance. Hence, it is likely that a susceptibility factor carried on wheat chromosome 4D has been lost in the 4H(4D) substitution line.

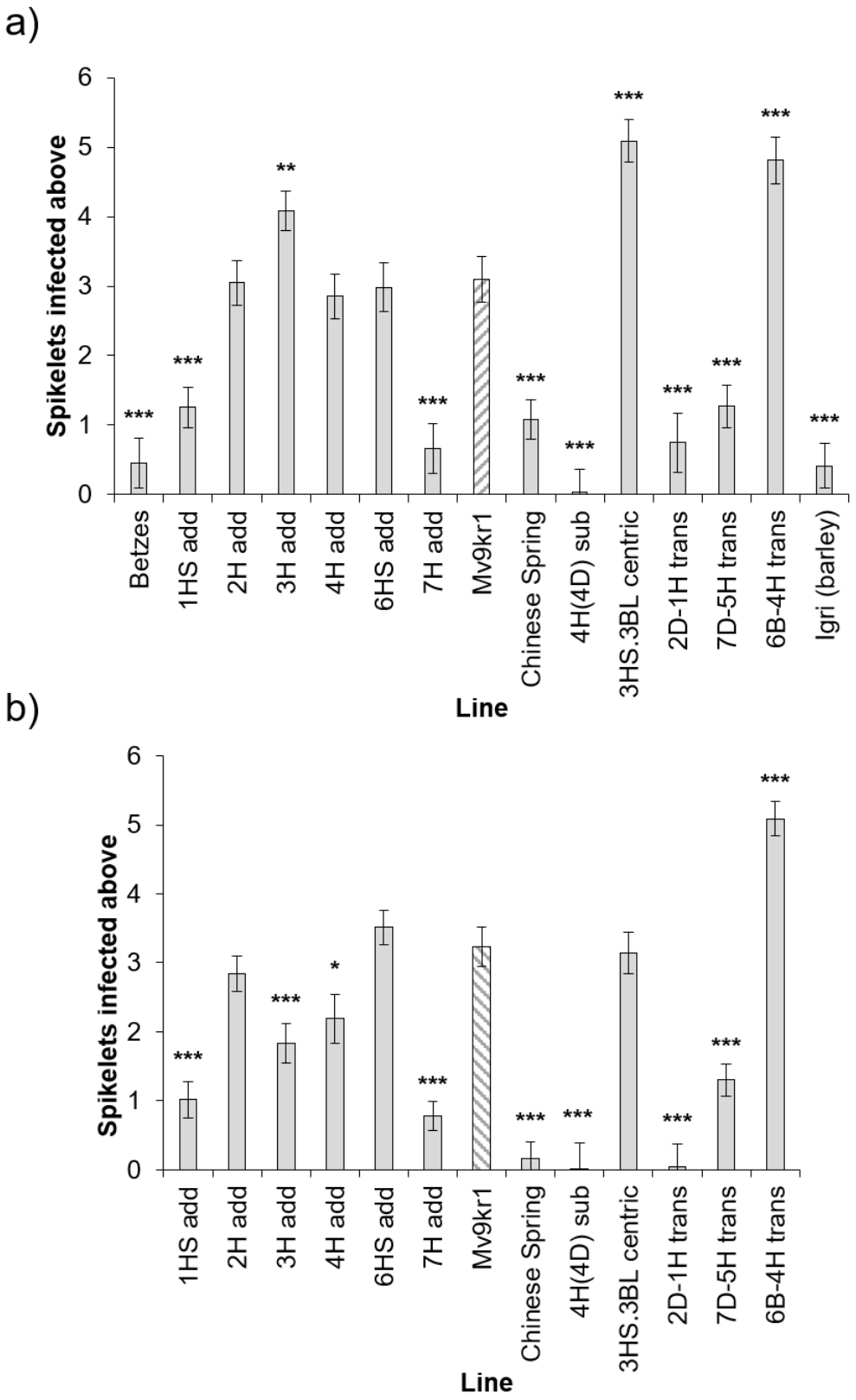

Figure 1.4 FHB disease above inoculation point in wheat-barley addition, substitution, translocation and centric fusion lines from a) polytunnel experiment 1 adapted from Giovannelli (2012), including barley parents Igri and Betzes as controls, and b) polytunnel experiment 2, adapted from data of Andrew Steed. Predicted means were generated using a general linear model. Error bars are ± standard error. * p< 0.05; ** p< 0.01; *** p< 0.001 compared with Mv9kr1.

1.4.2 Susceptibility factor isolated to short arm of 4D using Chinese Spring ditelosomic lines

One of the most established wheat resources are the cytogenetic stocks developed in the Asian spring variety Chinese Spring (Sears, 1954, Sears and Sears, 1978). As a consequence of redundancy due to its allohexaploid genome, wheat is tolerant to aneuploidy, which is the loss or gain of chromosomes or parts of chromosomes (Law *et al.*, 1987). The development of aneuploid wheat lines forms the basis of the cytogenetic stocks. Ditelosomic lines possess one chromosome pair where either the short or long arms are missing. Such lines can be used to identify a phenotype associated with a particular chromosome arm.

The contrast in the effect of adding 4H or substituting 4D with 4H indicated that the presence of 4D appeared to be responsible for a significant proportion of the susceptibility in Mv9kr1. To test this possibility, Chinese Spring and two ditelosomic lines: DT(4DL) and DT(4DS), missing 4DS and 4DL, respectively, were tested in two independent FHB point inoculation experiments (Steed and Nicholson, unpublished-a). Data is presented from a 2013 experiment conducted in a glasshouse (**Figure 1.5**), but the results were closely replicated in a 2013 experiment under controlled conditions (Steed and Nicholson, unpublished-a). The loss of 4DS (DT(4DL)) resulted in a high level of FHB resistance, whilst the loss of 4DL (DT(4DS)) showed little change in disease levels compared to euploid Chinese Spring. Ma *et al.* (2006) phenotyped Chinese Spring ditelosomic lines for FHB susceptibility and also reported an increase in FHB resistance in the ditelosomic line missing 4DS.

These results provide further evidence for the presence of an FHB susceptibility factor on 4D and isolate the effect to the short arm. The results also indicate that the susceptibility factor is present in both winter (Mv9kr1) and spring (Chinese Spring) wheat genetic backgrounds. The effect of disrupting the susceptibility factor has not

been detected in QTL studies and hence the susceptibility factor is likely to be widely present, or even ubiquitous, in wheat germplasm.

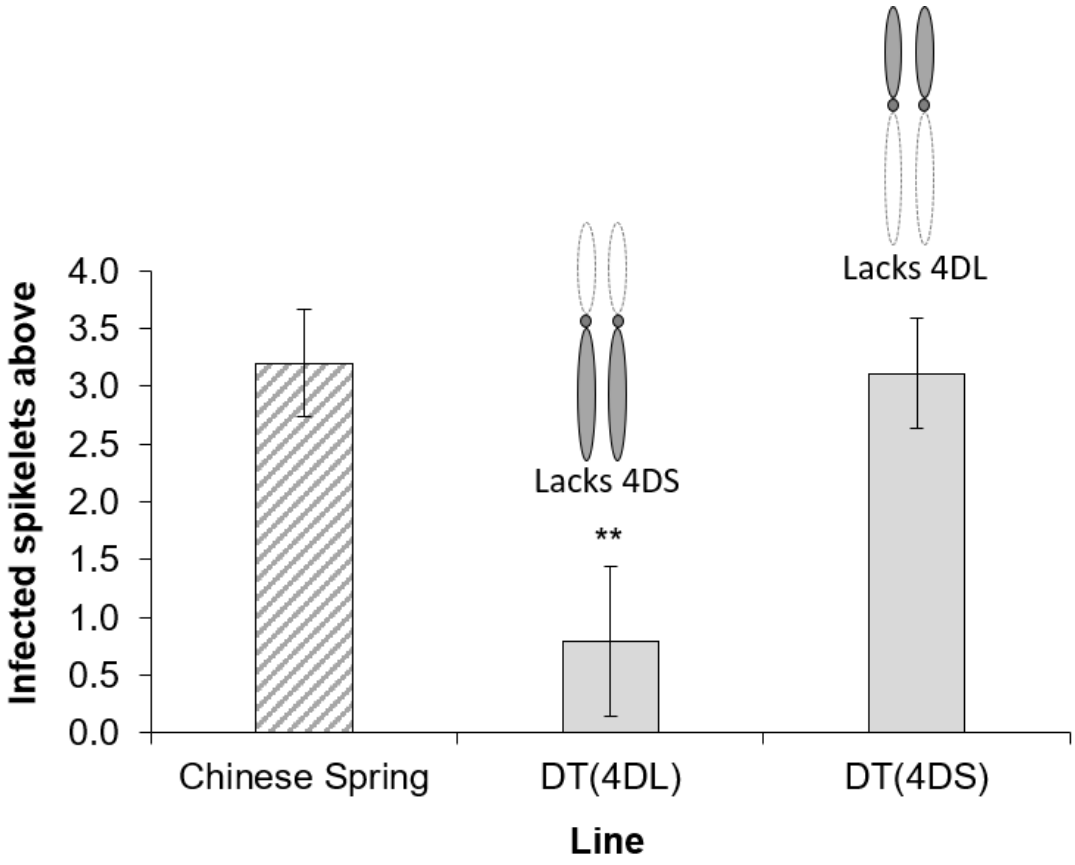

Figure 1.5 FHB disease at 17 dpi in euploid Chinese Spring and 4D ditelosomic lines DT(4DL) and DT(4DS), missing 4DS and 4DL, respectively. Diagrams of chromosome 4D are included above each aneuploid line to illustrate their genetic state. Predicted means were generated using a general linear model. Error bars are ± standard error. ** $p < 0.01$ compared with Chinese Spring. Data were provided by (Steed and Nicholson, unpublished-a).

1.5 Susceptibility factors

1.5.1 Defining a susceptibility factor

The interactions between host and pathogen are highly complex and a delicate balance must be maintained for the interaction to progress. Destabilising this interaction in favour of either host or pathogen will result in disease resistance or exacerbated susceptibility, respectively. Host resistance genes enable the plant to initiate a defence response which inhibits the progress of the fungus. In contrast, a susceptibility factor is a host gene which encodes a protein that, in some way, aids the fungus in its infection and colonisation. When a host gene encoding a susceptibility factor is deleted, the interaction is destabilised in favour of the plant host, thereby restricting the pathogenicity of the fungus. Until a host gene that alters a pathogenic interaction is fully characterised, it is not always possible to distinguish a resistance gene from a susceptibility gene. A naturally disrupted susceptibility gene will confer resistance and hence may be misidentified as a resistance gene. To complicate matters, plants must be able to defend against a range of different pathogens and there is likely to be trade-offs involved in this; in particular, between defending against fungal pathogens with biotrophic and necrotrophic lifestyles. Hence, a gene that confers resistance to one pathogenic interaction may compromise resistance to other pathogenic interactions; effectively the gene is functioning simultaneously as a resistance factor and a susceptibility factor.

1.5.2 Powdery mildew and *Mlo*

Powdery mildew is a fungal disease that infects many plant species, including wheat (caused by *Blumeria graminis* f. sp. *tritici*) and barley (caused by *Blumeria graminis* f. sp. *hordei*). The pathogen lives biotrophically in its host and gains nutrient from living plant cells. The *mildew resistance locus o* (*Mlo*), first described in barley, is one of the earliest and best characterised examples of how disrupting a susceptibility factor can be exploited to improve resistance to pathogens (Jorgensen, 1992). Mutant

alleles of *mlo* prevents the fungus from penetrating the plant cell wall and hence haustoria are not formed and spores are not produced (Acevedo-Garcia *et al.*, 2014). Induced and natural mutation of the *Mlo* locus results in a recessive, race nonspecific and durable resistance which has been widely deployed in European spring barley varieties (McGrann *et al.*, 2014, Lyngkjaer and Carver, 2000, Jorgensen, 1992). MLO proteins are highly conserved in plants, and possess seven transmembrane domains, an extracellular N terminus and an intracellular C terminus (Kusch *et al.*, 2016, Devoto *et al.*, 1999). *MLO*-based resistance has since been demonstrated in a number of other species affected by powdery mildew, reviewed by Kusch and Panstruga (2017). However, *mlo* mutations typically have pleiotropic effects (Kusch and Panstruga, 2017). Increased susceptibility to hemibiotrophic and necrotrophic pathogens has been reported under certain conditions. Barley possessing *mlo* mutant alleles suffer from enhanced susceptibility to *Magnaporthe grisea*, the causative agent of rice blast (Jarosch *et al.*, 1999). There have been reports that *mlo* mutants increased susceptibility to *F. graminearum* and *Ramularia colli-cygni* (Jansen *et al.*, 2005, McGrann *et al.*, 2014). However, Hofer *et al.* (2015) did not observe any change in susceptibility to *Fusarium* spp. or *Ramularia colli-cygni* of *mlo*5 under field conditions.

The deployment of *mlo* mutants in wheat is more challenging due to its allohexaploid nature (Acevedo-Garcia *et al.*, 2017). In contrast to barley, no natural *Mlo* mutants have been identified in wheat, presumably because all copies of *Mlo* must be mutated to obtain resistance to powdery mildew (Acevedo-Garcia *et al.*, 2017). However, TALENs and CRISPR Cas9- derived gene knockouts (Wang *et al.*, 2014) and *Mlo* TILLING mutants (Acevedo-Garcia *et al.*, 2017) have been used to demonstrate that mutation of all wheat copies does strongly enhance resistance to wheat powdery mildew.

1.5.3 *Parastagonospora nodorum* necrotrophic effectors and host sensitivity

R genes, which usually encode nucleotide binding site-leucine rich repeat (NBS-LRR) proteins, are typically used by plants to detect and respond to attack by biotrophic fungi. However, necrotrophic pathogens have evolved methods of exploiting such plant defences to aid infection. *Parastagonospora nodorum* and *Pyrenophora tritici-repentis* are necrotrophic pathogens of wheat that utilise this strategy. *Parastagonospora nodorum* causes Stagonospora nodorum blotch (SNB), whilst *Pyrenophora tritici-repentis* is responsible for tan spot (Faris *et al.*, 2013, Gao *et al.*, 2015). SNB and tan spot affect both tetraploid durum and hexaploid bread wheats. Susceptibility to these diseases operates in an inverse gene-for-gene interaction, in which a fungal necrotrophic effector is detected by a corresponding host sensitivity gene product (usually an NBS-LRR), triggering a hypersensitive response that results in necrosis that benefits the fungus (Faris *et al.*, 2010). If either necrotrophic effector or host sensitivity gene is absent, no interaction occurs and host resistance is maintained.

To date, eight necrotrophic effector proteins have been identified in *Parastagonospora nodorum*, called SnTox1, SnToxA, SnTox2, SnTox3, SnTox4, SnTox5, SnTox6 and SnTox7, which induce susceptibility in the presence of host genes *Snn1*, *Tsn1*, *Snn2*, *Snn3*, *Snn4*, *Snn5*, *Snn6* and *Snn7*, respectively (Shi *et al.*, 2015, Gao *et al.*, 2015, Friesen *et al.*, 2012, Friesen and Faris, 2010). *Snn1* and *Tsn1* are both believed to encode NBS-LRR proteins (Reddy *et al.*, 2008, Faris *et al.*, 2010). A toxin identical to SnToxA was originally identified in *Pyrenophora tritici-repentis*, called PtrToxA, which induces susceptibility to tan spot in the presence of host *Tsn1* (Friesen and Faris, 2010, Faris *et al.*, 1996). An additional two necrotrophic effectors have been identified that are exclusive to *Pyrenophora tritici-repentis*: PtrToxB and PtrToxC, associated with host sensitivity genes *Tsc2* and *Tsc1*, respectively (Friesen and Faris, 2004, Effertz *et al.*, 2002).

1.6 Project aims

Previous work by colleagues has demonstrated that there is an FHB susceptibility factor on the short arm of wheat chromosome 4D (Giovannelli, 2012, Steed and Nicholson, unpublished-a). Evidence to date suggests the susceptibility factor is fixed in wheat, which prevents the use of a typical mapping population in efforts to identify it. Incorporating a deletion or deleterious mutation of the susceptibility factor in elite wheat cultivars has the potential to greatly increase FHB resistance. Hence, a deletion line, or ideally a Cadenza TILLING line containing a mutation resulting in a premature stop codon in the susceptibility gene, would be of great value to wheat breeders (Uauy *et al.*, 2009). In an ideal situation, the mutation could be followed using DNA markers to the causal single nucleotide polymorphism (SNP). Whilst this is the ultimate aim, it is first necessary to characterise and fine-map the FHB susceptibility factor.

In the first step towards this aim, Chinese Spring aneuploid lines were used to confirm how the susceptibility factor functions in response to point and spray inoculation of *Fusarium* spp. and point application of DON. Terminal deletion lines of 4DS were then used to refine the position of the FHB susceptibility factor to a smaller physical interval along the chromosome arm.

Following this, a deletion mapping approach, using a gamma-irradiated Paragon population (Shaw *et al.*, 2013, Wheat Genetic Improvement Network, 2019), was adopted to further refine the physical interval containing the FHB susceptibility factor. This has eliminated the majority of the FHB susceptibility interval identified from the work on Chinese Spring, leaving several small intervals that require further investigation.

Thirdly, during the investigation into Chinese Spring aneuploid lines a resistance factor to bleaching induced by DON was also identified on 4DS. Therefore, this DON resistance interval was interrogated to attempt to identify candidate genes.

Chapter 2: Utilising Chinese Spring cytogenetic material to confirm, characterise and refine an FHB susceptibility factor

2.1 Introduction

Previous work, described in Chapter 1, identified an FHB susceptibility factor associated with wheat chromosome 4D in the Hungarian winter wheat variety Martonvasari9 (Giovannelli, 2012, Steed and Nicholson, unpublished-b). The effect was subsequently isolated to the short arm using 4D ditelosomic lines in a Chinese Spring genetic background (Steed and Nicholson, unpublished-a).

If the FHB susceptibility factor is indeed promoting the spread of infection, then this could be due to increased susceptibility to the fungus, or to the mycotoxin and virulence factor, DON. Furthermore, the material has never been subjected to spray inoculation and hence it remains possible that the susceptibility factor has an influence on initial infection (Type I resistance).

Endo and Gill (1996) developed deletion stocks, in a Chinese Spring genetic background, comprising of a series of lines with deletions assumed to be from the ends of chromosome arms. Examination of a specific phenotype using this material, where deletions are homozygous, can assist in reducing the physical position of genes with a particular function of interest; for example, disease resistance or susceptibility factors. Terminal deletions of the short arms of chromosomes 2A and 4B are unable to be maintained in a homozygous state because this results in sterility, and large deletions of the long arms of chromosome 4A and group 5 chromosomes were not obtained, although the reasons for this are not known (Endo and Gill, 1996).

In this chapter, Chinese Spring ditelosomic lines of 4D, lacking the entire long or short arms of the chromosome, are utilised to further characterise the FHB

susceptibility factor, using a combination of fungal point and spray inoculation experiments, in addition to point application with DON. In doing so, evidence of a resistance factor to DON on 4DS was found. Furthermore, the long arm of 4D appears to contain a Type I resistance factor.

Following this, Chinese Spring lines containing terminal deletions of 4DS and 4DL were genotyped to more precisely characterise the deletion breakpoints in the lines. The 4DS terminal deletion lines were phenotyped for Type II FHB susceptibility and DON susceptibility, to map the FHB susceptibility and DON resistance factors to refined physical intervals. In addition, 4DL terminal deletion lines were spray inoculated in order to refine the position of the Type I resistance factor.

2.2 Materials and Methods

2.2.1 Plant material

Euploid Chinese Spring, and its 4D ditelosomic (DT) lines, were acquired from the Germplasm Resource Unit, John Innes Centre, Norwich, UK. The lines DT(4DL) and DT(4DS) lack 4DS and 4DL, respectively.

Four homozygous Chinese Spring terminal deletion lines of 4DS, described by Endo and Gill (1996), were obtained from Kansas State University, Manhattan, Kansas, USA. The lines acquired were 4532 L1 (FL= 0.53), 4532 L2 (FL= 0.82), 4532 L3 (FL= 0.67) and 4532 L4 (FL= 0.77), henceforth referred to as del4DS-1, del4DS-2, del4DS-3 and del4DS-4, respectively.

An additional seven Chinese Spring terminal deletion lines of 4DL, also described by Endo and Gill (1996), were obtained from Kansas State University, Manhattan, Kansas, USA. The lines acquired were 4533 L14 (FL= 0.86), 4533 L2 (FL= 0.70), 4533 L11 (FL= 0.61), 4533 L13 (FL= 0.56), 4533 L1 (FL= 0.46), 4533 L6 (FL= 0.38) and 4533 L5 (FL= 0.09), henceforth referred to as del4DL-14, del4DL-2, del4DL-11, del4DL-13, del4DL-1, del4DL-6 and del4DL-5, respectively.

2.2.2 Marker development and genotyping

Homoeologue-nonspecific primers were designed to simultaneously amplify fragments of homoeologous genes on 4A, 4B and 4D. Sequence information of 4D genes and corresponding homoeologous genes were obtained from Ensembl Plants (EMBL-EBI, 2019). Gene names and the physical positions reported correspond to the IWGSC RefSeq v1.1 wheat genome assembly (IWGSC, 2018). Sequence insertions and deletions (indels) between homoeologous gene sequences were exploited to enable distinction of the three resulting PCR products. Forward primers were M13-tailed at the 5’ end (M13 sequence: TGTAAAACGACGGCCAGT) to enable incorporation of a fluorescent adaptor to PCR products, as described by

Schuelke (2000). Thirty-seven markers designed as such were used to characterise the deletions in the four Chinese Spring 4DS terminal deletion lines (**Table 2.1**).

Table 2.1 Primer sequences, fragment sizes (corresponding to the 4A, 4B and 4D homoeologous gene targets) and the 4D gene target of markers used to characterise the deletion sizes present in four Chinese Spring 4DS terminal deletion lines. The lowercase sequence in the forward primer indicates the M13 tail. All markers amplified at 58 °C annealing temperature.

Marker	Forward primer	Reverse primer	Fragment A; B; D (bp)	4D gene target
BH0001	tgtaaaacgacggccagtTCCTCCAATAAGAAGGTATGTC	TGGCACTGCCCTTATAGCAA	356; 330; 228	TraesCS4D02G001400
BH0002	tgtaaaacgacggccagtTGTCGTTGTTCCAGTTAAAG	TCAGGCGCATCAGACATTTG	205; 172; 163	TraesCS4D02G009200
BH0013	tgtaaaacgacggccagtGGGGAATTGTCCAAAGCGT	TGCAAGAGATGTTGGGATTTT	211; 155; 207	TraesCS4D02G014500
BH0003	tgtaaaacgacggccagtCTCCACTTTATCATTTGAAGACA	ACAAAACCTTTCACATGGCC	452; 264; 491	TraesCS4D02G017300
BH0004.2	tgtaaaacgacggccagtGTGTTCCCATTGTCGCCG	TAGTCCGCCTCCTTGCTCCT	168; 152; 194	TraesCS4D02G035700
BH0025.2	tgtaaaacgacggccagtACAATCCCGAGGTTGCCAGA	CGAAGAGGAGGGCATACATA	275; 359; 378	TraesCS4D02G039400
BH0005.2	tgtaaaacgacggccagtTGGTGCTTCATTATCCTTCTGAT	TGGTGTCCAGAGTAAACTCGATA	443; 448; 319	TraesCS4D02G040700
BH0020	tgtaaaacgacggccagtCGACCTCCTCTCAGCTTTTAG	ATGAGGATACACGGTGCTGC	304; 193; 220	TraesCS4D02G045500
BH0029	tgtaaaacgacggccagtGAGCAGATCTTCAACGTACG	ATCACAAAGGGATGGACCTG	183; 196; 159	TraesCS4D02G050300
BH0024	tgtaaaacgacggccagtAAAGTAAAATCCTCTTCCCTGAG	GCTAAACTTGCTGTCAGACAAG	274; 298; 389	TraesCS4D02G051400
BH0006.2	tgtaaaacgacggccagtGGCCAAGGTGCGTAATCCA	CGCGAGCTGAACACAAGC	265; 121; 313	TraesCS4D02G052300
BH0022	tgtaaaacgacggccagtAGTATTAGGCAATGTGTTCCACT	TGAGAAGGTTCCAAGAACCAAC	288; 459; 260	TraesCS4D02G057100
BH0021	tgtaaaacgacggccagtTCATTCAACATGCAGATCTAGGC	GACAAACTTCAATGGCATAAGC	123; 155; 130	TraesCS4D02G065300
BH0014	tgtaaaacgacggccagtCCATTGCATTCCTTCACTTGT	CGTCGTCCCATACTTCACAAA	110; 113; 107	TraesCS4D02G066900
BH0026	tgtaaaacgacggccagtCGATACACCAGTTAATTGAAATATG	CTAGGAGTTCCTTCATGGACATT	289; 471; 318	TraesCS4D02G073200
BH0015.2	tgtaaaacgacggccagtCACAACTTGTGCAGGTATAACC	GGAAAGTCAAGACAGGCACAA	198; 346; 426	TraesCS4D02G074200
BH0008	tgtaaaacgacggccagtGTATCGACGAAGCCGCAGTT	TTCCGGAGCGTCCTACGACAA	309; 190; 199	TraesCS4D02G074500
BH0040	tgtaaaacgacggccagtGCGCAGTGAGACAAAACTC	AAGTAGAAGAGCAGCGCCAT	442; 448; 451	TraesCS4D02G075300
BH0041	tgtaaaacgacggccagtAACAAATCCATGTGACCCC	CTACAAGGACGCGTGGTTAT	299; 338; 302	TraesCS4D02G076000
BH0042	tgtaaaacgacggccagtCGGACAACATTTCAGGATTTC	ACCGGAACAAGGCTGCAC	379; 135; 125	TraesCS4D02G077600
BH0027.3	tgtaaaacgacggccagtGGTAACATTCCTTTGGTATACTCGG	TGTGCTAAGATCTACAACATC	303; 350; 266	TraesCS4D02G078900
BH0032	tgtaaaacgacggccagtTTGTGGCCTGCTTACATTGC	TGATCTGCAGGTGTTGGC	317; 305; 300	TraesCS4D02G079900
BH0033	tgtaaaacgacggccagtTGCCCGTGTTTTATGCACTG	GGTAAGTAAAATGGGAAGAAAGC	201; 167; 185	TraesCS4D02G081000
BH0034	tgtaaaacgacggccagtCTGCCGTATCTCCAACTC	ATGAGCGCCATCAGGAAC	209; 297; 217	TraesCS4D02G082500
BH0035	tgtaaaacgacggccagtACGCGGACCCGAATTCAAA	TCCTTGGGCATAGAGGAAG	190; 167; 162	TraesCS4D02G083100

Table 2.1 (continued) Primer sequences, fragment sizes (corresponding to the 4A, 4B and 4D homoeologous gene targets) and the 4D gene target of markers used to characterise the deletion sizes present in four Chinese Spring 4DS terminal deletion lines. The lowercase sequence in the forward primer indicates the M13 tail. All markers amplified at 58 °C annealing temperature.

Marker	Forward primer	Reverse primer	Fragment A; B; D (bp)	4D gene target
BH0036	tgtaaaacgacggccagtATGTTAGCCGTCCTTTGTTTC	TGGCTGACAGCTATACTTCTAGT	246; 255; 223	TraesCS4D02G084000
BH0037	tgtaaaacgacggccagtGACGGACAATTCTTATGATTGTG	TATGTCCTGCCCCTTCTCCAT	191; 187; 166	TraesCS4D02G085100
BH0038	tgtaaaacgacggccagtATCTGCGTCCAGGTGAGC	TCAGCTAAGACAACTGGCAC	359; 341; 318	TraesCS4D02G085900
BH0009.3	tgtaaaacgacggccagtTAGAGGGAGCAGGGATGACAT	TCTCCGTCTGGTTCATTCGT	106; 103; 111	TraesCS4D02G087200
BH0010.2	tgtaaaacgacggccagtACGTGGTCTTCAAATCTGGC	CTGCAATATAAGGTGGCAAATC	189; 155; 159	TraesCS4D02G098400
BH0017	tgtaaaacgacggccagtCAGATTGTACGAACATCTTCTGC	AGCAGAACAAAATCTCATGG	252; 246; 263	TraesCS4D02G105100
BH0018	tgtaaaacgacggccagtGTGAGCAGAGCACCCTCC	CTGCACCACCACAGAAAAGA	226; 195; 214	TraesCS4D02G107300
BH0011	tgtaaaacgacggccagtATGCTCGTCTTCATCGAGGTAA	ATGCATTGCAGACACATCAAG	128; 160; 135	TraesCS4D02G114700
BH0012.2	tgtaaaacgacggccagtGGTCCTTCATGAAGCTTGTTC	GGCAAATAAGAGAGTTGCATAGG	275; 289; 280	TraesCS4D02G117800
BH0030	tgtaaaacgacggccagtGGCAATGTGATCCTGCAGTTC	GCCCAAAGAAATAGCAAGGGAAA	145; 174; 189	TraesCS4D02G126600
BH0057	tgtaaaacgacggccagtGCACATCCTGCTGTACCA	CTCCTTGGGAATCTTAATGCA	464; 356; 322	TraesCS4D02G147800
BH0058	tgtaaaacgacggccagtCCATTTAGATTCATGGCGAT	AGGCATATTGCAAACCCAAC	190; 315; 179	TraesCS4D02G149800

2.2.3 Leaf sampling and DNA extraction

At the second or third leaf stage, three approximately 1.5 cm sections of leaf material were collected from each plant and placed in to 96 well 1.2 mL deep-well plates. Plates containing the leaf samples were freeze dried overnight. Following this, a single tungsten bead was added to each well and samples were ground into a fine powder using a Spex GenoGrinder 2010 at 20 Hz for 2 - 5 min, checking the samples every minute. Prior to DNA extraction, the plates were centrifuged at 2232 x g for 10 min, to settle the ground leaf samples and prevent sample loss.

DNA was extracted from freeze-dried leaf tissue as described by Pallotta *et al.* (2003), with minor modifications. 500 µL of extraction buffer (preparation for 1 L: 100 mL Tris-HCl [1.0 M, pH 7.5], 100 mL EDTA [0.5 M, pH 8.0], 125 mL SDS [10% w/v], 675 mL dH_2O) was added to each occupied well and hand shaken to mix. Samples were incubated in a water bath at 65 ºC for 60 min, shaking every 15 min. Plates were moved to a fridge at 4 ºC for approximately 15 min to cool, before adding 250 µL 6.0 M ammonium acetate to each occupied well. Samples were inverted several times to mix, refrigerated for a further 20 min at 4 ºC, and then centrifuged at 2916 x g for 15 min. Leaving the pelleted leaf debris undisturbed, 600 µL of supernatant was transferred to 96 well 1.2 mL deep-well plates containing 360 µL chilled propan-2-ol. Plates were inverted several times to mix and centrifuged at 2916 x g for 15 min. The supernatant was discarded, and 500 µL 70 % v/v ethanol was added to each occupied well. Plates were shaken and centrifuged at 2916 x g for 15 min. The supernatant was discarded, and unsealed plates were placed in a pre-heated water bath at 65 ºC for 30 min, with no lids, to evaporate the remaining ethanol. DNA samples were resuspended in 100 µL dH_2O, vortexed, then stored overnight at 4 ºC. Samples were centrifuged at 2916 x g for 20 min and stored at -20 ºC until required.

2.2.4 Use of homoeologue nonspecific markers

PCR reactions were prepared using HotStarTaq Mastermix (Qiagen) following manufacturer's instructions and amplified using the following steps: 95 °C 15 min; 35 cycles of: 95 °C 1 min, 58 °C 1 min, 72 °C 1 min; with a final extension step of 72 °C 10 min. PCR products were diluted 1:30 and up to five markers were multiplexed to increase assay efficiency. 1 µL diluted and multiplexed PCR samples were added to 8.92 µL highly deionised formamide containing 0.08 µL LIZ500 size standard. PCR products were separated using an ABI 3730xl DNA analyser (Applied Biosystems) and resolved using Peak Scanner v2.0 software (Applied Biosystems).

2.2.5 Use of KASP markers

Kompetitive Allele Specific PCR (KASP) markers were used to characterise the deletions in the 4DL terminal deletion lines. Seven KASP markers obtained from RAGT Seeds mapped to 4DL, following BLAST searches of corresponding context sequences, and were capable of diagnosing deletions (**Table 2.2**).

An additional ten KASP markers were designed for deletion detection on 4DL, to increase coverage of the chromosome arm where there was poor marker coverage (**Table 2.3**). In order to design KASP markers, sequence data of 4D genes and homoeologues, on 4A and 4B, were extracted from Ensembl Plants (EMBL-EBI, 2019). Gene sequences were aligned using MUSCLE (Madeira *et al.*, 2019). Single nucleotide polymorphisms (SNPs) between the 4B and 4D copies were targeted for the HEX and FAM primers, respectively. A SNP distinguishing the 4B and 4D copies from the 4A copy was used for the common primer to prevent amplification from the 4A homoeologue. This method enables the detection of deletions in chromosome 4D and chromosome 4B by comparing their respective amplification.

Three DNA samples per line were transferred to KASP-compatible 384 or 1536 well PCR plates using a RepliKator liquid handling robot (LGC Genomics). DNA samples were placed in a 40 ºC cabinet for at least 90 min to dehydrate the DNA samples.

KASP reactions were prepared using a Meridian^2 dispenser (LGC Genomics) and amplified using a ThermoCycler^2 (LGC Genomics) using the following settings: 94 ºC 15 min; 35 cycles of: 94 ºC 20 s, 57 ºC 60 s. Plates were read using a PHERAstar fluorescent microplate reader (BMG LABTECH) and, where necessary, amplified for an additional 5 cycles of: 94 ºC 20 s, 57 ºC 60 s. KASP results were analysed using Kraken workflow management software (LGC Genomics).

Table 2.2 In-house RAGT KASP markers that mapped to 4DL (see 4D position) and were capable of detecting 4D deletions.

Marker ID	Primer sequences (FAM, HEX, Common)	4D position (bp)
RAGT_1	GAAGGTGACCAAGTTCATGCTAGTGCCCCCTTGGTTGGATTTG	393946590- 393946754
	GAAGGTCGGAGTCAACGGATTATAAGTGCCCCCTTGGTTGGATTTT	
	ACGAAGTAAAGAGAACTGGAAGGAGTA	
RAGT_2	GAAGGTGACCAAGTTCATGCTGAAAGAACTCTGTAGAAGATTGTACTG	404043537-404043325
	GAAGGTCGGAGTCAACGGATTGTGAAAGAACTCTGTAGAAGATTGTACTA	
	CGAGCAGAACCAAATTCTCGTGCAT	
RAGT_3	GAAGGTGACCAAGTTCATGCTGCATCATTAGCAGAGGTTACTGTAG	418228318-418228037
	GAAGGTCGGAGTCAACGGATTGGCATCATTAGCAGAGGTTACTGTAA	
	GGAGATGGGCTCGTTGGGCAAA	
RAGT_4	GAAGGTGACCAAGTTCATGCTAGTATTTGTTTTGATTTTTTTTTCTGAGTGGA	455783807-455784034
	GAAGGTCGGAGTCAACGGATTGTATTTGTTTTGATTTTTTTTTCTGAGTGGG	
	GCCTGTTTCTTGTTTGAAACAGGTTCTAA	
RAGT_5	GAAGGTGACCAAGTTCATGCTCCCAATACTTGAGGAAATATGGTTATTTTT	455895572-455895338
	GAAGGTCGGAGTCAACGGATTCCAATACTTGAGGAAATATGGTTATTTTC	
	TCCGTCTCAAAATAAGTGTCTCAACCTTA	
RAGT_6	GAAGGTGACCAAGTTCATGCTGCGTGGAAACCGTCGTCGTAC	456042202-456042415
	GAAGGTCGGAGTCAACGGATTGCGTGGAAACCGTCGTCGTAT	
	GACGCGAACCCTAATTGTGGTAGTT	
RAGT_7	GAAGGTGACCAAGTTCATGCTGTGAGCGTTGGAGATGCCTATC	475283518-475283716
	GAAGGTCGGAGTCAACGGATTGTGAGCGTTGGAGATGCCTATT	
	CTCACAAAAAGCGGTTCCTTTGGCT	

Table 2.3 KASP markers designed to detect deletions across 4DL, with their respective 4D gene target.

Marker name	Primer sequence: FAM (4D), HEX (4B), Common	4D gene
BH_4D160200	GAAGGTGACCAAGTTCATGCTAGGCTCCAGACCATTGAAGAAA	TraesCS4D02G160200
	GAAGGTCGGAGTCAACGGATTAGGCTCCAGACCATTGAAGAAG	
	GGCACCTTCTCAAAGCTCAC	
BH_4D164000	GAAGGTGACCAAGTTCATGCTGAAGAATCGACGTCGTCTCG	TraesCS4D02G164000
	GAAGGTCGGAGTCAACGGATTGAAGAATCGACGTCGTCTCA	
	CGCTTCACTGTTGAAGATGAC	
BH_4D168300	GAAGGTGACCAAGTTCATGCTGATGTCAGATACACAGTCTCCCAT	TraesCS4D02G168300
	GAAGGTCGGAGTCAACGGATTGATGTCAGATACACAGTCTCCCAC	
	AAACTCCTTTCCATGGGCTCG	
BH_4D207700	GAAGGTGACCAAGTTCATGCTTTCCCATGCAAGACATGAGTG	TraesCS4D02G207700
	GAAGGTCGGAGTCAACGGATTTTCCCATGCAAGACATGAGTA	
	CAGAACCTACTCGATCCCTTCT	
BH_4D227100	GAAGGTGACCAAGTTCATGCTCAGATCGAGGCGCTCATAC	TraesCS4D02G227100
	GAAGGTCGGAGTCAACGGATTCAGATCGAGGCGCTCATAT	
	GACATGCAGCGCGATGTAG	

Table 2.3 (continued) KASP markers designed to detect deletions across 4DL.

Marker name	Primer sequence: FAM (4D), HEX (4B), Common	4D gene
BH_4D247500	GAAGGTGACCAAGTTCATGCTGTGCAACAAGTTCACAGTTC	TraesCS4D02G247500
	GAAGGTCGGAGTCAACGGATTGTGCAACAAGTTCACAGTTG	
	GACGGAGGTGCAATTTAAGT	
BH_4D276200	GAAGGTGACCAAGTTCATGCTGAACTGTTCAGCTGATGTTACCC	TraesCS4D02G276200
	GAAGGTCGGAGTCAACGGATTGAACTGTTCAGCTGATGTTACCG	
	GTTGTTGCCTGCTATCTACTCTGC	
BH_4D312000	GAAGGTGACCAAGTTCATGCTGCAGCTTGTGCTTCTAGGG	TraesCS4D02G312000
	GAAGGTCGGAGTCAACGGATTGCAGCTTGTGCTTCTAGGA	
	GAATAAAGCAAAGCGTCTCCAG	
BH_4D360400	GAAGGTGACCAAGTTCATGCTACTTCGCCAGCGTCTCCT	TraesCS4D02G360400
	GAAGGTCGGAGTCAACGGATTACTTCGCCAGCGTCTCCC	
	GTAAGGGAGGGAAGGGTCGAAC	
BH_4D366100	GAAGGTGACCAAGTTCATGCTGGGAAACTTCGTGGTTTGGT	TraesCS4D02G366100
	GAAGGTCGGAGTCAACGGATTGGGAAACTTCGTGGTTTGGG	
	GCTCAAAGGCTCCATCAGGAT	

2.2.6 Fungal point inoculation of wheat heads

Fungal point inoculation experiments were performed in a polytunnel during the summer months of 2016 and 2017 at the John Innes Centre, Norwich, UK (**Table 2.4**). Experiments were arranged in a randomised complete block design consisting of four replicates with up to 20 plants per line distributed evenly between replicates.

Fungal inoculum was prepared using a highly virulent DON-producing strain of *F. graminearum* or *F. culmorum*, as described by Gosman *et al.* (2005). At mid-anthesis, a spikelet approximately halfway up the wheat head was injected with fungal conidia at a concentration of 1 *10^6 conidia/ mL. In polytunnel experiments, water was applied to the floor and the ventilation screens were sealed overnight, to increase the temperature and humidity following inoculation. The spread of infection through the rachis to spikelets above and below the point of inoculation was recorded at regular intervals post-inoculation.

2.2.7 Fungal spray inoculation of wheat heads

Fungal spray inoculation experiments took place in a polytunnel during the summer months of 2017 and 2018 at the John Innes Centre, Norwich, UK (**Table 2.4**). Plants were arranged in the same manner as fungal point inoculation experiments, described above.

Fungal inoculum was prepared using a highly virulent DON-producing strain of *F. graminearum* or *F. culmorum*, as described by Gosman *et al.* (2005). At mid-anthesis, wheat heads were sprayed until runoff with fungal conidia at a concentration of 1 *10^5 conidia/ mL, amended with 0.01 % Tween 20. The number of infected spikelets on each inoculated head was recorded at regular intervals post-inoculation.

2.2.8 DON application to wheat heads

DON application experiments were conducted in a polytunnel in the summers of 2016 and 2017 (**Table 2.4**). Plants were organised in a randomised complete block design with four replicates, each containing four plants per line.

DON application was carried out on wheat spikes at mid-anthesis, following a protocol modified from Lemmens *et al.* (2005). Purified DON (> 98 %) was kindly supplied by Dr Marc Lemmens (IFA-Tulln) and was purified as described by Altpeter and Posselt (1994). Two adjacent spikelets opposite to each other on the wheat head, approximately central on the head, were cut with scissors approximately central on the spikelet. The cut spikelets were left for 1 - 2 h before applying 10 µL of DON solution (10 mg / mL amended with 0.01 % v/v Tween 20) to the two outer florets of each cut spikelet, between the palea and lemma. To increase the humidity at the site of DON application, treated wheat heads were bagged. At 48 h post-application, the DON application was repeated, and heads bagged again. Hence, each wheat head received a total application of 0.8 mg DON. After a further 48 h, bags were removed from the heads. At regular intervals post-application (from first application), the severity of bleaching for each treated wheat head was scored out of ten. A score of zero was given when no evidence of DON damage was present and a score of ten was recorded when the spike was completely bleached above the point of DON application. Scores between one and nine were used to record the progressive yellowing and bleaching of the DON treated wheat heads, which occurred uniformly above the point of DON application. After the experiment, DON-treated and untreated heads from each plant were harvested. From each plant with a DON treated head, a comparable untreated head (with similar spikelet number and head length) was selected for grain weight analysis. Grain number and grain weight data were collected from DON treated and comparable untreated heads, to observe any difference in the effect of DON on grain filling.

Table 2.4 FHB point and spray inoculation, and DON application experiments conducted as part of Chapter 2. Each experiment has been assigned a unique code. Figures relating to each experiment are provided, in addition to brief descriptions of each experiment.

Experiment code	Figure(s)	Description
FHBpt_CSditelo_Poly_16	1A	Conidial point inoculation of Chinese Spring 4D ditelosomic lines
DON_ CSditelo_Poly_16	1B, 2	DON application to Chinese Spring 4D ditelosomic lines
FHBsp_CSditelo_Poly_17	1C	Conidial spray inoculation of Chinese Spring 4D ditelosomic lines
FHBpt_CSterm_Poly_17	5	Conidial point inoculation of Chinese Spring 4DS terminal deletion lines
DON_CSterm_Poly_17	7	DON application to Chinese Spring 4DS terminal deletion lines
FHBsp_CSterm_Poly_18	10	Conidial spray inoculation of Chinese Spring 4DL terminal deletion lines

2.2.9 FHB disease and DON experiment data analysis

Scoring data from experiments conducted on Chinese Spring 4D ditelosomic lines (experiments FHBpt_CSditelo_Poly_16, DON_CSditelo_Poly_16 and FHBsp_CSditelo_Poly_17) were analysed using a general linear model (GLM), accounting for genotype and replicate. Residuals were visually checked to confirm they were normally distributed and independent of fitted values. In all cases, data were log10 transformed, which corrected for the necessary assumptions regarding the residuals. Predicted means and standard errors were generated for each line included in the GLM. Predicted means and standard errors generated from transformed data were back transformed to the original scale for presentation purposes.

All other experiments were analysed using linear mixed modelling (REML). In all cases, line was included as a fixed effect and replicate as a random effect in the linear mixed model. During construction of the model, inoculation date, and the interaction between inoculation date and line were included in the model as fixed effects and plant nested within replicate as a random effect. However, inclusion of these terms did not have a significant effect on the model. Hence, the terms were omitted from the model. In all cases except FHBsp_CSterm_Poly_18, the final model included line as a fixed effect and replicate as a random effect. The model for FHBsp_CSterm_Poly_18 also included inoculation date as a fixed term. Residuals were visually assessed for normality and independence from fitted values. Data from experiments FHBpt_CSterm_Poly_17 and FHBsp_CSterm_Poly_18, and grain data from DON_CSterm_Poly_17, were log10 transformed to achieve normality of residuals and to make residuals independent of fitting values.

Predicted means and standard errors were generated for each line included in the linear mixed model. Predicted values generated from transformed data were back transformed to the original scale for presentation purposes. Pairwise differences

between wild type Chinese Spring and the studied lines were tested by Fisher's Protected Least Significant Difference.

All statistical analyses were carried out using GenStat (18th edition, VSN International). ANOVA tables for all statistical analyses conducted are presented in the appendix (p. 195-7).

2.3 Results

2.3.1 The loss of 4DS alters FHB and DON susceptibility in Chinese Spring

Previous work identified a potential Fusarium head blight susceptibility factor on the short arm of wheat chromosome 4D. To characterise the susceptibility factor, Chinese Spring 4D ditelosomic lines were point and spray inoculated to assess Type II and Type I FHB resistance, respectively. Additionally, a DON application experiment was performed on the same material.

An FHB point inoculation experiment was conducted in a polytunnel in summer 2016 to assess Type II resistance in Chinese Spring 4D ditelosomic lines (FHBpt_CSditelo_Poly_16). Euploid Chinese Spring was susceptible to the spread of disease (mean= 1.16). DT(4DS), lacking 4DL, was not significantly different from the wild type (mean= 0.81, p=0.473) (**Figure 2.1A**). In contrast, DT(4DL), lacking 4DS, showed very limited disease spread and was significantly more resistant than Chinese Spring (mean= 0.26, p= 0.043) (**Figure 2.1A**). These data are consistent with the previous findings of Steed and Nicholson (unpublished-a).

A DON application experiment was also performed in a polytunnel in summer 2016 (DON_CSditelo_Poly_16). In this experiment, the bleaching in response to DON did not spread gradually within the head. Instead, the entire portion of the wheat head above the DON application point bleached uniformly. However, the speed and severity of bleaching, in response to DON application, varied between lines. A score out of ten was used to indicate the level of bleaching in response to DON. Euploid Chinese Spring (mean= 3.42) and DT(4DS) (mean= 2.94, p= 0.259) showed similar bleaching in response to DON application (**Figure 2.1B**). Conversely, DT(4DL) was significantly more susceptible to bleaching than Chinese Spring (mean= 7.60, p< 0.001) (**Figure 2.1B**).

An FHB spray inoculation experiment was conducted in a polytunnel in summer 2017 to assess Type I resistance in the Chinese Spring 4D ditelosomic lines

(FHBsp_CSditelo_Poly_17). Disease symptoms were very low in both Chinese Spring (mean= 1.55 %) and the line missing 4DS, DT(4DL) (mean= 2.65 %, p= 0.601) (**Figure 2.1C**). However, the line lacking 4DL, DT(4DS), was significantly more susceptible than Chinese Spring (mean= 11.53 %, p<0.001) (**Figure 2.1C**).

DON-treated and untreated heads from each plant were harvested following the DON application experiment (DON_CSditelo_Poly_16). The grain above and below the application point were dissected out, counted and weighed. The ratio between average grain weight of treated and untreated heads were calculated for each plant and these values were used to compare the effect of DON application on grain weight. Chinese Spring (mean= 0.522) and DT(4DS) (mean= 0.454, p= 0.193), lacking 4DL, showed similar grain weight ratios to each other above the point of application (**Figure 2.2A**). In contrast, DT(4DL) showed a significantly reduced grain weight ratio and this was significantly different when compared to Chinese Spring (mean= 0.228, p< 0.001) (**Figure 2.2A**). This difference is evident when visually comparing treated and untreated grain of the three lines, with treated grain from DT(4DL) being visibly smaller than Chinese Spring and DT(4DS) (**Figure 2.2B**).

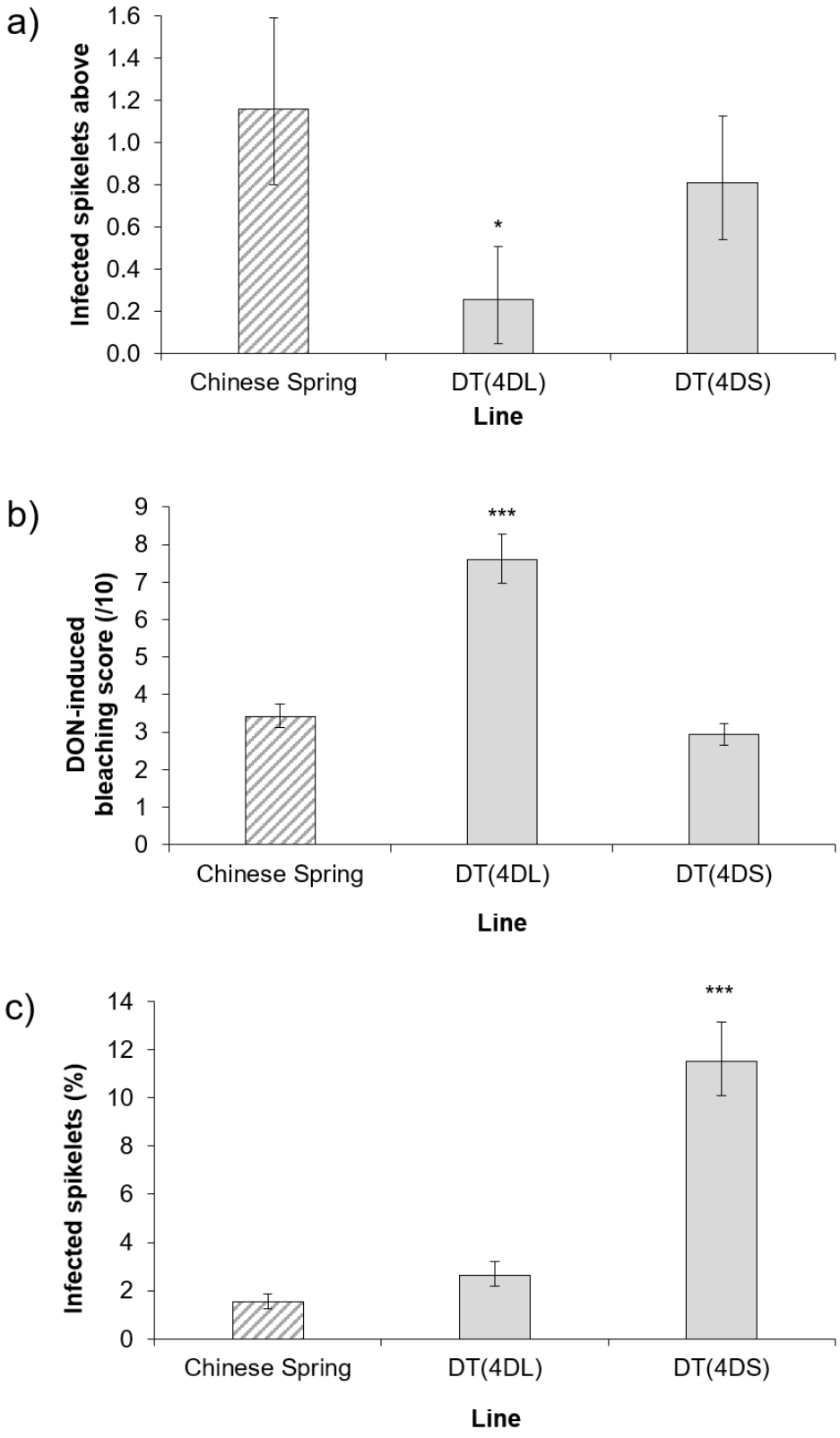

Figure 2.1 a) FHB point inoculation at 14 dpi, b) DON application at 7 days post application, and c) FHB spray inoculation at 14 dpi, of euploid Chinese Spring and 4D ditelosomic lines DT(4DL) and DT(4DS), missing 4DS and 4DL, respectively. Predicted means were generated using a general linear model. In all cases, statistical analyses were performed on Log10 transformed values. The predicted means and standard error bars presented have been back transformed. Error bars are ± standard error. * $p < 0.05$; *** $p < 0.001$ compared with Chinese Spring.

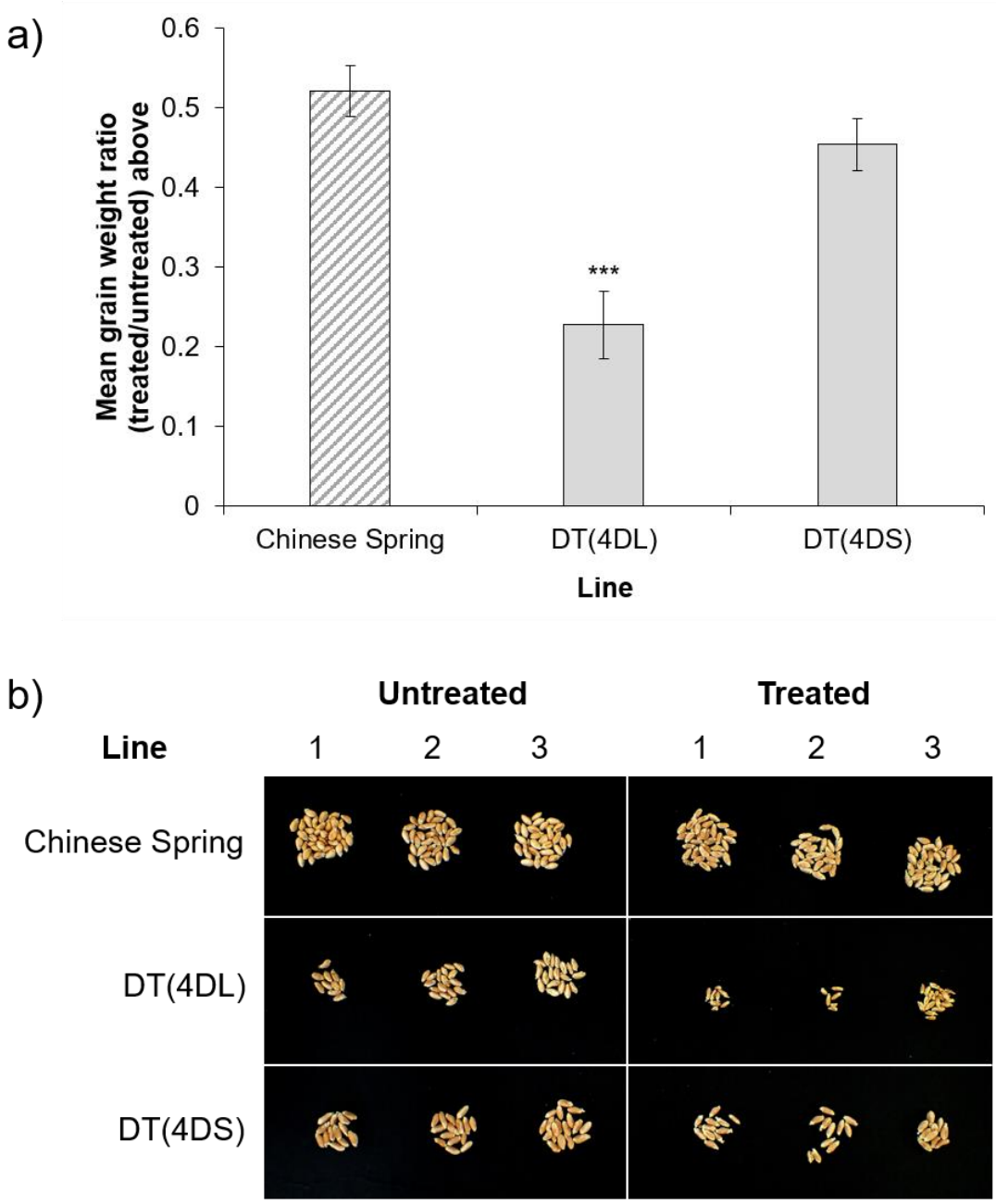

Figure 2.2 a) the mean ratio of DON treated/ untreated average grain weight above the DON application point, or comparable point in untreated heads, of euploid Chinese Spring and 4D ditelosomic lines DT(4DL) and DT(4DS), missing 4DS and 4DL, respectively. Predicted means were generated using a linear mixed model. Error bars are ± standard error. *** p< 0.001 compared with Chinese Spring. b) photograph showing three representative examples of untreated and DON treated grain taken from above the DON application point, or comparable point in untreated heads, of euploid Chinese Spring and 4D ditelosomic lines DT(4DL) and DT(4DS), missing 4DS and 4DL, respectively.

2.3.2 Precise characterisation of deletion sizes in Chinese Spring 4DS terminal deletion lines

Experiments using 4D ditelosomic lines strongly suggested that the susceptibility attributed to chromosome 4D is isolated to the short arm (4DS). These experiments also provided evidence that a DON resistance factor is also located on 4DS. Genotyping was performed on four Chinese Spring lines with terminal deletions on 4DS to verify the deletions present and more precisely position the deletion breakpoint in each line, relative to the physical map. Markers were designed that can reliably detect genes on 4D and their homoeologues on 4A and 4B. The ability to detect and distinguish all three homoeologues provides two internal positive controls for each marker when identifying deletions of any particular homoeologue. Up to five markers, tagged using different fluorophores, were multiplexed into a single sample for efficiency, using markers designed to produce PCR product sizes sufficiently different for each gene target and its respective homoeologues to be resolved following capillary electrophoresis (**Figure 2.3**).

Genotyping was successful in identifying genes, and their respective physical positions, flanking the deletion breakpoint in all four 4DS terminal deletion lines (**Figure 2.4**). A marker (BH0001) targeting the gene TraesCS4D02G001400 at the extreme distal end of 4DS confirmed that all four lines were true terminal deletions. The terminal deletion in del4DS-2 extends to between 50.6 and 51.6 Mbp. Line del4DS-4 is deleted up to between 53.9 and 54.8 Mbp. The deletion in del4DS-3 ends between 83.3 and 85.6 Mbp. The deletion breakpoint in the largest terminal deletion line, del4DS-1, ends between 111.1 and 140.9 Mbp.

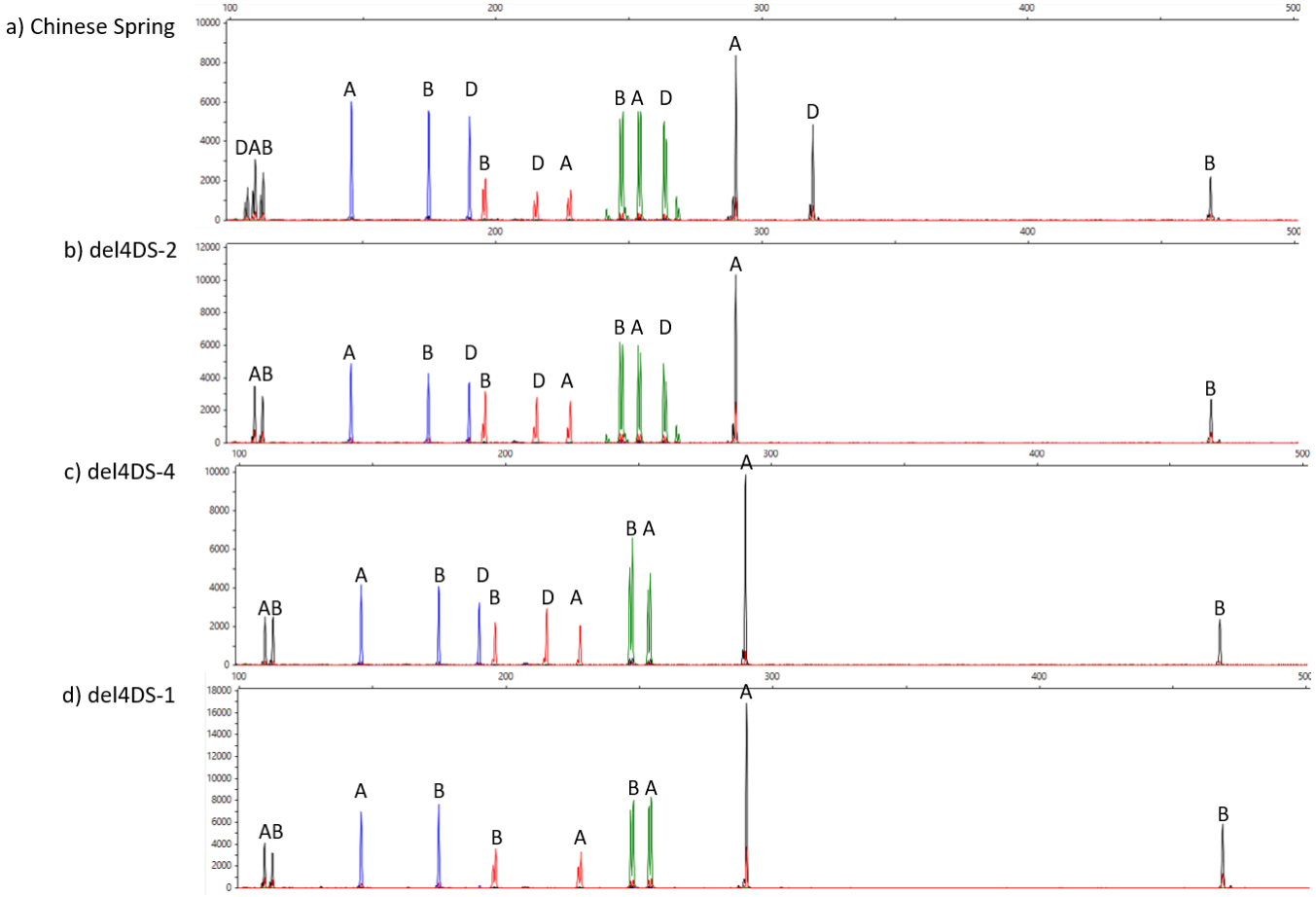

Figure 2.3 Example outputs of five multiplexed markers BH0014 (left black), BH0030 (blue), BH0018 (red), BH0017 (green) and BH0026 (right black) in a) Chinese Spring; b) del4DS-2; c) del4DS-4; d) del4DS-1. The line del4DS-3 showed the same deletion pattern as del4DS-4 for the markers visible in the selected multiplex and was hence omitted. X axis is fragment size (bp) and Y axis is the strength of fluorescence (relative fluorescence units). Images were extracted as screenshots from Peak Scanner 2 software (Applied Biosystems).

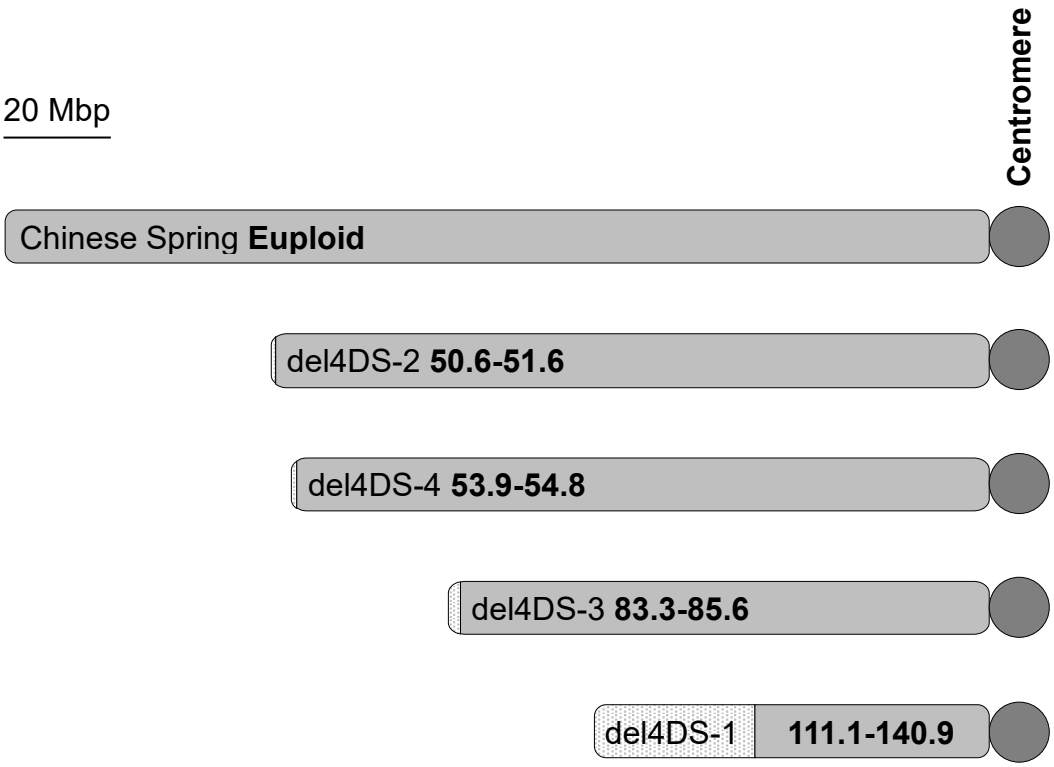

Figure 2.4 Diagram of 4DS in euploid Chinese Spring and four 4DS terminal deletion lines, as characterised by genotyping with 37 markers. The spotted interval indicates the breakpoint interval; the distance between two markers where the 4D signal was retrieved. Values in bold indicate the physical positions of the deletion breakpoints (Mbp).

2.3.3 Assessing Type II susceptibility of Chinese Spring 4DS terminal deletion lines

Euploid Chinese Spring and the four Chinese Spring 4DS terminal deletion lines that were genotyped (del4DS-2, del4DS-4, del4DS-3 and del4DS-1, in ascending order of terminal deletion size) were point inoculated in a polytunnel experiment in summer 2017 (FHBpt_CSterm_Poly_17). Chinese Spring showed moderate levels of disease in this experiment, with mean disease above the inoculation point of 1.24 bleached spikelets at 13 dpi (**Figure 2.5**). Lines del4DS-2 (mean= 1.17, p= 0.573) and del4DS-4 (mean= 1.06, p=0.145) showed similar disease levels to that of euploid Chinese Spring (**Figure 2.5**). Lines del4DS-3 (mean= 0.51, p< 0.001) and del4DS-1 (mean= 0.37, p< 0.001) both had significantly reduced disease with respect to euploid Chinese Spring (**Figure 2.5**).

These disease data were used to infer that the susceptibility factor was present in the two deletion lines carrying the smaller deletions (del4DS-2 and del4DS-4) but was lost in the two lines containing the larger deletions (del4DS-3 and del4DS-1). Hence, the susceptibility factor appears to reside between the deletion breakpoints of del4DS-4 and del4DS-3; a 31.73 Mbp interval (**Figure 2.6**).

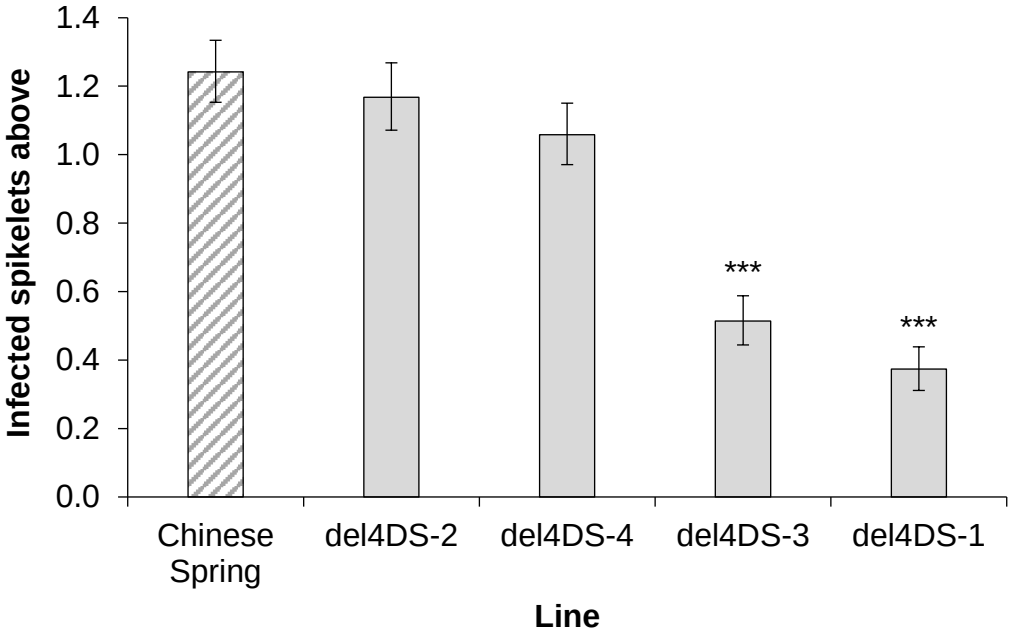

Figure 2.5 FHB disease above the inoculation point at 13 dpi, following point inoculation of euploid Chinese Spring and four terminal deletion bins; del4DS-2, del4DS-4, del4DS-3 and del4DS-1. Predicted means were generated using a linear mixed model. Statistical analysis was performed using Log10 transformed values. The predicted means and standard error bars presented have been back transformed. Error bars are ± standard error. *** $p < 0.001$ compared with Chinese Spring.

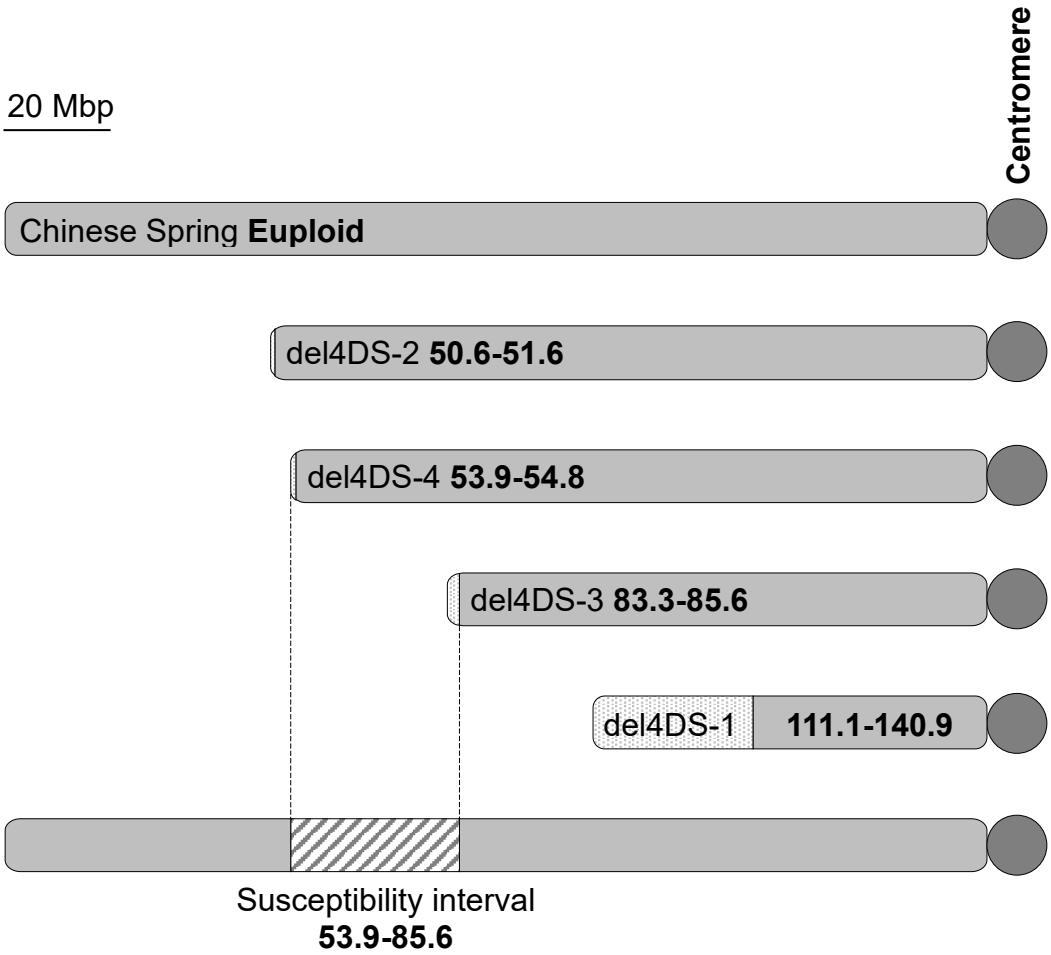

Figure 2.6 Diagram of 4DS in euploid Chinese Spring and four 4DS terminal deletion lines, as characterised by genotyping with 37 markers. The spotted interval indicates the breakpoint interval; the distance between two markers where the 4D signal was retrieved. The bottom diagram indicates the interval on 4DS inferred to contain an FHB susceptibility factor (diagonal stripes), following point inoculation of the Chinese Spring terminal deletion lines. Values in bold indicate the physical positions of the deletion breakpoints (Mbp).

2.3.4 Assessing DON susceptibility of Chinese Spring 4DS terminal deletion lines

Euploid Chinese Spring and the four terminal deletion lines of 4DS were used in a DON application experiment in a polytunnel in summer 2017 (DON_CSterm_Poly_17). In this experiment, DON treated heads were scored for bleaching out of ten both above and below the point of application. There was little bleaching observed below the application point. Hence, data are presented of the scores above the DON application point. A second head of each plant received a mock treatment using water amended with 0.01 % v/v Tween 20. No spikelet bleaching symptoms were observed and grain developed normally in the mock treated heads. Chinese Spring was the most resistant line to spikelet bleaching in response to DON, with a mean score of 3.91. The line del4DS-2 showed a small but significant increase in DON susceptibility (mean= 4.66, p=0.019) (**Figure 2.7A**). However, the lines del4DS-4 (mean= 5.73, p< 0.001), del4DS-3 (mean= 5.83, p< 0.001) and del4DS-1 (mean= 6.32, p< 0.001) were all significantly more susceptible to DON bleaching (**Figure 2.7A**).

Grain weight data were collected from DON treated and mock treated wheat heads in the experiment (DON_CSterm_Poly_17). As with the previous DON application experiment, grain data is presented as a ratio between the average grain weight of DON treated and mock treated heads. The bleaching scores suggest the strongest differential is expected between del4DS-2 and del4DS-4, and hence grain data in Chinese Spring and the two smaller deletion lines were collected. The grain weight of Chinese Spring above the application point, was less affected by DON treatment than del4DS-2 or del4DS-4 (mean= 0.488) (**Figure 2.7B**). Grain in del4DS-2 were significantly reduced compared to Chinese Spring (mean= 0.282, p=0.013) (**Figure 2.7B**). A significant effect was also observed in del4DS-4 compared with Chinese Spring (mean=0.235, p= 0.003) (**Figure 2.7B**).

Based on the DON bleaching data, the greatest increase in DON susceptibility was observed between del4DS-2 and del4DS-4. These data would suggest that, whilst there may be additional factors that have an influence on DON susceptibility on the distal end of 4DS, there appears to be a DON resistance factor present between 50.6 Mbp and 54.8 Mbp (**Figure 2.8**). This relatively small interval contains 49 genes. However, the effect of DON on grain weight is similarly pronounced in both del4DS-2 and del4DS-4, which would suggest a DON resistance factor may be present distal to 50.6 Mbp.

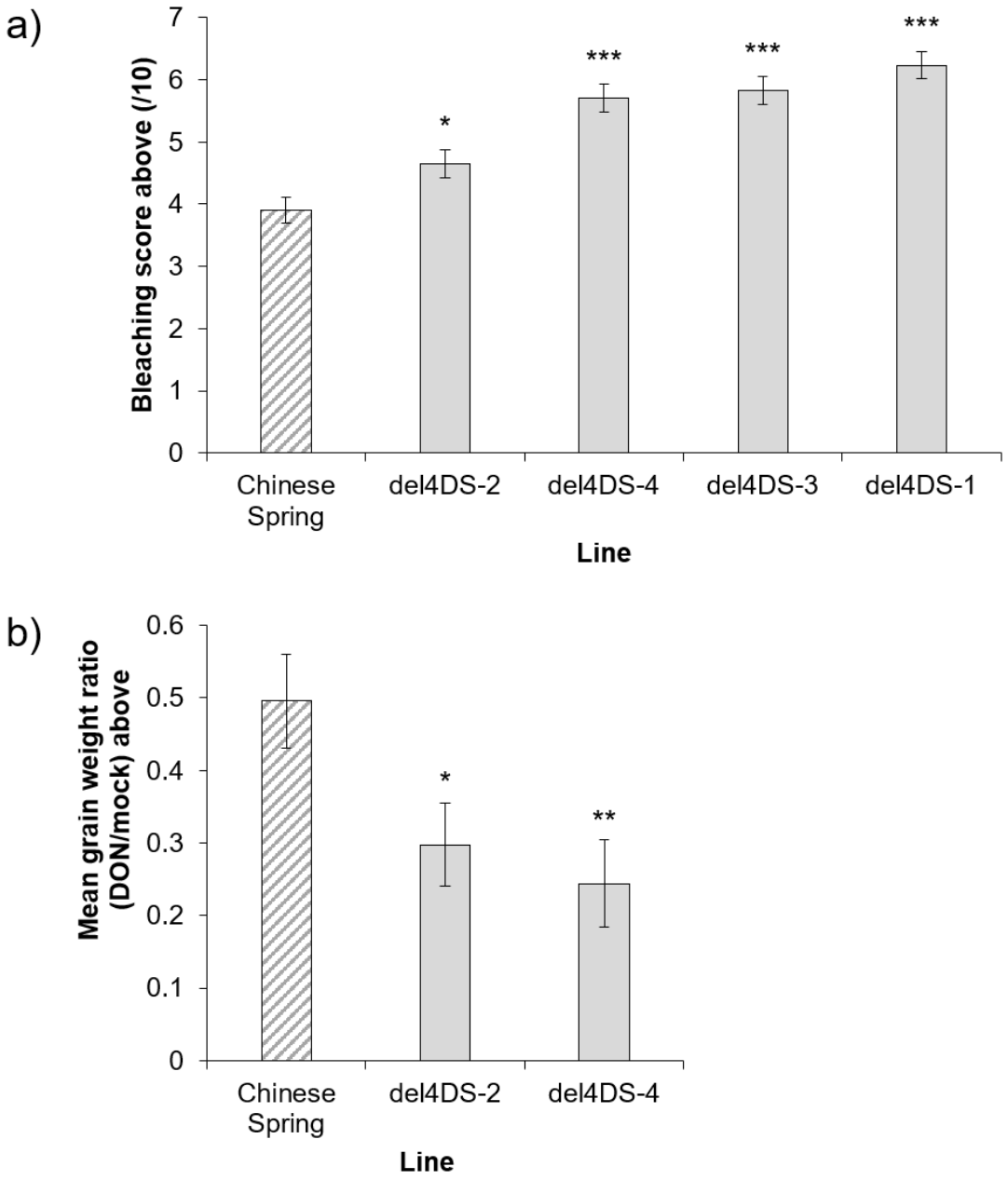

Figure 2.7 a) Bleaching score in response to DON at 8 days post application, in euploid Chinese Spring and four 4DS terminal deletion lines: del4DS-2, del4DS-4, del4DS-3 and del4DS-1. Untransformed values were used analyse DON bleaching data. B) The mean ratio of DON/ mock treated average grain weight above the DON application point, of euploid Chinese Spring and two 4DS terminal deletion lines: del4DS-2 and del4DS-4. Statistical analysis for grain ratio data were performed on Log10 transformed values. The predicted means and standard error bars presented have been back transformed. In both cases, predicted means were generated using a linear mixed model. Error bars are ± standard error. * $p < 0.05$; ** $p < 0.01$; *** $p < 0.001$ compared with Chinese Spring.

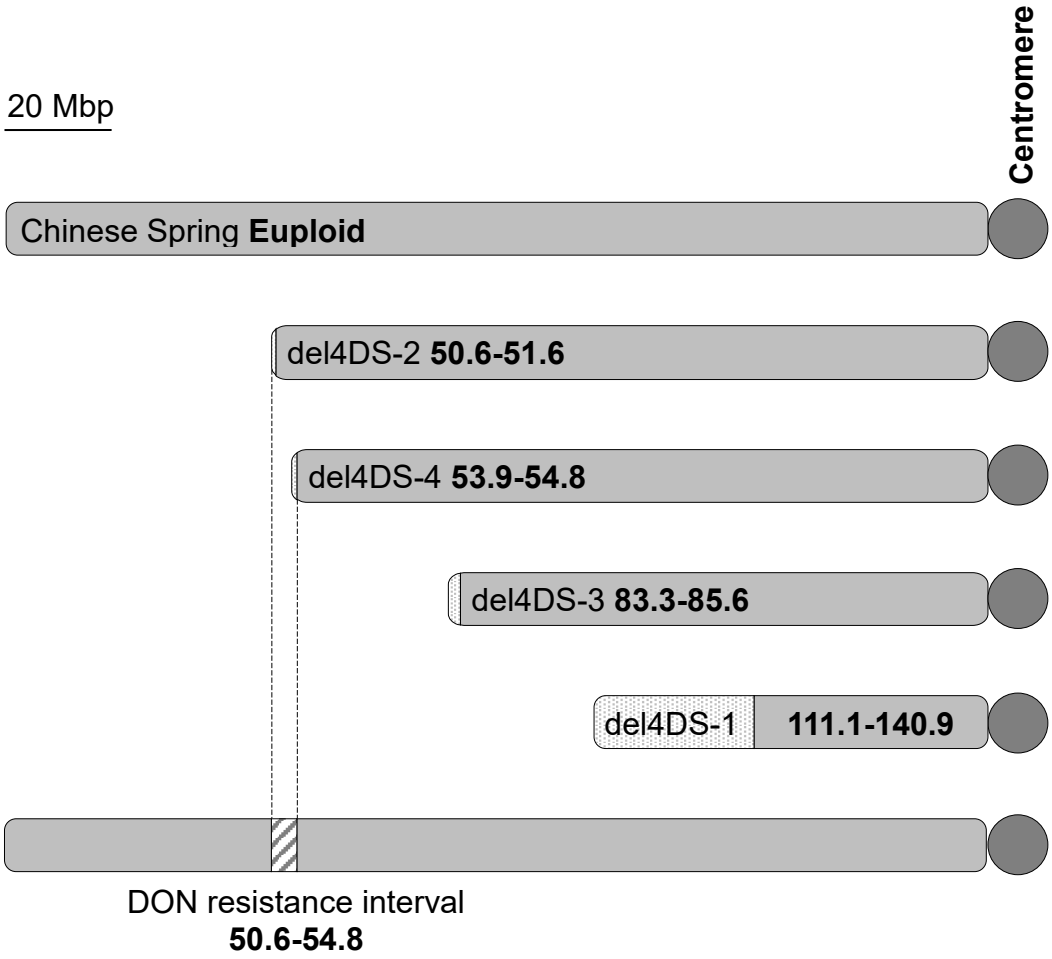

Figure 2.8 Diagram of 4DS in euploid Chinese Spring and four 4DS terminal deletion lines, as characterised by genotyping with 37 markers. The spotted interval indicates the breakpoint interval; the distance between two markers where the 4D signal was retrieved. The bottom diagram indicates the interval on 4DS inferred to contain a DON resistance factor (diagonal stripes), following DON application of the Chinese Spring terminal deletion lines. Values in bold indicate the physical positions of the deletion breakpoints (Mbp).

2.3.5 Characterisation of deletion sizes in Chinese Spring 4DL terminal deletion lines

Euploid Chinese Spring and seven 4DL terminal deletion lines were genotyped using KASP markers with three biological replicates per line. The deletion breakpoint in del4DL-14 (FL value 0.86) was between 478.03 Mbp (TraesCS4D02G312000) and 507.35 Mbp (TraesCS4D02G360400) (**Figure 2.9**). The line del4DL-2 is deleted to between 418.23 Mbp (marker RAGT_3) and 447.34 Mbp (TraesCS4D02G276200). The lines del4DL-11 and del4DL-13, with FL values of 0.61 and 0.56, respectively, could not be distinguished with the current marker density and the breakpoints in both lines are between 393.95 Mbp (marker RAGT_1) and 404.04 Mbp (marker RAGT_2). Only one marker, at 386.37 Mbp (TraesCS4D02G227100), showed a wild type-like signal in del4DL-1 (FL value 0.46). All other markers showed a deletion-like signal. The deletion breakpoint in del4DL-6 (FL value 0.38) is between 292.91 Mbp (TraesCS4D02G168300) and 356.88 Mbp (TraesCS4D02G207700). Line del4DL-5 (FL value 0.09) possessed a deletion-like signal for all markers, with the exception of RAGT_1 at 393.95 Mbp, which showed an inconsistent signal between the three replicate samples. Markers that showed inconsistent results between replicates were all from markers obtained from RAGT Seeds, and hence were not designed specifically for detection of deletions.

			4D position (Mbp)																
Line	Sample	FL value	234.40	261.25	292.91	356.88	386.37	393.95	404.04	416.43	418.23	447.34	455.78	455.90	456.04	475.28	478.03	507.35	509.83
Chinese Spring	1	1.00																	
Chinese Spring	3	1.00																	
Chinese Spring	5	1.00																	
Del 4DL-14	3	0.86																	
Del 4DL-14	4	0.86																	
Del 4DL-14	5	0.86																	
Del 4DL-2	1	0.70																	
Del 4DL-2	2	0.70																	
Del 4DL-2	3	0.70																	
Del 4DL-11	1	0.61																	
Del 4DL-11	2	0.61																	
Del 4DL-11	5	0.61																	
Del 4DL-13	2	0.56																	
Del 4DL-13	3	0.56																	
Del 4DL-13	4	0.56																	
Del 4DL-1	1	0.46																	
Del 4DL-1	2	0.46																	
Del 4DL-1	4	0.46																	
Del 4DL-6	1	0.38																	
Del 4DL-6	2	0.38																	
Del 4DL-6	3	0.38																	
Del 4DL-5	2	0.09																	
Del 4DL-5	5	0.09																	
Del 4DL-5	5	0.09																	

Figure 2.9 Genotyping of Chinese Spring and seven 4DL terminal deletion lines using 24 KASP markers spanning the chromosome arm. The fraction length (FL) values, estimated by Endo and Gill (1996), provided for each line. A green box indicates a present signal and a red box indicates an absent signal at the marker position (Mbp).

Assessing Type I susceptibility of Chinese Spring 4DL terminal deletion lines

Euploid Chinese Spring and the seven 4DL terminal deletion lines were spray inoculated, to assess Type I FHB susceptibility, in a polytunnel trial conducted in summer 2018 (FHBsp_CSterm_Poly_18). Chinese Spring was resistant to infection, with only 1.95 % infected spikelets (**Figure 2.10**). The smallest 4DL terminal deletion, del4DL-14 was significantly more susceptible than Chinese Spring (mean= 7.44 %, $p< 0.001$) (**Figure 2.10**). Lines del4DL-2 (mean= 3.06 %, $p= 0.287$), del4DL-11 (mean= 3.22 %, $p= 0.194$) and del4DL-13 (mean= 2.87 %, $p= 0.331$) were not significantly different from Chinese Spring. Significantly increased susceptibility was observed in del4DL-1 compared to Chinese Spring (mean= 6.87 %, $p= 0.002$). Neither del4DL-6 (mean= 2.65 %, $p= 0.497$) nor del4DL-5 (mean= 1.92 %, $p= 0.971$) were significantly different from Chinese Spring (**Figure 2.10**).

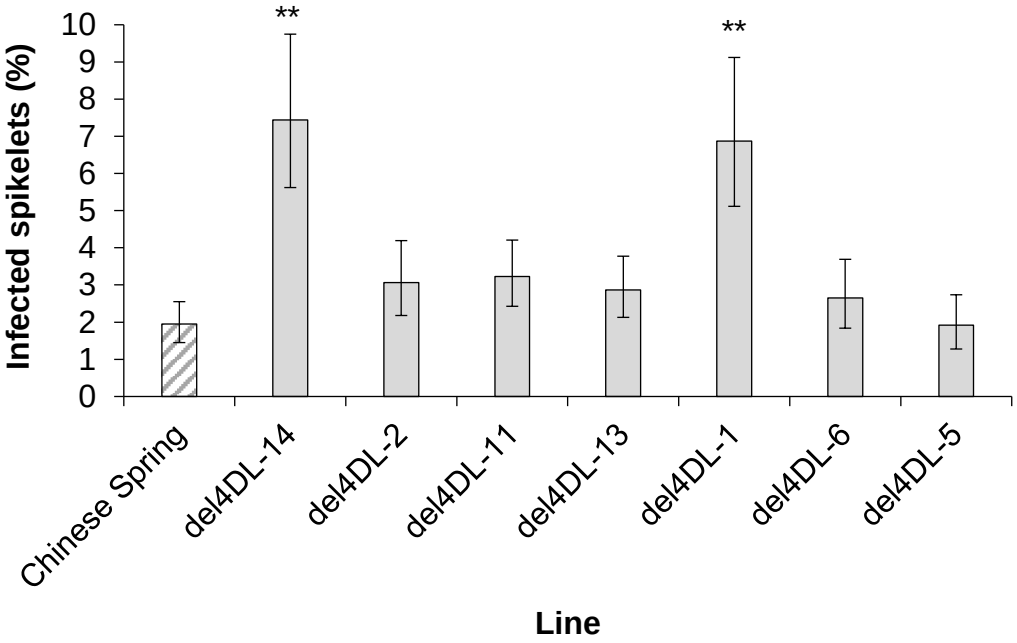

Figure 2.10 FHB disease above the inoculation point at 17 dpi, following spray inoculation of euploid Chinese Spring and seven 4DL terminal deletion bins; del4DL-14, del4DL-2, del4DL-11, del4DL-13, del4DL-1, del4DL-6 and del4DL-5. Predicted means were generated using a linear mixed model. Statistical analysis was performed on log10 transformed values. The predicted means and standard error bars presented have been back transformed. Error bars are ± standard error. ** p< 0.01 compared with Chinese Spring.

2.4 Discussion

2.4.1 Characterising the FHB susceptibility factor

Data arising from the Masters thesis of Giovannelli (2012) suggested that there is an FHB susceptibility factor on wheat chromosome 4D in the winter wheat variety Martonvasari 9. To confirm this, Steed and Nicholson (unpublished-a) point inoculated Chinese Spring ditelosomic lines, missing the long or short arm of chromosome 4D. In two independent experiments, it was demonstrated that the loss of 4DS results in high levels of Type II resistance. No such effect was observed following the loss of 4DL, which clearly demonstrates that the FHB susceptibility factor is present on the short arm of chromosome 4D. These data also confirm that the FHB susceptibility factor is present in a spring wheat genetic background and is not specific to Martonvasari 9. Ma *et al.* (2006) performed FHB point inoculation experiments on 30 Chinese Spring ditelosomic lines and also reported an increase in FHB resistance in the line missing 4DS.

To confirm these results, an FHB point inoculation experiment was performed on Chinese Spring 4D ditelosomic lines to assess Type II resistance of the lines. As expected, the line missing 4DS showed higher levels of Type II resistance compared to Chinese Spring and the Chinese Spring line lacking the long arm of 4D.

DON is known to act as a virulence factor in wheat, by promoting the spread of infection (Langevin *et al.*, 2004, Bai *et al.*, 2001). Hence, susceptibility to DON may be underlying the Type II susceptibility observed. To understand whether the susceptibility factor is causing increased susceptibility to DON, purified DON was applied to wheat heads of Chinese Spring and the 4D ditelosomic lines. Chinese Spring was relatively resistant to bleaching in response to DON and DT(4DS), missing 4DL, showed similar symptoms to the wild type. In contrast, DT(4DL), missing 4DS, was significantly more susceptible to bleaching following DON application. DON treated and untreated heads were harvested following the

experiment and the grain above and below the application point were removed, counted and weighed following the experiment. These data supported the DON bleaching data, with DT(4DL) showing a much greater reduction in grain weight in response to DON application, compared to Chinese Spring and DT(4DS). These data suggest that the susceptibility associated with 4DS is not promoted by DON. Were this the case, the line missing 4DS would possess enhanced resistance to DON bleaching, but increased susceptibility was observed in this experiment. Hence, these data suggest that there is an independent resistance factor to DON, which has been lost in DT(4DL), thereby increasing DON susceptibility in this line.

Due to the nature of the preceding work, which focussed on whether the potent Type II resistance in barley could be transferred to wheat, no experiments had been conducted to assess resistance to initial infection (Type I resistance). Spray inoculation is typically used to assess resistance to initial infection. To determine whether the susceptibility factor influenced initial infection, the 4D ditelosomic lines were spray inoculated with *Fusarium* conidia. Both Chinese Spring and the line missing 4DS showed very low levels of infection following spray inoculation. This confirms that the susceptibility factor does not have a Type I effect and is instead involved in promoting the spread of infection. On the other hand, the loss of 4DL resulted in significantly greater FHB susceptibility. Hence, a Type I resistance factor is likely to reside on the long arm of chromosome 4D in Chinese Spring.

The results of the point and spray inoculation experiments and the DON application experiments were sufficient to better characterise the FHB susceptibility factor. The FHB susceptibility factor is likely to be promoting the spread of the fungus and DON is not implicated. However, in confirming this, two additional resistance factors were identified on 4D: a resistance factor to DON on the short arm and a Type I resistance factor on the long arm.

2.4.2 Refining the physical position of the FHB susceptibility factor

Endo and Gill (1996) developed a set of terminal deletion lines in Chinese Spring. The lines have deletions from the ends of each chromosome arm, varying in size. These stocks are a valuable resource for physically mapping genes to a defined interval of a chromosome arm. The lines were originally characterised using C-banding and the deletion sizes were reported as a fraction length (FL) value; effectively the proportion of the chromosome arm estimated to have been retained (Endo and Gill, 1996). C-banding is unlikely to be capable of reliably detecting more complex deletions, such as interstitial deletions or chromosome substitutions. Since their development, the Chinese Spring terminal deletion stocks have not been more precisely characterised using more recent advances in genotyping. Four lines containing terminal deletions of 4DS were genotyped using a total of 37 novel homoeologue nonspecific markers spanning the chromosome arm. These markers take advantage of the hexaploid nature of wheat to create a robust genotyping assay for the detection of deletions on 4DS, and its homoeologous regions on 4BS and 4AL. Most gene homoeologues from 4DS and 4BS map to 4AL, as a result of a pericentric inversion of all but the extreme distal end of the ancestral 4AS (Hernandez *et al.*, 2012). A similar assay was used by Chia *et al.* (2017) to verify deletions across homoeologous regions, but this study expands on this technique, using a much higher density of markers to characterise deletion size. Homoeologous genes are simultaneously amplified with a single pair of primers but are distinguishable due to differences in the size of PCR products corresponding to the A, B and D genome copies. The signal from the retained homoeologues act as internal controls for detecting a deletion in any homoeologue; in the case of this study, the 4D copy.

This technique verified that all four Chinese Spring 4DS terminal deletion lines were indeed true terminal deletions. The most distal marker used, BH0001, maps to 4AS for the 4A homoeologue, indicating that the marker is targeting the small distal

portion of the ancestral 4AS that remains on the short arm. The size of the deletions were approximately consistent with the FL values calculated by Endo and Gill (1996). For the lines del4DS-2, del4DS-4 and del4DS-3, the physical positions of the deletion endpoints have been restricted to a small physical interval. For both del4DS-2 and del4DS-4, this interval is smaller than 1 Mbp. The interval containing the deletion endpoint in del4DS-3 has been refined to approximately 2.3 Mbp. The breakpoint in the largest deletion, del4DS-1, was less precisely characterised and the deletion breakpoint was isolated to a 29.8 Mbp interval. For the purposes of this study, it was not necessary to more precisely characterise the deletion in del4DS-1, because the FHB susceptibility factor appears to be situated between the deletion breakpoints of del4DS-4 and del4DS-3.

FHB disease experiments were performed on the four Chinese Spring 4DS terminal deletion lines that were genotyped. This clearly demonstrated that the lines with the two smaller deletions, del4DS-2 and del4DS-4, retained the susceptibility factor and showed a similar phenotype to euploid Chinese Spring. In contrast, the lines del4DS-3 and del4DS-1, containing the larger terminal deletions, showed significantly improved FHB resistance and hence the FHB susceptibility factor has presumably been lost. As the susceptibility factor was present in del4DS-4 but was lost in del4DS-3, the susceptibility factor must be situated between the deletion breakpoints of these two lines, thereby restricting the FHB susceptibility factor to a 31.7 Mbp interval containing 274 high confidence genes (IWGSC RefSeq v1.1). The deletion of 4D alone is sufficient to strongly improve FHB resistance. This suggests that the gene responsible may be 4D specific and does not possess homoeologues, or that the 4D copy is preferentially expressed. Alternatively, the 4D homoeologue may have diverged from the 4A and 4B copies and performs a different function. BLAST searches of each 4D gene in the interval identified 20 genes that are likely to be 4D-specific.

A population possessing smaller deletions across the FHB susceptibility interval is required to further refine the position of the susceptibility factor. In the next chapter, the utilisation of a gamma-irradiated population of the UK spring wheat variety Paragon (2019, Shaw *et al.*, 2013) is described in the effort to improve the resolution for the physical mapping of the FHB susceptibility factor.

It may be considered surprising that an FHB susceptibility factor with such a strong effect has not been detected before now. However, I hypothesise that the susceptibility factor is highly conserved among wheat cultivars. The FHB susceptibility factor exists both in the Hungarian winter wheat cultivar Martonvasari 9 and in the Asian variety Chinese Spring. If there were sufficient allelic variation at the locus, the effect of the FHB susceptibility factor is likely to have been detected as a QTL in biparental mapping populations. In the absence of such reports, it is probable that the FHB susceptibility factor is fixed in both spring and winter wheats and that utilising a deletion population is necessary to physically map the FHB susceptibility factor. Providing that any agronomic penalties, as a result of the eliminated FHB susceptibility factor, can be minimised, this provides an opportunity to immediately improve FHB resistance levels in any future hexaploid wheat variety. Furthermore, demonstrating how the elimination of an FHB susceptibility factor can be exploited in plant breeding may open up a new method for improving disease resistance. Once the gene has been identified, any potential pleiotropic effects of knocking out the FHB susceptibility factor will also need to be assessed.

Genetic resistance to fungal diseases is critical to the protection of food crops such as wheat. The search and incorporation of resistance factors is common practice in crop plant breeding. However, identifying novel sources of resistance to FHB is challenging and time consuming. FHB resistance is quantitative, highly polygenic, and often environmentally labile. Few large-effect FHB QTL have been identified. Attempts to clone the gene underlying the best-known source of FHB resistance, the

Fhb1 QTL, have been inconsistent and controversial (Su *et al.*, 2017, Steiner *et al.*, 2017, Rawat *et al.*, 2017, Ma *et al.*, 2017). Until recently, *Fhb1* was believed to encode, or regulate the expression of, a glucosyl transferase (Lemmens *et al.*, 2005). Rawat *et al.* (2016) reported that they had cloned a pore-forming toxin-like (*PFT*) gene underlying the *Fhb1* QTL. However, Jia *et al.* (2018) provided evidence that refuted the findings of Rawat *et al.* (2016). Su *et al.* (2018) identified that the presence of a deletion at the 5' end of a histidine-rich calcium-binding protein within the *Fhb1* locus was sufficient in identifying varieties carrying *Fhb1*. If this is indeed the case, it may be that the resistance conferred by *Fhb1* is, at least in part, caused by the loss of function of a susceptibility factor. The implications being that removal of a gene conferring susceptibility to FHB has the potential to provide an immediate increase in resistance.

Despite this, there has been relatively little research into susceptibility factors in wheat and other cereals, and how they may be exploited in plant breeding. The barley *mildew resistance locus o* (*Mlo*) is one of the earliest and best characterised examples of how disruption of a susceptibility factor could be exploited to improve disease resistance; in this case, to powdery mildew caused by the biotrophic fungus *Blumeria graminis* f. sp. *hordei* (Jorgensen, 1992). Induced and natural mutation of the *Mlo* locus result in a recessive, race nonspecific and durable resistance which has been widely deployed in European spring barley varieties (McGrann *et al.*, 2014, Lyngkjaer and Carver, 2000, Jorgensen, 1992). *Mlo*-based resistance has since been demonstrated in a number of other species affected by powdery mildew, reviewed by Kusch and Panstruga (2017). The deployment of *mlo* in wheat is more challenging due to its allohexaploid nature (Acevedo-Garcia *et al.*, 2017). However, TALENs and CRISPR Cas9 - derived gene knockouts (Wang *et al.*, 2014) and *Mlo* TILLING mutants (Acevedo-Garcia *et al.*, 2017) have been used to demonstrate that mutation of all wheat copies strongly enhances resistance to wheat powdery mildew.

R genes, usually nucleotide binding site-leucine rich repeat (NBS-LRR) genes, are typically used by plants to detect and respond to attack by biotrophic fungi. However, necrotrophic pathogens have evolved methods of exploiting such plant defences to aid infection. *Parastagonospora nodorum* and *Pyrenophora tritici-repentis* are necrotrophic pathogens of wheat that utilise this strategy. Susceptibility to these diseases operates in an inverse gene-for-gene interaction, in which a fungal necrotrophic effector is detected by a corresponding host sensitivity gene product (usually an NBS-LRR), triggering a hypersensitive response that results in necrosis that benefits the fungus (Faris *et al.*, 2010). If either necrotrophic effector or host sensitivity gene is absent, the interaction is impossible and host resistance is maintained. There have been few reports of how NBS-LRRs are involved in interactions with *Fusarium* spp. However, Zhang *et al.* (2019) found that the expression of an LRR gene was associated with increase susceptibility to *F. graminearum* in soybean (*Glycine max*).

Fusarium graminearum leads a hemibiotrophic lifestyle whereby the hyphal front remains surrounded by living tissue, but cell death is triggered soon after colonisation (Brown *et al.*, 2010). Phytohormones play important roles in defence and there is considerable evidence indicating that *F. graminearum* modifies phytohormone expression for its own benefit. Disruption of ethylene signalling in wheat (Chen *et al.*, 2009) and brassinosteroid signalling in barley and *Brachypodium distachyon* (Goddard *et al.*, 2014) results in enhanced resistance to FHB infection, suggesting that the fungus is exploiting phytohormone signalling in order to progress its infection. Expression of 9-lipogenases are also manipulated by *F. graminearum* in both bread wheat and *Arabidopsis thaliana*, which appear to be involved in balancing salicylic acid (SA) and jasmonic acid (JA) signalling (Nalam *et al.*, 2015). It is possible that the susceptibility factor on 4D is involved in the biosynthesis or signalling of a phytohormone.

Two known factors on the short arm of 4D may influence FHB susceptibility: *Reduced height-D1* (*Rht-D1*) and *Male Sterility 2* (*MS2*). *Rht-D1* is a DELLA protein present on 4DS. The mutant alleles *Rht-D1b* and homoeologous *Rht-B1b* (on chromosome 4B) result in reduced GA sensitivity, causing decreased stem elongation and hence reduced plant height. These semi-dwarfing alleles were widely deployed during the Green Revolution and resulted in greatly increased crop yields (Hedden, 2003). However, *Rht-D1b* and *Rht-B1b* have also been implicated in increased susceptibility to FHB (Buerstmayr and Buerstmayr, 2016, Saville *et al.*, 2012, Srinivasachary *et al.*, 2009). Both Chinese Spring and Paragon possess the wild type allele *Rht-D1a* (TraesCS4D02G040400) (Nicholson, personal communication) and *Rht-D1* is at 18.78 Mbp on chromosome 4D (EMBL-EBI, 2019).

The gene *MS2* is also present on 4DS and expression of the mutant *Ms2* is known to result in complete male sterility (Xia *et al.*, 2017, Ni *et al.*, 2017). Anthers are known to be important during infection by *Fusarium* spp. and male sterility is believed to result in increased FHB resistance. *Ms2* was found to co-segregate with the *Rht-D1c* dwarf allele, indicating that it is close, at least in genetic distance, to the *Rht-D1* locus (Ni *et al.*, 2017).

Both *Rht-D1* and *MS2* are distal to the FHB susceptibility interval being investigated in the present study. Hence, both will have been deleted in the smallest terminal deletion line (del4DS-2), which did not show altered FHB symptoms. Furthermore, no obvious signs of male sterility or altered plant height were observed in any of the Chinese Spring 4D ditelosomic or terminal deletion lines (data not shown). For these reasons, neither *Rht-D1* nor *MS2* are likely to be responsible for the altered FHB susceptibility observed in the lines containing deletions of 4DS.

2.4.3 Refining the physical position of the DON resistance factor

To refine the position of the DON resistance factor, which also appears to be present on the short arm of chromosome 4D, the four 4DS Chinese Spring terminal deletion

lines that were genotyped were used in DON application experiments. The smallest deletion, del4DS-2, showed a small but significant increase in DON susceptibility compared to euploid Chinese Spring. However, a greater increase in DON susceptibility was observed in the three larger deletion lines, del4DS-4, del4DS-3 and del4DS-1. These data suggest that, although there may also be a small effect DON resistance factor on the distal end of 4DS, a stronger differential was observed in the three larger terminal deletion lines. Hence, a DON resistance factor is likely to be present between the deletion breakpoints in del4DS-2 and del4DS-4, which would refine the DON resistance factor to a 4.2 Mbp interval, containing 49 genes.

Whilst the DON bleaching data suggests that the DON resistance factor is present in this small interval, the lines del4DS-2 and del4DS-4 showed similar grain weight reductions above the DON application point. These data alone would suggest the DON resistance factor is distal to the breakpoint of del4DS-2, between 50.6 and 51.6 Mbp, which contains 775 genes. It is possible that there is a DON resistance factor that affects grain filling on the distal end of 4DS and an additional DON resistance factor in the 4.2 Mbp interval that reduces visible bleaching in response to DON. The interval containing 49 genes is small enough to easily interrogate the interval for the DON resistance factor. Additionally, it must be noted that grain weight data were not collected immediately after harvesting heads from the DON application experiment. Grain data from the experiment were collected in autumn 2018, over a year after harvesting the grain. For these reasons, the 4.2 Mbp interval is the focus of experiments conducted in Chapter 4.

Glucosylation of DON to the less toxic DON-3-*O*-glucoside by UPD-glucosyltransferase (UGT) proteins is the best studied mechanism of host detoxification of DON. Previous studies have shown that barley is able to detoxify DON through glucosylation by the UDP-glucosyltransferase UGT13248 (Schweiger *et al.*, 2010). This gene has been transgenically expressed in Arabidopsis, where it

has been demonstrated to increase resistance to DON (Schweiger *et al.*, 2010). Furthermore, expression of UGT13248 in wheat, under the maize ubiquitin promoter, increased FHB resistance and transformants were demonstrated to more efficiently convert DON to the less toxic DON-3-*O*-glucoside (Li *et al.*, 2015). However, Xing *et al.* (2018) demonstrated that overexpression of a wheat UGT also increased FHB resistance and reduced the DON concentration in grain. How the barley UGT performs in transgenic wheat under its native barley promoter has not yet been demonstrated and hence the increase in resistance attributed to the barley UGT in wheat may be due to its overexpression.

Whilst glucosylation appears to be the primary means of detoxifying DON in plants, other forms of DON detoxification have been described in bacteria. The epimerisation of DON to 3-*epi*-DON by a two-step catalysis has been demonstrated (He *et al.*, 2017, Hassan *et al.*, 2017). In a strain of *Devosia mutans*, the oxidation of DON to 3-*keto*-DON by a dehydrogenase protein, followed by the conversion of 3-*keto*-DON to 3-*epi*-DON by an NADPH-dependent aldo-keto reductase (Carere *et al.*, 2018b, Carere *et al.*, 2018a). He *et al.* (2017) found an aldo-keto reductase in a strain of *Sphingomonas* sp. that is responsible for the first step, by converting DON to 3-keto-DON. Whilst such pathways have not been identified in plants, there may be more diverse means of DON detoxification possible, beyond glucosylation.

Of the 49 genes in the DON resistance interval, there are no glucosyltransferase genes. However, there are two aldo-keto reductase genes that warrant further study.

2.4.4 Refining the physical position of the Type I resistance factor

In characterising the FHB susceptibility factor on 4D, it was observed that the loss of the long arm of 4D resulted in significantly increased susceptibility to initial infection following spray inoculation, compared to Chinese Spring. Seven Chinese Spring terminal deletion lines of 4DL were obtained to study the effect further. The lines were genotyped using 24 KASP markers that can detect deletions across 4DL.

Whilst a lower density of markers was used compared to the characterisation of the 4DS terminal deletion lines, they were sufficient in distinguishing between most of the 4DL terminal deletion lines, in addition to obtaining a physical interval of the deletion breakpoint in most of the lines. The FL values in del4DL-11 and del4DL-13 (0.61 and 0.56, respectively) indicate they differ in size by about 5 % of the chromosome arm (approximately 16 Mbp). Hence, whilst C-banding is not an especially precise means of characterising deletion size, it is somewhat surprising that these two terminal deletions cannot be distinguished at the current marker density. The deletion breakpoints of both del4DL-11 and del4DL-13 are present within a 10.1 Mbp interval. The line 4DL-1 (FL=0.46) was deleted accorded to the loss of signal from all markers, except BH_4D227100, which targets TraesCS4D02G227100 at 386.4 Mbp. Hence, the deletion appears to be significantly larger than estimated by Endo and Gill (1996). At the resolution of the markers used, it appears that only a small interstitial segment of 4DL is retained. Presumably there has been substitution in del4DL-1 on 4DL from another chromosome, which would explain why the FL value may be proportionally greater, relative to the size estimated using DNA markers in this line. Further analysis is necessary to establish the origin of the DNA responsible for the 0.46 region of long arm in this line.

The results of the FHB spray inoculation of the 4DL terminal deletion lines were somewhat inconsistent across the lines. The line containing the smallest deletion, del4DL-14, was significantly more susceptible than Chinese Spring. In isolation, this would suggest there is a Type I resistance factor on the distal end of 4DL, that has been lost in the del4DL-14. The lines del4DL-2, del4DL-11 and del4DL-13 showed similar disease levels compared to Chinese Spring that were not statistically significant in any line. The line missing almost all of 4DL, del4DL-1, was significantly more susceptible compared to Chinese Spring. However, del4DL-6 and del4DL-5 were not significantly different to Chinese Spring.

These data provide some support for a possible Type I resistance factor on the long arm of 4D in Chinese Spring, although the effect is inconsistent and appears to be of relatively small effect. The weak effect, combined with relatively high disease variation, may explain why a statistically significant difference was not detected across all lines. The smallest 4DL deletion line was significantly more susceptible and hence the Type I FHB resistance factor may be distal to 487.0 Mbp. However, the results of this experiment were undoubtedly inconsistent and hence no reliable conclusions can be drawn. It is necessary to repeat the experiment to do so.

Whilst many FHB QTL have been reported in wheat, studies have generally focussed on resistance limiting the spread of infection through the rachis. Few QTL with a Type I effect have been described. Whilst breeding for Type II resistance is likely to protect the crop from severe FHB disease, this protection typically breaks down under high disease pressure, in which many initial infection events may occur within individual wheat heads. Barley possesses strong Type II resistance that prevents the spread of infection through the rachis (Langevin *et al.*, 2004). However, during the FHB epidemics across the Northern Great Plains of North America during the 1990s, significant economic losses were suffered in barley as well as wheat (McMullen *et al.*, 1997). Hence, a combination of Type I and Type II resistance is critical to achieve robust FHB resistance. This can be further supplemented by an understanding of susceptibility factors, such as that identified on 4DS in the present study, and the generation of novel deletions for these factors that can be utilised by plant breeders to combine with FHB resistances.

A resistance factor on 5A, originating from Sumai 3, was demonstrated to contribute to Type I resistance (Buerstmayr *et al.*, 2003). Further study found the 5A resistance is due to two closely linked QTL that both contribute to Type I resistance (Steiner *et al.*, 2019). Both QTL are associated with increased anther extrusion (Steiner *et al.*, 2019). Chromosome 4A of *Triticum macha* contains a Type I resistance factor that

was introgressed to hexaploid wheat variety Hobbit Sib (Steed *et al.*, 2005). Lin *et al.* (2006) identified a Type I resistance factor derived from the variety Wangshuibai on chromosome 4B. In neither instance was any possible relationship between FHB susceptibility and anther extrusion examined.

2.4.5 Concluding remarks

Convincing evidence has been found for an FHB susceptibility factor present on the short arm of chromosome 4D. The effect has been refined to a 31.7 Mbp interval, using terminal deletion lines of 4DS. In order to refine the location, in Chapter 3, a deletion mapping approach is utilised, using a gamma-irradiated population of Paragon, to physically map the FHB susceptibility factor. In Chapter 4, similar methods are used to attempt to fine map the DON resistance factor, which is also present on the short arm of 4D in Chinese Spring. It is intended that these approaches will provide deletion lines that can be utilised by plant breeders to provide novel sources of genetic control of FHB.

Chapter 3: Deletion mapping of a Fusarium head blight susceptibility factor on chromosome 4D in wheat

3.1 Introduction

A gamma-irradiated population of the UK spring wheat variety, Paragon, has been developed at the John Innes Centre. The gamma-irradiation treatment has resulted in deletions within chromosomes (Wheat Genetic Improvement Network, 2019, Shaw *et al.*, 2013). However, other genetic aberrations, such as duplications and inversions, are also likely to be present in the population (Puchta, 2005). Gamma irradiation-induced deletions provide an opportunity to knock-out entire gene clusters or to effectively convert intervals containing a deletion to a tetraploid state. Screening for lines containing deletions across an interval of interest, followed by phenotyping for a particular trait, can be an effective way of refining the physical interval and reducing the list of gene candidates associated with the trait. Screening of a deletion population, followed by TILLING for candidate genes, provides a very powerful combination of techniques to identify the genes responsible for particular traits. Paragon is very closely related to Cadenza with both varieties having the same pedigree; Axona x Tonic (Dobrotvorskaya *et al.*, 2017a, Dobrotvorskaya *et al.*, 2017b). Cadenza is the variety used to produce the large hexaploid wheat TILLING population for which it is possible to screen for variants *in silico* using the Ensembl Plants database (EMBL-EBI, 2019, Uauy *et al.*, 2009). Hence, refining an interval using the Paragon population can be directly used to substantially reduce the number of candidate genes that need to be phenotyped using the TILLING population.

In this chapter, the gamma-irradiated Paragon population was screened for deletions across the FHB susceptibility interval on the short arm of chromosome 4D. Point

inoculation of identified lines confirmed whether any of them show any increase in FHB resistance that would indicate a deletion of the susceptibility factor.

3.2 Materials and Methods

3.2.1 Plant material and population development

A gamma irradiated population in the UK spring wheat variety Paragon, previously generated by Shaw *et al.* (2013), was used for this work. A single seed each of 886 lines, at the M4 generation, were bulked in summer 2016 to obtain sufficient seed for future work (M4B1). An additional 974 lines, at the M3 generation, were progressed to M4 by single seed descent in summer 2016. The newly generated M4 lines were subsequently bulked in summer 2017 using a single seed per line (M4B2). During the M4 bulking step of both M4B1 and M4B2, leaf material was taken from all germinated lines to enable DNA extraction for genotyping. Following development of the population, a total of 1860 gamma-irradiated lines at the M4 generation were produced (i.e. M4B1 and M4B2 combined).

3.2.2 Marker design and genotyping

Five homoeologue nonspecific markers spanning the 31.7 Mbp FHB susceptibility factor were used to screen for deletions on 4D, and homoeologous regions of 4A and 4B, in the M4B2 lines of the gamma-irradiated Paragon population. The markers used were BH0027.2, BH0009.3, BH0010.2, BH0017, BH0018 (**Table 3.1**). Ten additional homoeologue nonspecific markers were designed to refine the positions of deletion breakpoints in selected gamma-irradiated Paragon lines (**Table 3.1**)

The design and use of homoeologue nonspecific markers are described in detail in Chapter 2 (p. 34). To briefly describe marker design: sequences from homoeologous genes on 4A, 4B and 4D were obtained from Ensembl Plants (EMBL-EBI, 2019) and aligned using multiple sequence comparison by log-expectation (MUSCLE; EMBL-EBI). Identical sequences between the three homoeologues were used for primer design. Insertions and deletions (indels) between forward and reverse primers, with specificity between each homoeologue, were used to enable distinction of PCR

fragments corresponding to each homoeologue by size. An M13 sequence (TGTAAAACGACGGCCAGT) was added to the 5' end of the forward primer.

For PCR reactions using homoeologue nonspecific markers, HotStarTaq Mastermix (Qiagen) was used and prepared following manufacturer's instructions and were amplified using the following steps: 95°C 15 min; 35 cycles of: 95°C 1 min, 58°C 1 min, 72°C 1 min; 72°C 10 min. The five markers used were multiplexed for improved efficiency following PCR. PCR products were separated using an ABI 3730xl DNA analyser (Applied Biosystems) and resolved using Peak Scanner software (v2.0, Applied Biosystems).

Kompetitive Allele Specific PCR (KASP) markers were designed and utilised to detect deletions across 4DS, in the same way as described in Chapter 2 (p. 34-5). A total of 23 markers were designed within genes between 50.76 Mbp and 62.73 Mbp on 4D (**Table 3.2** and **Table 3.3**: KASP marker tables are separated based on the fluorophore attached to the 4D/ 4B homoeologue).

KASP markers were used to genotype all 1860 lines of the gamma-irradiated population, as described in Chapter 2 (p. 34-5).

Table 3.1 Homoeologue nonspecific markers used in genotyping the gamma-irradiated Paragon population. The gene targets on 4DS and their corresponding physical positions (bp) are provided for each marker.

Marker	Primer sequence	4D gene	Physical position (bp)
BH0027.2.For	tgtaaaacgacggccagtGGTAACATTCCTTTGGTATACTCGG	TraesCS4D02G078900	52,775,746-52,779,088
BH0027.2.Rev	TGTGCTAAGATCTACAACATC		
BH0009.3.For	tgtaaaacgacggccagtTAGAGGGAGCAGGGATGACAT	TraesCS4D02G087200	62,479,751-62,483,165
BH0009.3.Rev	TCTCCGTCTGGTTCATTCGT		
BH0059.1.For	tgtaaaacgacggccagtTGCCGCTTAGCACAAACGA	TraesCS4D02G088200	63,251,469-63,257,122
BH0059.1.Rev	ATATGCCTCTGCCTAGTGGCTG		
BH0060.1.For	tgtaaaacgacggccagtGTATATGCTGGTTTCCCCAAGAGC	TraesCS4D02G090400	65,531,283-65,539,548
BH0060.1.Rev	AGGCCCATACCAAACAAACAGG		
BH0061.1.For	tgtaaaacgacggccagtCATGTCTGAGATGATTAGACCAGAG	TraesCS4D02G091400	66,315,527-66,322,939
BH0061.1.Rev	CCTCACCTTAACCTGCCATGAT		
BH0062.For	tgtaaaacgacggccagtGTTCTCGTCATATCAGCCTGGA	TraesCS4D02G094500	69,846,691-69,850,833
BH0062.Rev	CCTCGTAGCCTCTCCCACAC		
BH0064.For	tgtaaaacgacggccagtCTCAGCAAGATGCACTTGTTGG	TraesCS4D02G096600	73,219,301-73,224,757
BH0064.Rev	GCCATAACAAAGGTCACAACTGAG		
BH0010.2.For	tgtaaaacgacggccagtACGTGGTCTTCAAATCTGGC	TraesCS4D02G098400	75,228,376-75,232,368
BH0010.2.Rev	CTGCAATATAAGGTGGCAAATC		

Table 3.1 (continued) Homoeologue nonspecific markers used in genotyping the gamma-irradiated Paragon population. The gene targets on 4DS and their corresponding physical positions (bp) are provided for each marker.

Marker	Primer sequence	4D gene	Physical position (bp)
BH0065.For	tgtaaaacgacggccagtCCAAAGTCTACTGGTTCATCTGC	TraesCS4D02G099100	76,017,896-76,019,693
BH0065.Rev	CAATGCCATGCAAGATCAGTC		
BH0066.For	tgtaaaacgacggccagtCTGGTTAGGTGGGCTTGAGTG	TraesCS4D02G101500	79,211,788-79,222,841
BH0066.Rev	GAGACCATCTGGATGATTGTCG		
BH0068.For	tgtaaaacgacggccagtAGTGTCGAGGCCGTAGCA	TraesCS4D02G102600	81,664,710-81,666,516
BH0068.Rev	GCAGCTTGGATTCTACCACAT		
BH0067.For	tgtaaaacgacggccagtTCGAACTCTGCGTATCCGTG	TraesCS4D02G104100	82,723,737-82,730,645
BH0067.Rev	CACCAAATCGGATCGAGACA		
BH0017.For	tgtaaaacgacggccagtCAGATTGTACGAACATCTTCTGC	TraesCS4D02G105100	83,275,376-83,280,800
BH0017.Rev	AGCAGAACAAAATCTCATGG		
BH0069.For	tgtaaaacgacggccagtGTACCGCTTACTCAATCACTTGC	TraesCS4D02G105300	83,852,778-83,873,785
BH0069.Rev	GCTGTTCTACTTGAACCTCTCCTTG		
BH0018.For	tgtaaaacgacggccagtGTGAGCAGAGCACCCTCC	TraesCS4D02G107300	85,587,783-85,593,810
BH0018.Rev	CTGCACCACCACAGAAAAGA		

Table 3.2 Primer sequences for the KASP markers designed to detect deletions on the short arm of chromosome 4D, including the genes targeted on 4D and their corresponding physical positions (bp). In all cases, the HEX tail was attached to the primer corresponding to the 4D homoeologue and the FAM tail to the 4B homoeologue.

Marker	Sequence (HEX 4D, FAM 4B, Common)	4D gene	Physical position (bp)
BH_4D078800	GAAGGTCGGAGTCAACGGATTGCAAGAAGACGAAAAGACTCGA GAAGGTGACCAAGTTCATGCTGCAAGAAGACGAAAAGACTCGT TCACGGTTTCTTTGATGTTCA	TraesCS4D02G078800	52,763,212-52,765,266
BH_4D081100	GAAGGTCGGAGTCAACGGATTGCACTAAATCGCCTTAAAACTGTA GAAGGTGACCAAGTTCATGCTGCACTAAATCGCCTTAAAACTGTC GATCAACCCAAGAAGCAAGTGT	TraesCS4D02G081100	55,046,522-55,052,757
BH_4D082100	GAAGGTCGGAGTCAACGGATTCAAGAGATGACAAGTGCACATTC GAAGGTGACCAAGTTCATGCTCAAGAGATGACAAGTGCACATTT CTTGGCATAATAGGAGGCTATG	TraesCS4D02G082100	55,559,928-55,564,146
BH_4D082800	GAAGGTCGGAGTCAACGGATTTATCAACCTTATCAGCACTACCT GAAGGTGACCAAGTTCATGCTTATCAACCTTATCAGCACTACCA GCAAAGTAGTTGCTACCCC	TraesCS4D02G082800	56,716,994-56,723,032
BH_4D084000	GAAGGTCGGAGTCAACGGATTCACATTCGTCAATGGCGAGTTT GAAGGTGACCAAGTTCATGCTCACATTCGTCAATGGCGAGTTC AACAAGGGTGTGCGTGTACTCA	TraesCS4D02G084000	57,835,189-57,838,699
BH_4D084700	GAAGGTCGGAGTCAACGGATTGTTTCCTTTGCCCCTACTCG GAAGGTGACCAAGTTCATGCTGTTTCCTTTGCCCCTACTCT ATGGGCTCTGAAGTGCATT	TraesCS4D02G084700	58,276,390-58,280,000

Table 3.2 (continued) Primer sequences for the KASP markers designed to detect deletions on the short arm of chromosome 4D, including the genes targeted on 4D and their corresponding physical positions (bp). In all cases, the HEX tail was attached to the primer corresponding to the 4D homoeologue and the FAM tail to the 4B homoeologue.

Marker	Sequence (HEX 4D, FAM 4B, Common)	4D gene	Physical position (bp)
BH_4D085100	GAAGGTCGGAGTCAACGGATTATCCGGCGGTGAGAAAGGC GAAGGTGACCAAGTTCATGCTATCCGGCGGTGAGAAAGGT CGGGAACTACATCAATGGCGT	TraesCS4D02G085100	59,622,464-59,625,174
BH_4D085400	GAAGGTCGGAGTCAACGGATTGCACGGTTAACCCACACTTAG GAAGGTGACCAAGTTCATGCTGCACGGTTAACCCACACTTAA TATGACCCTGCTTCTCCTGGGA	TraesCS4D02G085400	60,133,190-60,134,377
BH_4D085700	GAAGGTCGGAGTCAACGGATTGGTGTAATGGAAGAACTTGCC GAAGGTGACCAAGTTCATGCTGGTGTAATGGAAGAACTTGCA CCATCCATACCAACAGTAGTTGTG	TraesCS4D02G085700	60,876,765-60,881,228
BH_4D086000	GAAGGTCGGAGTCAACGGATTCTGGGGCTATTCTCTCCCTTAC GAAGGTGACCAAGTTCATGCTCTGGGGCTATTCTCTCCCTTAT GGTACAATCACTTAGTAATGCCATC	TraesCS4D02G086000	61,585,793-61,593,158
BH_4D086700	GAAGGTCGGAGTCAACGGATTCTTGATGGGTGACGAGGACA GAAGGTGACCAAGTTCATGCTCTTGATGGGTGACGAGGACC GGCGGGGAAAATCTAACAAACG	TraesCS4D02G086700	62,096,216-62,097,196
BH_4D087100	GAAGGTCGGAGTCAACGGATTAATTGCCAGCGTTGAAACTCG GAAGGTGACCAAGTTCATGCTAATTGCCAGCGTTGAAACTCA CTGTAGTGCAGGAAGTATTGGAAG	TraesCS4D02G087100	62,458,860-62,469,401

Table 3.3 Primer sequences for the KASP markers designed to detect deletions on the short arm of chromosome 4D, including the genes targeted on 4D and their corresponding physical positions (bp). In all cases, the FAM tail was attached to the primer corresponding to the 4D homoeologue and the HEX tail to the 4B homoeologue.

Marker	Sequence (FAM 4D/ HEX 4B/ Common)	4D gene	Physical position (bp)
BH_4D078200	GAAGGTGACCAAGTTCATGCTGACCGCCCTTTCACAGCA GAAGGTCGGAGTCAACGGATTGACCGCCCTTTCACAGCT ACTGATCCATGGTGGTTGCTC	TraesCS4D02G078200	52,492,099-52,496,665
BH_4D078600	GAAGGTGACCAAGTTCATGCTCATTCAGTGCTGCAATGGAGC GAAGGTCGGAGTCAACGGATTCATTCAGTGCTGCAATGGAGT CGTCAGTGTATATCATTGTTCTGG	TraesCS4D02G078600	52,751,281-52,754,472
BH_4D079900	GAAGGTGACCAAGTTCATGCTTGGAAGGAGGTGTTCGACA GAAGGTCGGAGTCAACGGATTTGGAAGGAGGTGTTCGACC CAGGTCCTCGGGCCACTT	TraesCS4D02G079900	53,862,557-53,864,923
BH_4D080200	GAAGGTGACCAAGTTCATGCTGAAGCCATCCAACTCGAAGCC GAAGGTCGGAGTCAACGGATTGAAGCCATCCAACTCGAAGCA ACCAGGATGTAATGCCCTTTC	TraesCS4D02G080200	54,261,815-54,266,356
BH_4D084600	GAAGGTGACCAAGTTCATGCTCCAAATACTGCAAAGAGGCATC GAAGGTCGGAGTCAACGGATTCCAAATACTGCAAAGAGGCATA CGAAGTAGTTCGGTATGACAAC	TraesCS4D02G084600	58,269,253-58,270,644
BH_4D087200	GAAGGTGACCAAGTTCATGCTGGACTAACAAATCAAAGCTGAC GAAGGTCGGAGTCAACGGATTGGACTAACAAATCAAAGCTGAT GCTCTCTACAGTTCACCATCC	TraesCS4D02G087200	62,479,799-62,483,162
BH_4D087400	GAAGGTGACCAAGTTCATGCTTGTACTCCCGTCGTTTGGTC GAAGGTCGGAGTCAACGGATTTGTACTCCCGTCGTTTGGTT AAGTGTGTCTATGCGTCTTCCA	TraesCS4D02G087400	62,727,949-62,734,054

3.2.3 Fungal point inoculation of wheat heads

Conidial point inoculation experiments on gamma-irradiated Paragon lines were conducted in a polytunnel or controlled environment room (CER) in 2018 and 2019 (**Table 3.4**). Polytunnel FHB point inoculation experiments were organised in a randomised complete block design, with four replicates containing four or five plants per line. FHB experiments conducted under controlled conditions were organised in a randomised complete block design, with three replicates containing five or six plants per line. The CER was set to 18 h days at 20 ºC/ 18 ºC day/ night temperature and 70 % relative humidity. Point inoculation was conducted as described in Chapter 2 (p.39).

3.2.4 FHB disease experiment data analysis

FHB point inoculation data were analysed using a linear mixed model (REML), accounting for line as a fixed effect and replicate as a random effect. During model construction, application date and the interaction between application date and line were tested as fixed terms and plant number nested within replicate was tested as a random term. However, these terms were not significant and, for this reason, the terms were removed from the model for clarity. In all cases, the final model included line as a fixed term and replicate as a random term. Residuals were visually checked for normality and equal variance between lines. With the exception of data from experiment FHBpt_PG_Poly_18, data were log10 transformed prior to statistical analysis, which achieved normality of the residuals and made the residuals typically independent of the fitted values. Predicted means and standard errors were generated for lines included in the linear mixed model. Predicted values that were generated from transformed data were back transformed for presentation. Pairwise differences between wild type Paragon and deletion lines were tested by Fisher's Protected Least Significant Difference. All statistical analyses were carried out using GenStat (18th edition, VSN International). ANOVA tables of statistical analyses are presented in the appendix (p. 195-7).

Table 3.4 FHB point inoculation experiments conducted as part of Chapter 3. Each experiment has been assigned a unique code. Figures relating to each experiment are provided, in addition to brief descriptions of each experiment.

Experiment code	Figure	Description
FHBpt_PG_CER_18	2	Conidial point inoculation of Paragon T20 L65
FHBpt_PG_Poly_18	3	Conidial point inoculation of Paragon 4DS deletions identified from initial marker screen
FHBpt_PGkasp_CER_19	8	Conidial point inoculation of Paragon 4DS deletions identified from focussed KASP marker screen
FHBpt_PGskim_CER_19	13B	Conidial point inoculation of Paragon 4DS deletions identified from skim sequencing data
FHBpt_PGhom_Poly_19	14	Conidial point inoculation of Paragon 4A and 4B deletions homoeologous to 4D susceptibility factor interval

3.3 Results

3.3.1 Initial screen of gamma-irradiated Paragon population

M4B2, consisting of 974 lines of the gamma-irradiated Paragon population, was genotyped using five homoeologue nonspecific markers, spanning the 31.7 Mbp susceptibility interval on 4D. Six lines were identified that contained homozygous deletions on 4D: T17 L65, T19 L19, T15 L49, T17 L20, T13 L38 and T20 L65 (**Figure 3.1**). T17 L65 and T19 L19 showed the same deletion pattern, with a single marker, BH0027.2 at 52.78 Mbp, missing the signal from the 4D copy, indicating a deletion on 4D in both lines. The deletions in T17 L65 and T19 L19 end before BH0009.3, which targets the gene TraesCS4D02G087200 at 62.48 Mbp. T15 L49 was missing a 4D signal at three markers BH0027.2, BH0009.3 and BH0010.2, targeting the physical positions 52.78 Mbp, 62.48 Mbp and 75.23 Mbp, respectively. The 4D signal was retrieved at 83.3 Mbp, indicating that the deletion extends no further than this position. T17 L20 and T13 L38 lost the 4D signal at a single marker: BH0010.2 (TraesCS4D02G098400 at 75.23 Mbp) and BH0017 (TraesCS4D02G105100 at 83.28 Mbp), respectively. T20 L65 showed no signal on 4D for any of the five markers, indicating that it contains a deletion spanning the entire FHB susceptibility interval.

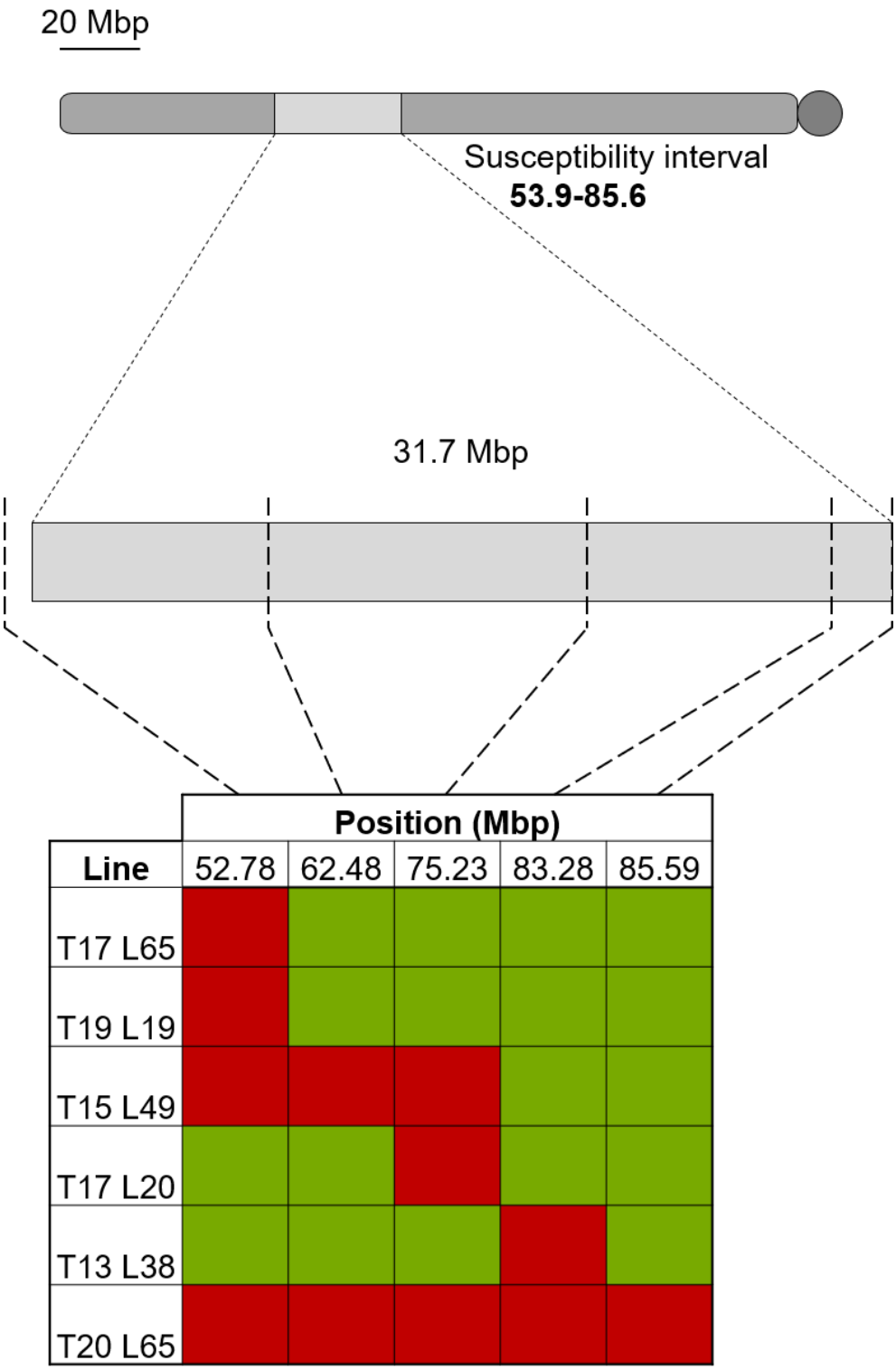

Figure 3.1 Five markers, spanning the 31.7 Mbp FHB susceptibility factor interval on 4DS, were used to screen for deletions in a gamma-irradiated Paragon population. Six lines were identified with homozygous 4D deletions across the interval. Red boxes indicate a missing signal of the 4D copy, indicating a deletion. Green boxes indicate the 4D homoeologue is present at the corresponding marker. The physical distance between markers, based on gene locations on the IWGSC Refseq v1.1 sequence is indicated above the genotyping diagram. The inferred interval containing the susceptibility factor is indicated by the grey bar.

3.3.2 The FHB susceptibility factor is present in a Paragon genetic background

To confirm that the FHB susceptibility factor is present in a Paragon genetic background, wild type Paragon and T20 L65 were point inoculated in a controlled environment chamber (FHBpt_PG_CER_18). The seed of T20 L65 was taken from the M4B2 stock. The plants were genotyped using the five homoeologue nonspecific markers, to confirm the state of the 4D deletion. From the seed used in this experiment, T20 L65 was found to be segregating for the 4D deletion. Of a total of 22 seeds, eight of the resulting T20 L65 plants possessed a homozygous 4D deletion and seven plants contained the deletion in a hemizygous state. The additional seven seed either did not contain the 4D deletion or did not germinate. T20 L65 plants, containing the 4D deletion in a homozygous or hemizygous state, were included in the point inoculation experiment. Paragon was susceptible to the spread of infection (mean= 2.87) (**Figure 3.2**). T20 L65, possessing the 4D deletion in a homozygous state, was highly resistant to the spread of infection (mean= 0.11, $p< 0.001$), compared with wild type Paragon (**Figure 3.2**). T20 L65 containing a hemizygous 4D deletion showed intermediate levels of FHB resistance but were still significantly more resistant compared to Paragon (mean= 1.08, $p= 0.003$) (**Figure 3.2**).

The effect of dosage of the 4D deletion on FHB susceptibility demonstrates that the enhanced resistance is associated with the 4D deletion in T20 L65 and confirms that the FHB susceptibility factor is present in Paragon.

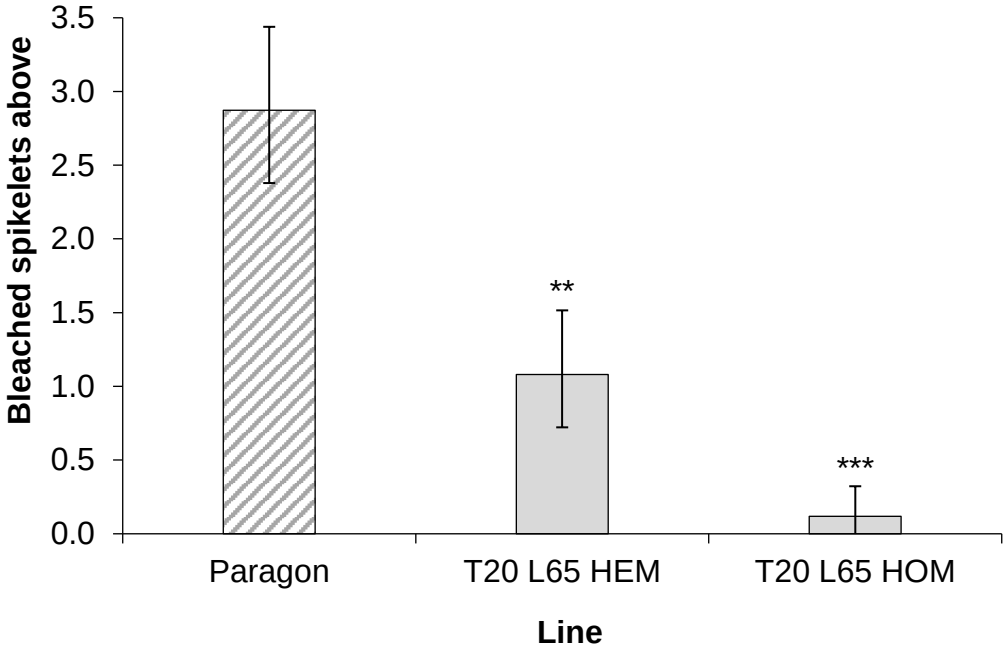

Figure 3.2 FHB point inoculation experiment of wild type Paragon, and a gamma-irradiated deletion line, T20 L65. T20 L65 possesses a deletion across the entire FHB susceptibility interval, in a hemizygous (HEM) or homozygous (HOM) state. Infection scores presented for each line above the point of inoculation, scored at 17 dpi. Experiment was performed under controlled conditions. Statistical analysis was performed using log10 transformed values. Predicted means were generated using a linear mixed model. Error bars are ± standard error. ** p< 0.01; *** p< 0.001 compared with Paragon.

3.3.3 Selected 4D deletion lines across the susceptibility interval show altered FHB susceptibility

The lines identified in the marker screen (**Figure 3.1**) were bulked in a heated glasshouse. DNA was extracted from leaf material taken from the plants of each line being bulked and the five homoeologue nonspecific markers were used to confirm that the bulked plants possessed homozygous deletions on 4D. Bagged seed obtained from parent plants possessing homozygous deletions were used in a point inoculation experiment conducted in a polytunnel in summer 2018 (FHBpt_PG_Poly_18).

FHB infection in wild type Paragon spread above the point of inoculation (mean= 4.33) (**Figure 3.3**). The spread of disease above inoculation in T19 L19 (mean= 5.03, p= 0.056), T17 L20 (mean= 4.27, p= 0.888) and T13 L38 (mean= 3.79, p=0.205) were not significantly different to Paragon (**Figure 3.3**). T15 L49 was significantly more susceptible to FHB spread compared to Paragon (mean= 5.84, p< 0.001) (**Figure 3.3**). In contrast, T17 L65 was significantly more resistant than Paragon (mean= 0.82, p< 0.001) (**Figure 3.3**). Consistent with the previous experiment, T20 L65 was also significantly more resistant than Paragon to the spread of infection above the inoculation point (mean= 1.58, p< 0.001) (**Figure 3.3**). Representative photographs of Paragon, and lines T19 L19 (Paragon-like), T17 L65 (resistant) and T20 L65 (resistant) were taken at 18 dpi and are provided in **Figure 3.4**.

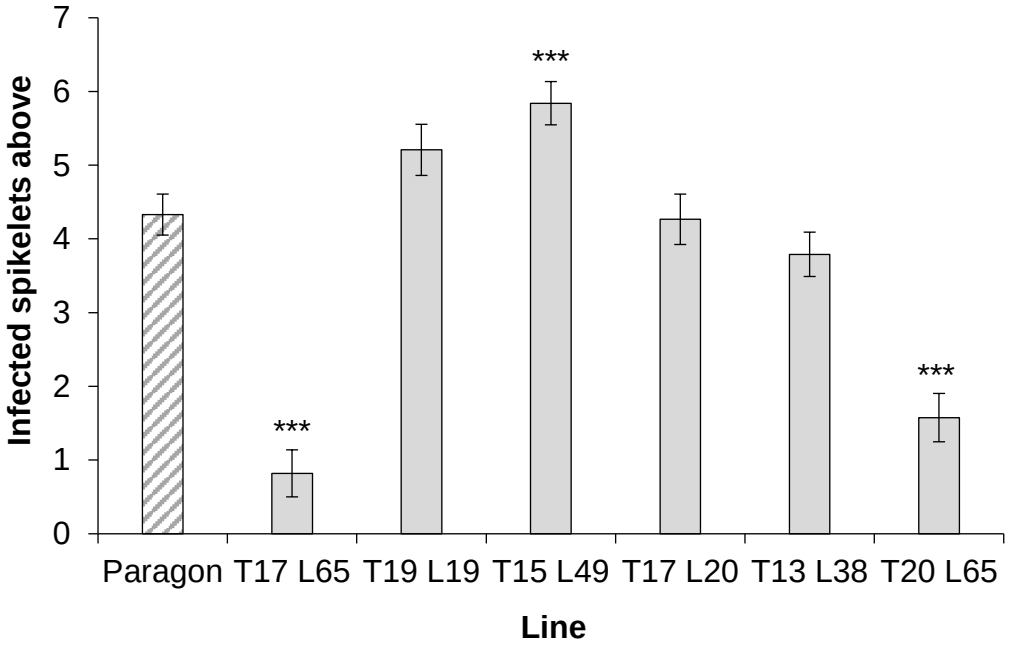

Figure 3.3 FHB point inoculation polytunnel experiment of wild type Paragon and six gamma-irradiated Paragon lines, possessing homozygous deletions across the FHB susceptibility interval on 4D. Disease scores presented are scores above the inoculation point at 14 dpi. Predicted means were generated using a linear mixed model. Error bars are ± standard error. *** $p < 0.001$ compared to Paragon.

Figure 3.4 Representative photographs of wild type Paragon and three gamma-irradiated Paragon lines that have been point inoculated centrally on the spikelet: T17 L65, T19 L19 and T20 L65. Paragon and T19 L19 show a similar susceptible phenotype. Lines T17 L65 and T20 L65 both show very limited signs of disease spread. Photographs were taken at 18 dpi.

3.3.4 Improved marker saturation can distinguish deletions in T17 L65 and T19 L19

The gamma-irradiated deletion lines, T17 L65 and T19 L19, possessed the same 4D deletion profile in the initial screen of the Paragon M4B2. However, T17 L65 was highly resistant to FHB, whilst T19 L19 was not significantly different from wild type Paragon.

Nineteen KASP markers were designed across the distal flank of the susceptibility interval and were used to genotype wild type Paragon, T17 L65, T19 L19 and T20 L65 (**Figure 3.6**). Example outputs of this KASP assay are displayed in **Figure 3.5**. Paragon showed a wild type-like signal across all markers. T20 L65 showed a signal indicating a 4D deletion across all markers. The distal end of the deletion in T17 L65 extends beyond the region to which the markers were designed. The proximal deletion breakpoint of T17 L65 ends between 62.46 Mbp and 62.48 Mbp. The distal deletion breakpoint in T19 L19 is between 52.49 Mbp and 52.75 Mbp and the proximal breakpoint is between 55.56 Mbp and 56.72 Mbp.

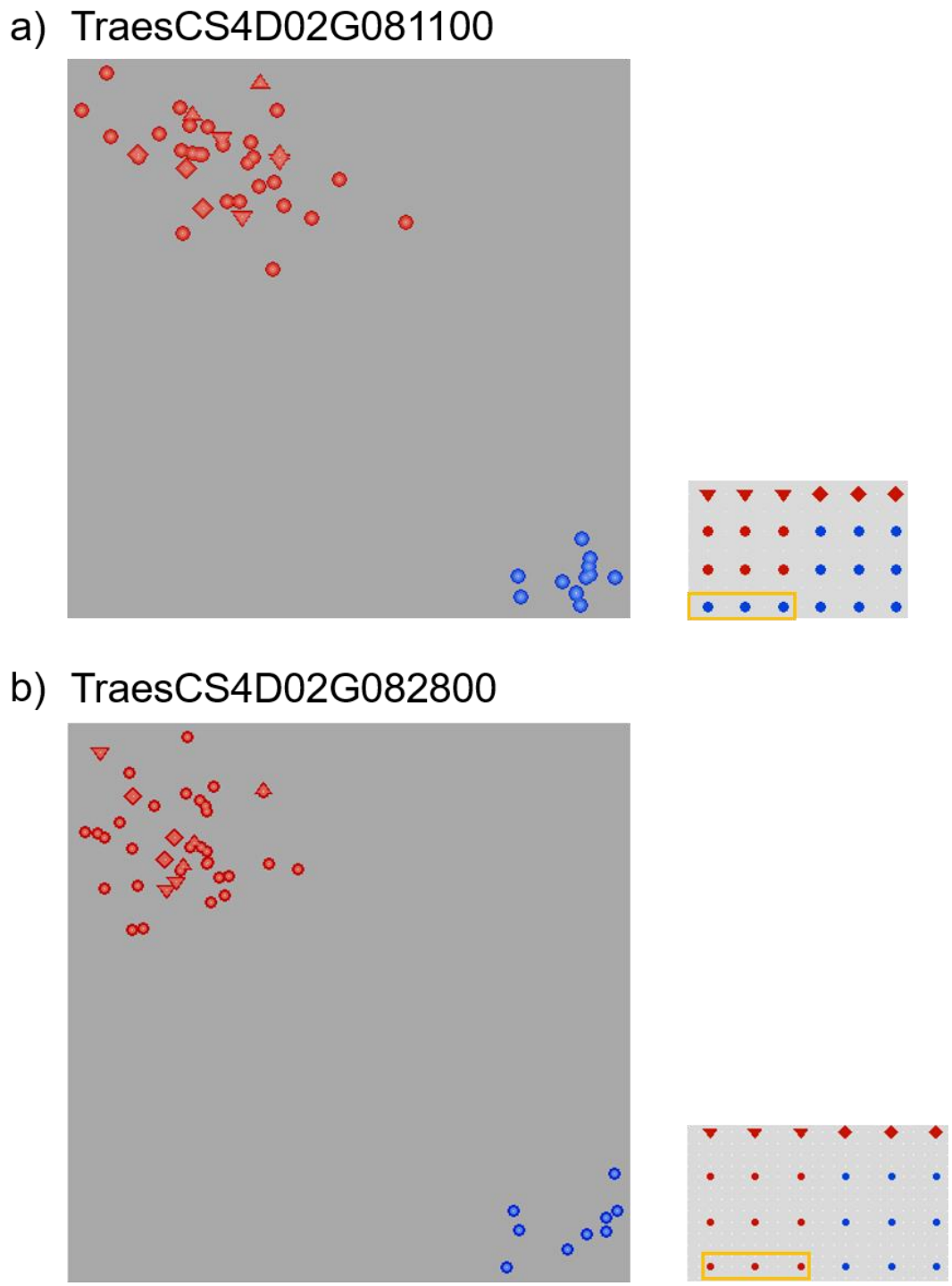

Figure 3.5 Example KASP outputs at markers targeting A TraesCS4D02G081100 and B TraesCS4D02G082800, captured from Kraken software (LGC Genomics). Wild type-like samples are displayed in red. Blue samples indicate a deletion at the marker position on 4D. T19 L19 is deleted at TraesCS4D02G081100 but the wild type-like signal is retrieved at TraesCS4D02G082800 (wells corresponding to T19 L19 samples are bordered by a yellow box). Three samples each of T17 L65, T15 L49 and T20 L65 are also visible. Wild type Paragon samples are red triangles and diamonds.

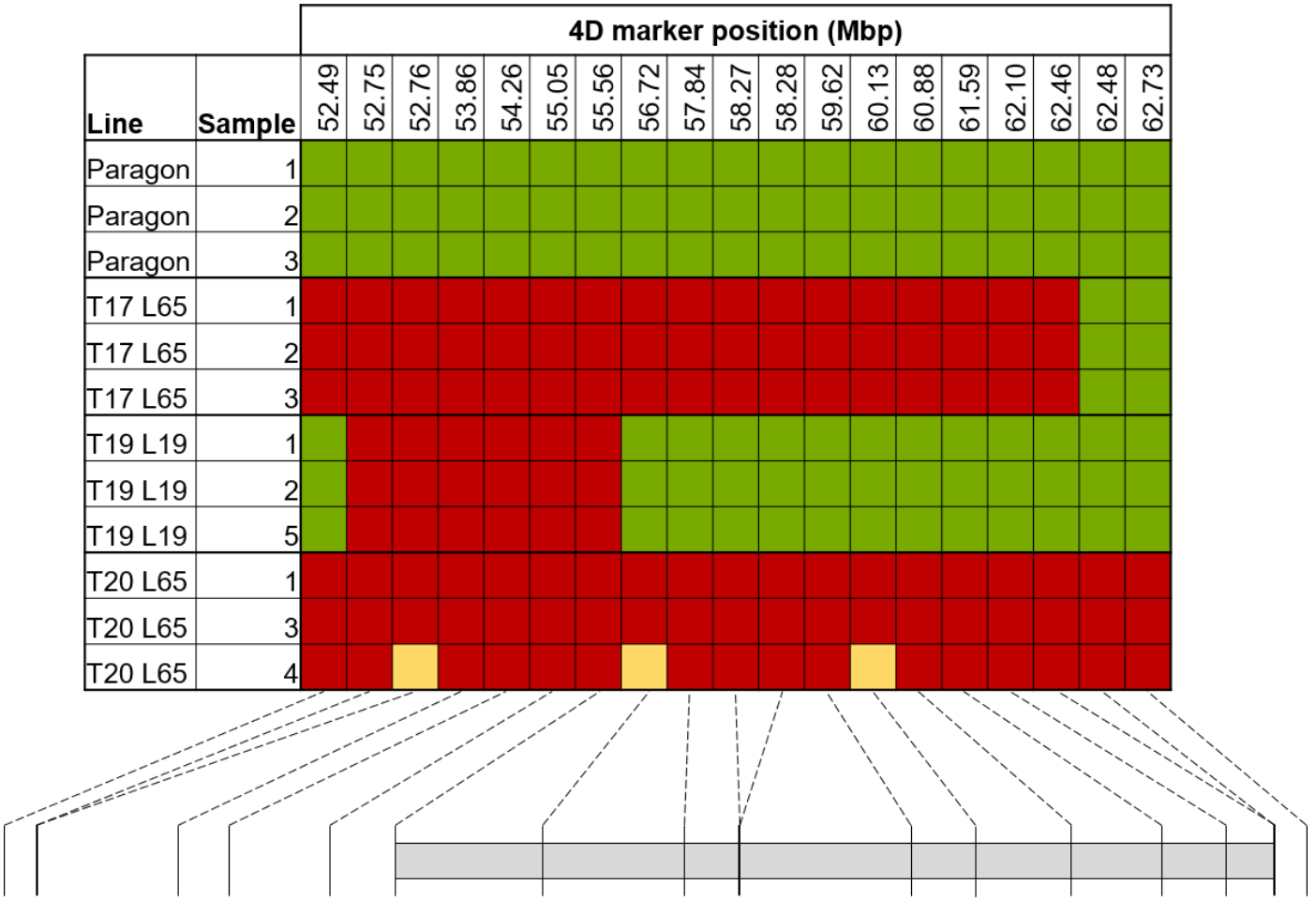

Figure 3.6 Genotyping Paragon and three gamma irradiated deletion lines: T17 L65, T19 L19 and T20 L65. Red boxes indicate a 4D deletion at the position of the marker. Green boxes indicate a wild type signal. Yellow boxes indicate an inconclusive signal. The physical distance between markers is indicated below the genotyping diagram. The inferred interval containing the susceptibility factor is indicated by the grey bar.

3.3.5 Focussed screen of gamma-irradiated Paragon population

The line T17 L65 has high levels of FHB resistance and contains a deletion within the susceptibility interval on 4D. T19 L19 has wild type-like levels of FHB resistance and contains a 4D deletion on the distal end of the susceptibility interval. Hence, the deletion in T17 L65 is likely to have eliminated the susceptibility factor but the susceptibility factor cannot be in the deleted region in common between T17 L65 and T19 L19 (at least between 52.75 and 55.56 Mbp).

Eighteen KASP markers (as used above, in **Figure 3.6**) were used to screen the entire gamma-irradiated Paragon population, consisting of 1860 lines. All samples were of the same genetic background (Paragon) and hence wild type samples clustered as a 'heterozygous-like' signal (example displayed in **Figure 3.7**). This is because both 4B and 4D homoeologues are amplified, contributing both FAM and HEX fluorescences. In the event of a deletion being present at the position of the marker on either 4D or 4B, the SNP corresponding to the deleted homoeologue cannot be amplified and hence the associated fluorescence will not be detected. The marker BH_4D087100, targeting TraesCS4D02G087100 at 62.46 Mbp, was not used in the screen because it was unreliable in providing a clear differential between lines with and without deletions.

A total of fourteen lines were identified that appeared to contain deletions across the interval on 4D. Four of these lines had previously been detected in the original screening of the gamma-irradiated Paragon population (T19 L19, T17 L65, T15 L49 and T20 L65). All new lines in which 4D deletions were detected were sown for experimental use. Leaf samples were taken from at least 16 plants per line and DNA was extracted from the samples. These DNA samples were rescreened using the same KASP markers, to verify the presence of the deletions detected. Five of the new 4D deletion lines were verified through this process: J10-89, T21 L56, J8-70, J4-50 and J7-35 (**Figure 3.8**). The deletions in the additional five lines could not be

detected in the verification screen and hence these were excluded as false positives. All lines that could not be verified had appeared to indicate the presence of a deletion at only a single marker in the preliminary screen.

Lines T17 L65 and T19 L19 were also prepared for experimental use and these were also genotyped to confirm that all plants contained the expected deletion. For T17 L65, the deletion could not be detected in five out of 36 plants. The remaining 31 plants of T17 L65 appeared to have retained the 4D deletion.

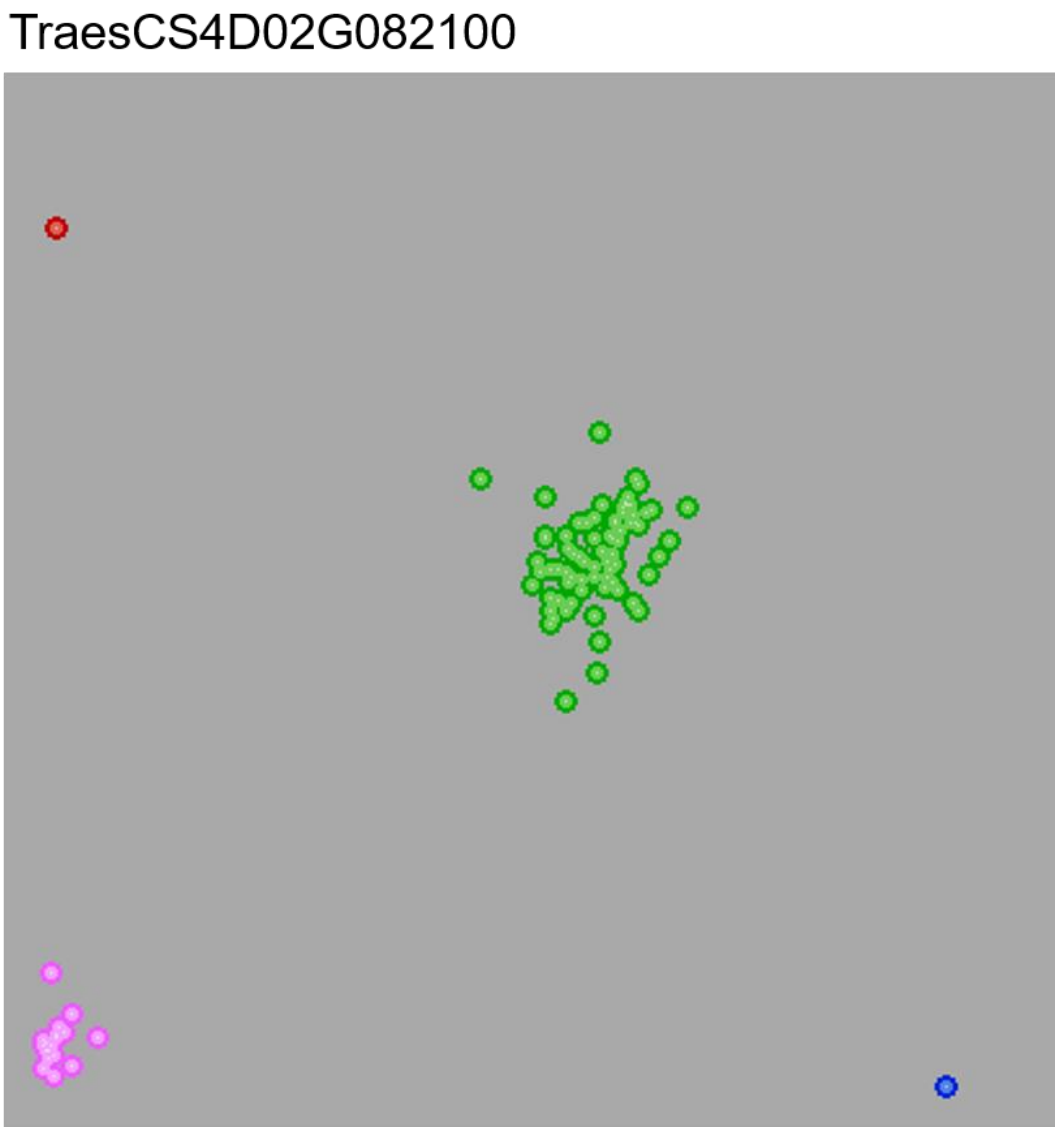

Figure 3.7 Example output of the KASP screen of the gamma-irradiated Paragon population. Image is a screenshot from Kraken software (LGC Genomics). The example shows the lines of T20 at the marker BH_082100, corresponding to TraesCS4D02G082100 at 55.56 Mbp on 4D. Wild type-like samples are clustered together as a heterozygous-like signal (green circles). No template controls are pink circles. A 4D deletion (blue circle) is visible, corresponding to line T20 L65. A possible 4B deletion (red circle) is also visible in line T20 L13.

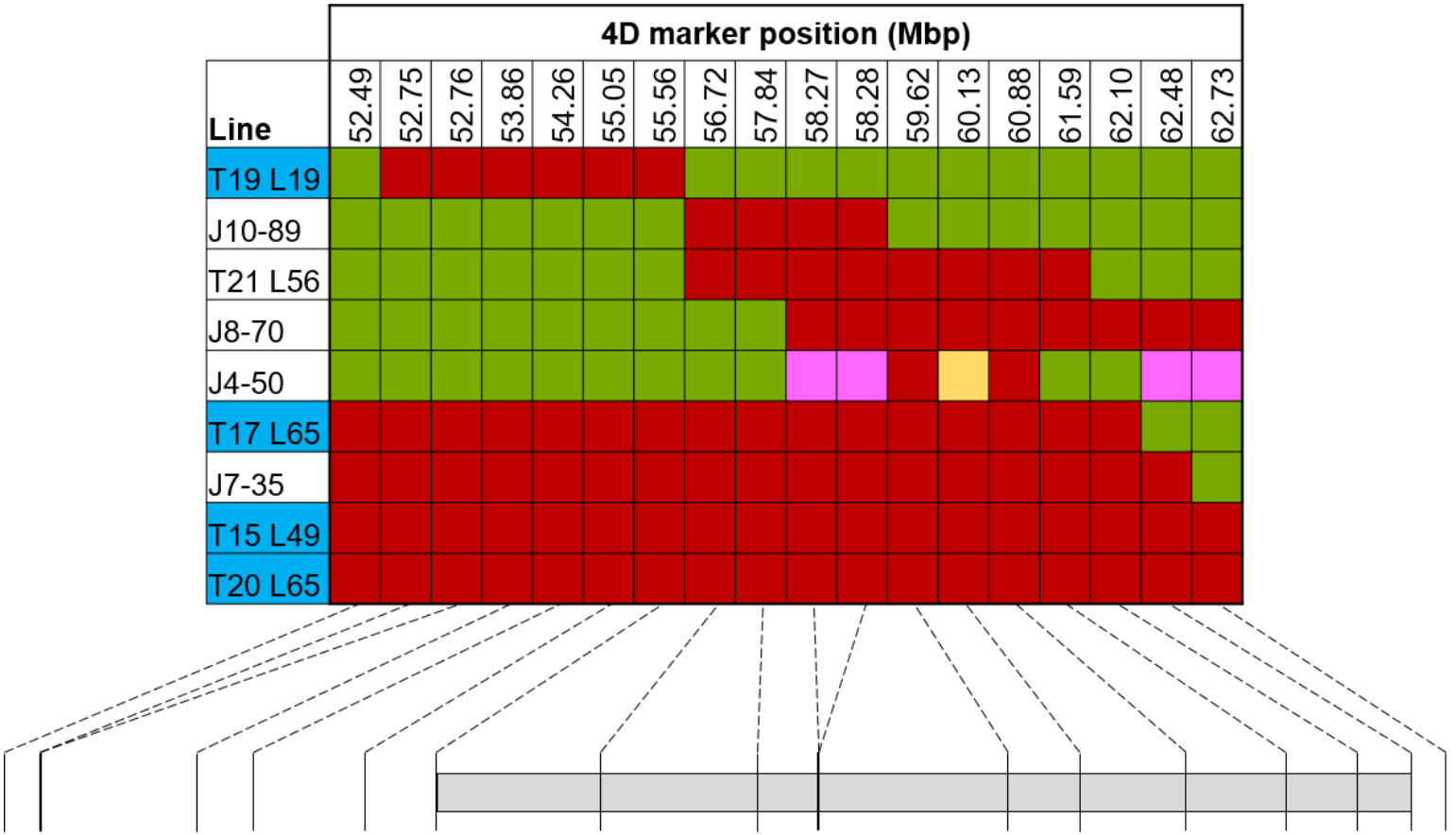

Figure 3.8 Genotyping of the gamma-irradiated Paragon population using KASP markers designed for detecting deletions on 4D and 4B. The lines displayed were subsequently verified by genotyping at least 16 plants per line. Green box indicates a wild type signal. Red box indicates a deletion on 4D at the position of the marker. Pink box represents a possible deletion of the 4B homoeologue. Yellow box indicates an inconclusive signal. Lines marked in blue were detected in the original screen. The physical distance on 4D between markers is indicated below the genotyping diagram. The inferred position of the susceptibility factor is indicated by the grey bar.

3.3.6 High levels of FHB resistance in T17 L65 is independent of the presence of the 4D deletion

The gamma-irradiated Paragon lines, that contained deletions across the interval of interest on 4D, were point inoculated in an experiment performed under controlled conditions (FHBpt_PGkasp_CER_19). J7-35 was very late flowering and hence escaped point inoculation. Hence, results for J7-35 are not presented. Paragon showed clear disease spread from the inoculation point (mean= 2.26) (**Figure 3.9**). T19 L19 (mean= 2.01, p= 0.712), J10-89 (mean= 1.21, p= 0.074), T21 L56 (mean= 2.12, p= 0.827), J8-70 (mean= 1.10, p= 0.058) and J4-50 (mean= 1.97, p= 0.724) all showed similar disease to wild type Paragon and were not significantly different in any case (**Figure 3.9**). T17 L65 plants containing the homozygous 4D deletion (4D del+) and the five plants where the 4D deletion was at least partially lost (4D del-) were both point inoculated. The line was highly resistant to FHB infection, regardless of whether the 4D deletion was present (4Ddel+; mean=0.181, p< 0.001) or at least partially absent (4Ddel-; mean= 0.146, p= <0.001) (**Figure 3.9**).

Leaf samples were taken from the five T17 L65 (4Ddel-) plants, in addition to five randomly selected T17 L65 (4Ddel+) and five wild type Paragon plants and DNA was extracted from these samples. Three KASP markers spanning the deletion in T17 L65 (BH_076500, BH_082100 and BH_085400) were used to confirm the lines possessed the expected genotype (**Figure 3.10**). T17 L65 (4Ddel-) samples showed a similar signal to Paragon, although each line did cluster separately, suggesting the deletion may be hemizygous in these plants (**Figure 3.10**). However, the T17 L65 (4Ddel+) samples all showed a 4D deletion-like signal (**Figure 3.10**). Hence, this assay confirms that the plants from T17 L65 (4Ddel-) and T17 L65 (4Ddel+) are genotypically distinct and resistance in T17 L65 appears to be independent of whether the 4D deletion is present or at least partially absent from the line. Furthermore, J10-89, T21 L56 and J8-70, that carry deletions across the interval thought to contain the putative FHB susceptibility factor, all possess wild type-like

levels of FHB resistance. Hence, the susceptibility factor does not appear to be present within the 4D deletion in T17 L65 (52.49-62.48 Mbp). This means that the FHB susceptibility factor is likely to be proximal to this interval and T17 L65 is resistant as a result of an unknown background deletion.

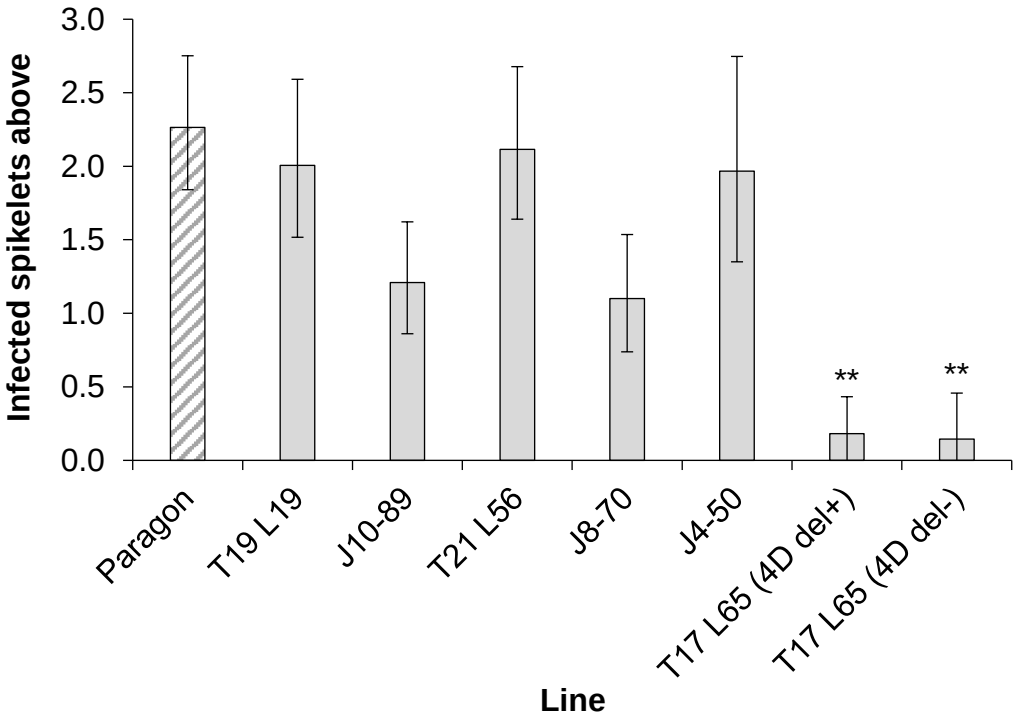

Figure 3.9 Point inoculation experiment scored at 17 dpi, conducted under controlled conditions, of Paragon and six deletion lines possessing deletions across an interval on 4D inferred to contain the FHB susceptibility factor. Genotyping identified that five plants of T17 L65 had retrieved the deleted region on 4D, (4D del-) whilst the remaining plants had retained the deletion (4D del+). Statistical analysis was conducted on log10 transformed values. Predicted means were generated using a linear mixed model. Error bars are ± standard error. ** $p < 0.01$ compared with Paragon.

a) TraesCS4D02G076500

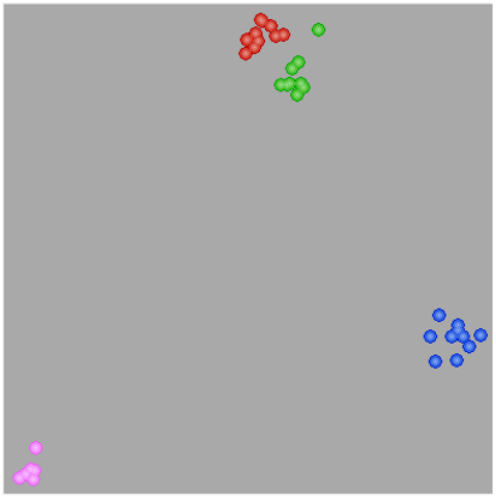

b) TraesCS4D02G082100

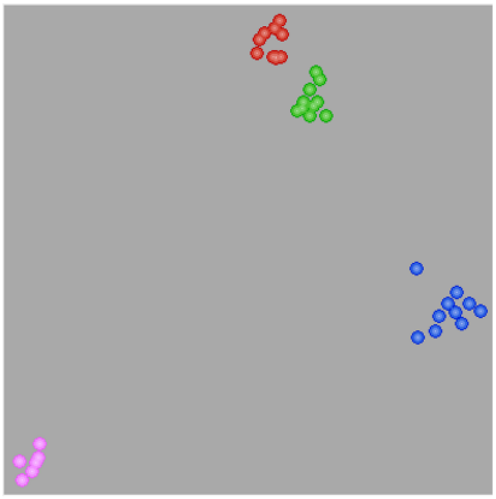

c) TraesCS4D02G085400

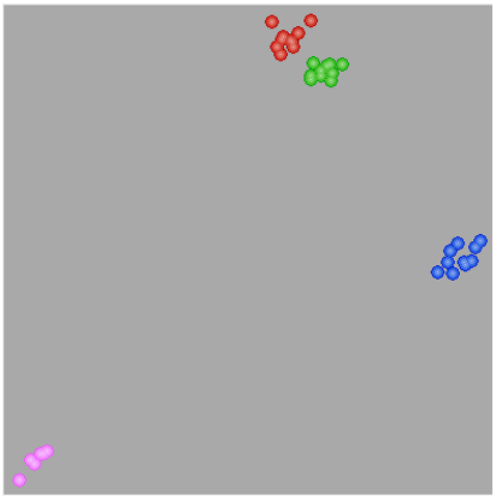

Figure 3.10 KASP outputs of markers targeting a) TraesCS4D02G076500, b) TraesCS4D02G082100, and c) TraesCS4D02G085400. Pink circle= no template control. Red circle= wild type Paragon. Green circle= T17 L65 (4Ddel-) samples. Blue circles= T17 L65 (4Ddel+) samples.

3.3.7 Interrogating line T17 L65

T17 L65 was highly resistant to the spread of FHB but the deletion on 4D does not appear to be responsible for this. Returning to the initial screen of the M4B2 Paragon lines, it was observed that T17 L65 showed an unusual signal at the homoeologue nonspecific marker BH0010.2, targeting the 4D gene TraesCS4D02G098400 located at 75.23 Mbp (**Figure 3.11A**). The signal from BH0010.2 shows increased amplification from the D genome in T17 L65 compared to Paragon and Chinese Spring, which suggests that there is a duplication of 4D at this position. The assay had previously been used to detect copy number variation in Chinese Spring nullisomic-tetrasomic lines (**Figure 3.12**) and both hemizygous deletions and duplications were evident in the initial screen of the Paragon population (data not shown). The marker BH0010.2 was used to test the T17 L65 plants from the CER experiment (FHBpt_PGkasp_CER_19). The same pattern was evident in all plants, indicating that the 4D duplication is fixed in the T17 L65 line (**Figure 3.11B**).

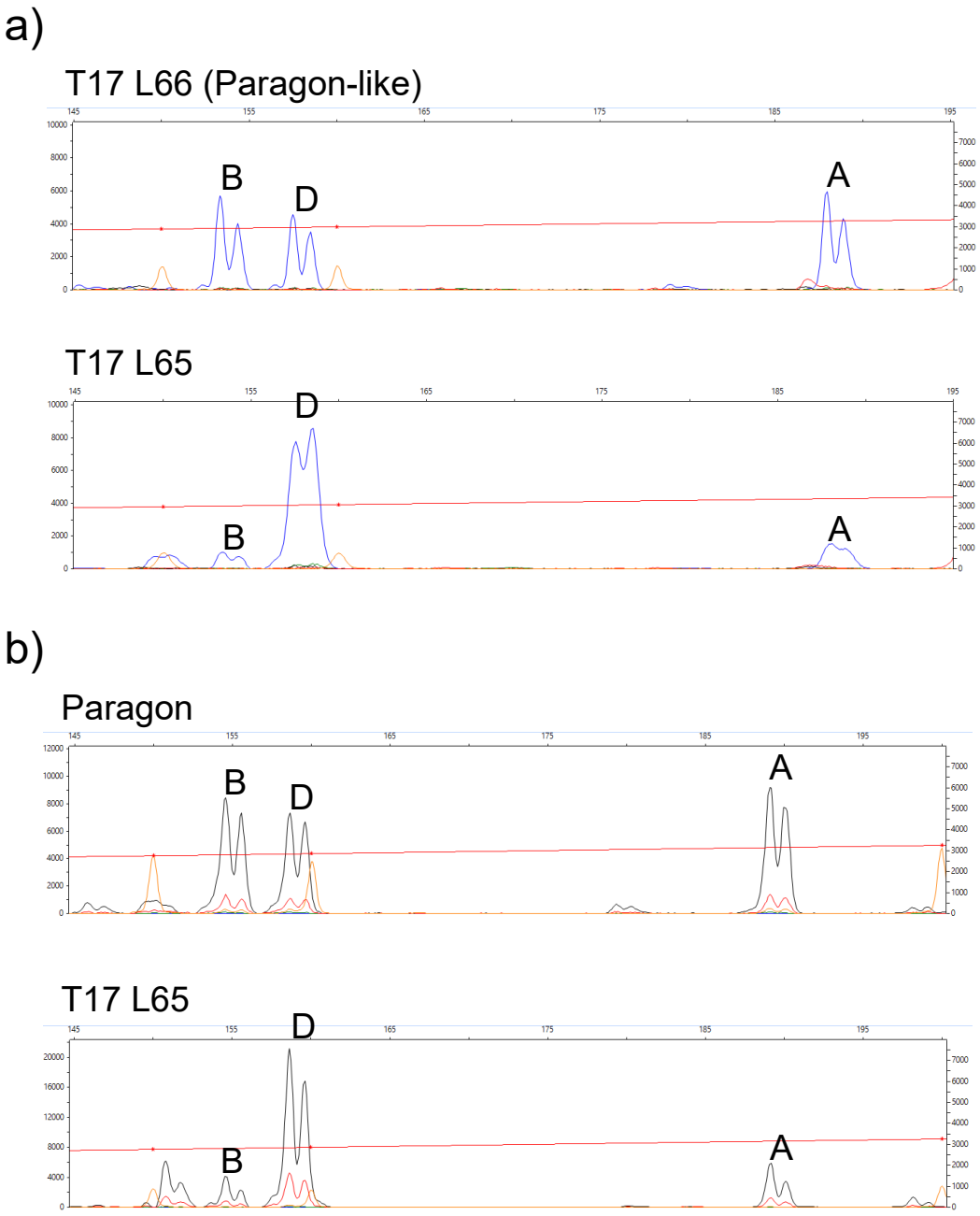

Figure 3.11 Peak Scanner (v2.0, Applied Biosystems) output of homoeologue nonspecific marker BH0010.2. Labels above the relevant peaks correspond to the 4A (A), 4B (B) and 4D (D) homoeologues. a) Output from the initial screen of the M4B2 Paragon lines, showing T17 L66 with a wild type-like signal (above), and T17 L65, showing an increased signal strength corresponding to the 4D homoeologue (below). b) Genotyping of T17 L65 plants from a 2019 CER experiment with BH0010.2 showed the same increased signal corresponding to the 4D homoeologue (below) compared to Paragon, showing a typical signal from BH0010.2 (above). X axis is fragment size (bp) and Y axis is the strength of fluorescence (relative fluorescence units). Images were extracted as screenshots from Peak Scanner 2 software (Applied Biosystems).

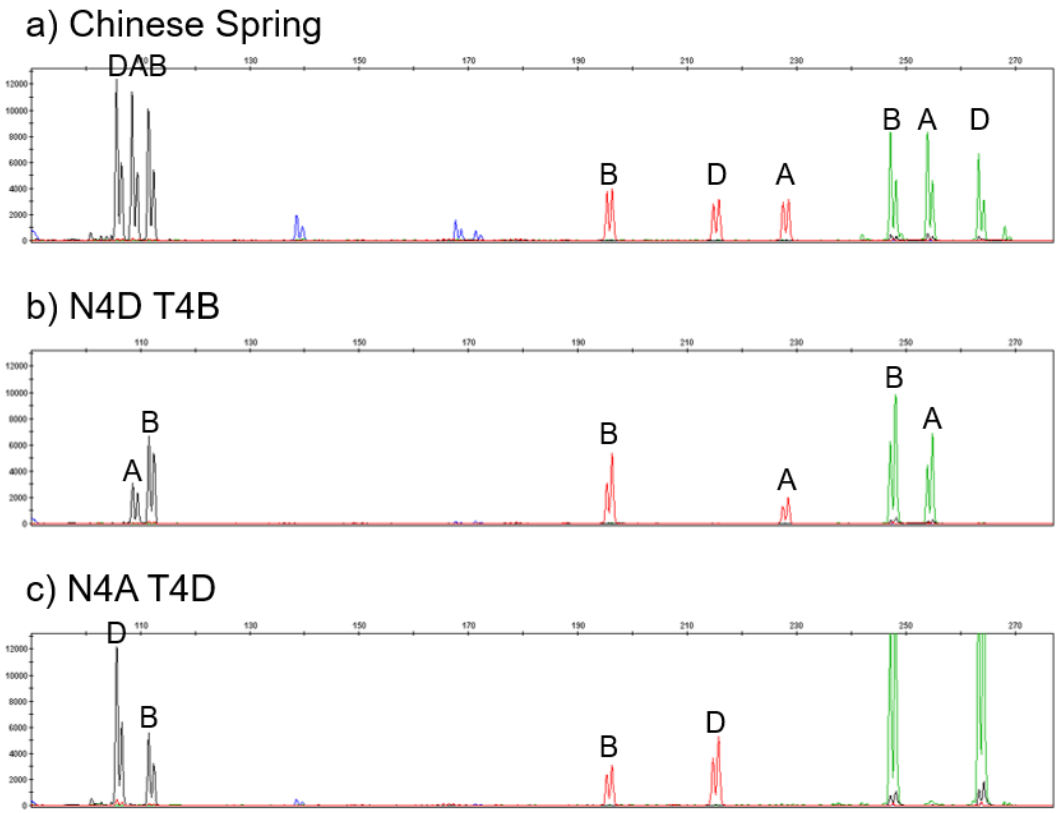

Figure 3.12 Peak Scanner (v2.0, Applied Biosystems) output of homoeologue nonspecific markers BH0014 (TraesCS4D02G066900, black peaks) BH0018 (TraesCS4D02G107300, red peaks) and BH0017 (TraesCS4D02G105100, green peaks), demonstrating the ability of the markers to detect copy number variation. Labels above the relevant peaks correspond to the 4A (A), 4B (B) and 4D (D) homoeologues. a) Chinese Spring; b) N4D T4B; c) N4A T4D. X axis is fragment size (bp) and Y axis is the strength of fluorescence (relative fluorescence units). Images were extracted as screenshots from Peak Scanner 2 software (Applied Biosystems).

3.3.8 Additional genotyping of 4D deletion lines

The 4D deletion in J8-70 extends beyond the most proximal KASP marker (BH_4D087400, targeting TraesCS4D02G087400). The line possesses Paragon-like levels of FHB susceptibility and hence the deletion is unlikely to contain the susceptibility factor. T17 L65 appears to contain a duplication on 4D at the position of TraesCS4D02G098400 but it is not known how far the duplication extends. Hence, four homoeologue nonspecific markers were designed between TraesCS4D02G087400 and TraesCS4D02G098400 to better characterise the deletion/ duplication present in these lines. The markers BH0059.1, BH0060.1, BH0061.1 and BH0062 targeted the 4D genes TraesCS4D02G088200, TraesCS4D02G090400, TraesCS4D02G91400 and TraesCS4D02G94500, respectively. In T17 L65, the duplication on 4D was evident across all four markers (**Figure 3.13A**). In the initial screen of the Paragon population, no duplication was evident in T17 L65 at BH0009.3 (TraesCS4D02G087200 at 62.48 Mbp). Hence, the distal deletion breakpoint is likely to be between 62.48 Mbp and 63.25 Mbp. The 4D deletion in J8-70 was visible in the most distal marker (BH0059.1 targeting TraesCS4D02G088200 at 63.25 Mbp) but the signal was retrieved at BH0060.1 (targeting TraesCS4D02G090400 at 65.53 Mbp) (**Figure 3.13A**). Hence, the proximal deletion breakpoint in J8-70 is between 63.25 Mbp and 65.53 Mbp (**Figure 3.13B**).

T17 L20 and T13 L38 contain deletions in the FHB susceptibility interval and both possess a Paragon-like FHB phenotype. The deletions in these lines are unlikely to contain the susceptibility factor, so these intervals can be eliminated from investigation. However, they were identified from the initial population screen using only five markers and hence additional genotyping was necessary to better characterise the size of the deletions.

Ten additional homoeologue nonspecific markers were used to genotype T17 L20 and T13 L38. Markers BH0010.2 (TraesCS4D02G098400; 75.23 Mbp), BH0017 (TraesCS4D02G105100; 83.28 Mbp) and BH0018 (TraesCS4D02G107300; 85.59 Mbp) are also included for reference (**Figure 3.14)**. T17 L65 was also genotyped to identify how far the 4D duplication extends proximally. T17 L20 did not have a deletion at the position of any of the new markers. The deletion in T17 L20 extends no further than the markers at 73.22 Mbp (BH0064; TraesCS4D02G096600) and 76.02 Mbp (BH0065; TraesCS4D02G099100) (**Figure 3.14**). Four new markers detected the deletion in T13 L38. The distal breakpoint in T13 L38 is between 76.02 Mbp (BH0065; TraesCS4D02G099100) and 79.21 Mbp (BH0066; TraesCS4D02G101500), and the proximal breakpoint is between 83.86 Mbp (BH0069; TraesCS4D02G105300) and 85.59 Mbp (BH0018; TraesCS4D02G107300) (**Figure 3.14**). The 4D duplication in T17 L65 was not detected in markers proximal to BH0010.2, so the duplication must end between 75.23 Mbp (BH0010.2; TraesCS4D02G098400) and 76.02 Mbp (BH0065; TraesCS4D02G099100) (**Figure 3.14**).

a) Paragon

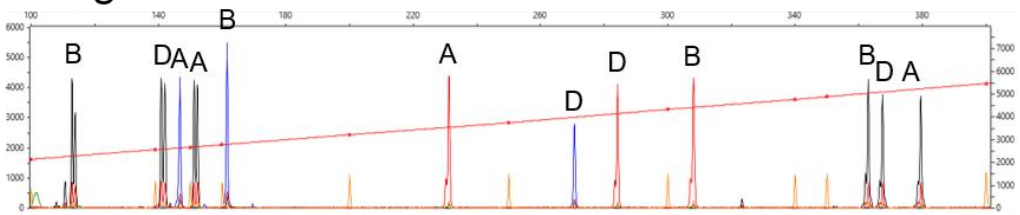

T17 L65

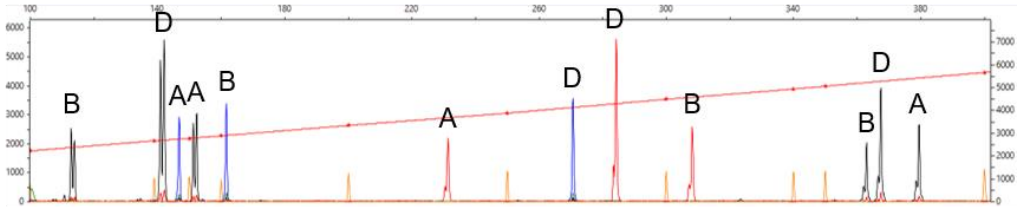

J8-70

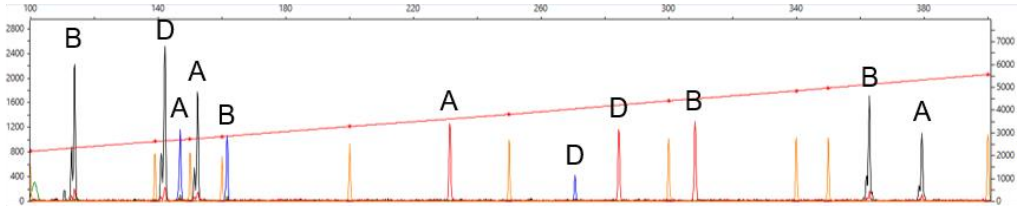

b)

		4D position (Mbp)			
Line	**Sample**	63.25	65.53	66.32	69.85
Paragon	1				
Paragon	2				
Paragon	3				
T17 L65	7				
T17 L65	10				
T17 L65	11				
J8-70	1				
J8-70	2				
J8-70	3				

Figure 3.13 a) Peak Scanner (v2.0, Applied Biosystems) output of homoeologue nonspecific markers BH0059.1 (TraesCS4D02G088200, black peaks clustered right), BH0060.1 (TraesCS4D02G090400, blue peaks), BH0061.1 (TraesCS4D02G91400, red peaks) and BH0062 (TraesCS4D02G94500, black peaks clustered left) in the lines Paragon, T17 L65 and J8-70. X axis is fragment size (bp) and Y axis is the strength of fluorescence (relative fluorescence units). Images were extracted as screenshots from Peak Scanner 2 software (Applied Biosystems). b) Interpreted results of homoeologue nonspecific markers of three biological replicate samples each of lines Paragon, T17 L65 and J8-70. Green box indicates signal present on 4D. Red box indicates a deletion present on 4D at the position of the marker. Blue box indicates a duplication of 4D at the position of the marker.

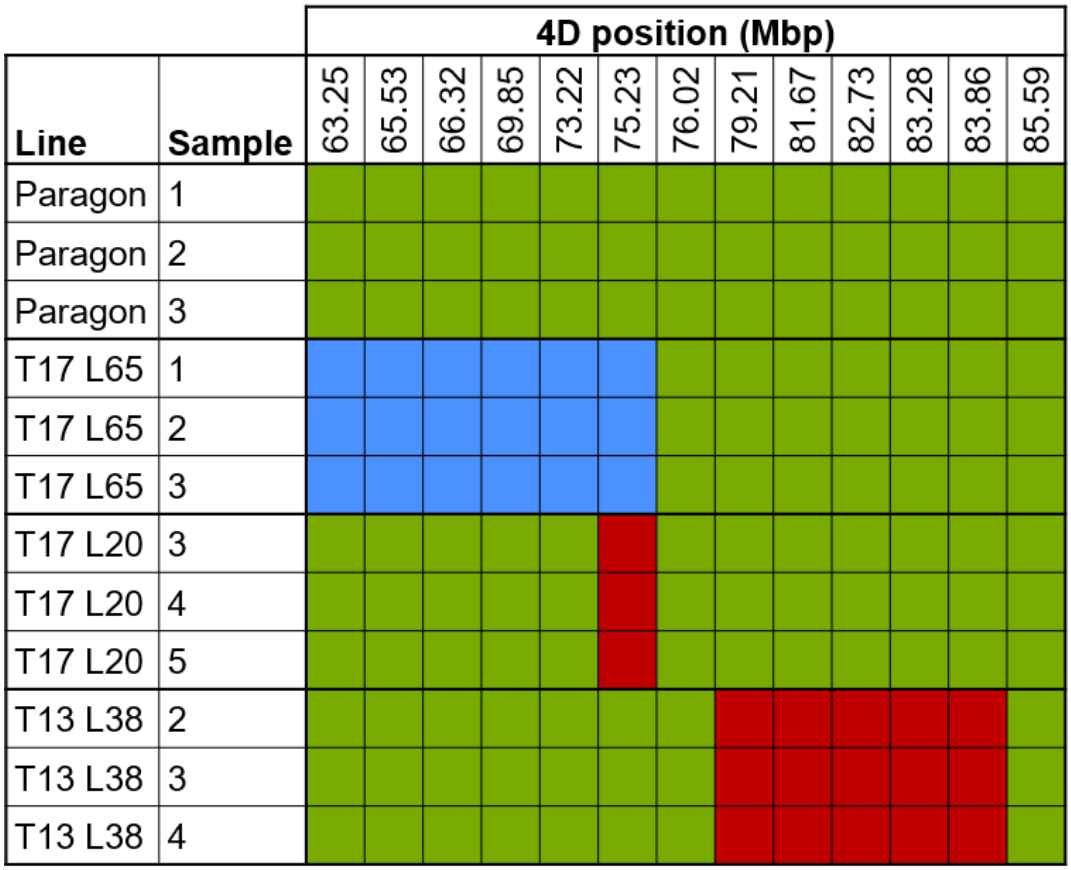

Figure 3.14 Improved genotyping of lines T17 L65, T17 L20 and T13 L38 using homoeologue nonspecific markers. Green box indicates signal present on 4D. Red box indicates a deletion present on 4D at the position of the marker. Blue box indicates a duplication of 4D at the position of the marker.

3.3.9 Skim sequenced Paragon deletion lines containing 4D deletions

Skim sequencing (to a sequencing depth of 0.2 x) was performed on 665 gamma-irradiated Paragon lines from M4B1 (Ramirez-Gonzalez *et al.*, unpublished). Bioinformatic analysis was performed by Dr Ricardo Ramirez-Gonzalez. Within the remaining 22.34 Mbp susceptibility interval, two lines were identified with deletions in the interval: J3-92 and J3-88 (**Figure 3.15A**).

Lines J3-92 and J3-88 were point inoculated, in addition to the gamma-irradiated Paragon lines previously identified that contain deletions in the refined FHB susceptibility interval (T17 L20, T13 L38 and T20 L65; FHBpt_PGskim_CER_19). Neither J3-92 (mean= 1.60, p= 0.855) nor J3-88 (mean= 2.26, p= 0.121) were significantly different from wild type Paragon (mean= 1.52) (**Figure 3.15B**). T17 L20 (mean= 0.86, p= 0.069) and T13 L38 (mean= 1.45, p= 0.850) were also not significantly different from Paragon (**Figure 3.15B**). Consistent with previous experiments, T20 L65 was significantly more resistant than wild type Paragon (mean= 0.15, p<0.001) (**Figure 3.15B**).

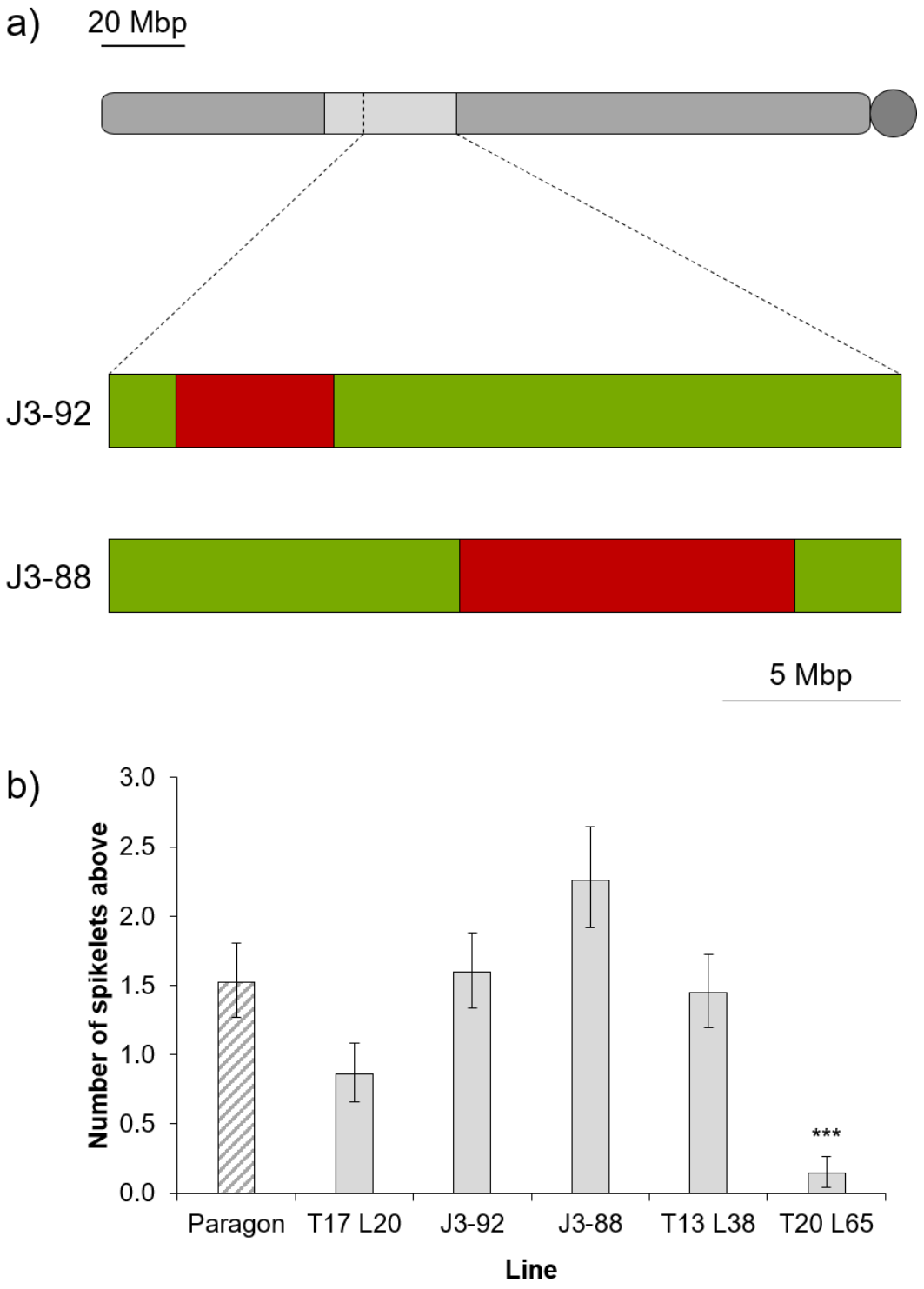

Figure 3.15 a) 4D deletions in the skim sequenced gamma-irradiated Paragon lines J3-92 and J3-88 across remaining 22.34 Mbp interval. The red interval indicates the position of the deletion in each line. b) FHB point inoculation experiment of lines containing deletions across the remaining FHB susceptibility interval, including J3-92 and J3-88 identified from skim sequencing data. Predicted means were generated using a linear mixed model, using count data above the inoculation point at 16 dpi. Data were log10 transformed prior to statistical analysis to improve normality. Presented data were back transformed. Error bars are ± standard error. *** p< 0.001 compared with Paragon.

3.3.10 Genes in the FHB susceptibility intervals

Ten gamma-irradiated Paragon lines have been identified that contain deletions (and a duplication, in the case of T17 L65) of the FHB susceptibility interval and were phenotyped for FHB susceptibility (**Figure 3.16**). In combining genotyping and phenotyping information from the lines, there are three small intervals that cannot be eliminated from the investigation. The distal, central and proximal intervals contain 15, 33, and 18 high confidence genes, respectively. In these intervals, there are a number of genes containing domains associated with disease resistance, including protein kinase, NB-ARC and leucine rich repeat domains (**Table 3.5**). Additionally, there is a gene annotated to encode an MLO-like protein (**Table 3.5**). The FHB susceptibility factor may also be 4D specific. There are eight genes in the interval that do not possess homoeologoues on either 4A or 4B: TraesCS4D02G088600, TraesCS4D02G089300, TraesCS4D02G093400, TraesCS4D02G095200, TraesCS4D02G095300, TraesCS4D02G096300, TraesCS4D02G106600 and TraesCS4D02G107000. Furthermore, TraesCS4D02G088600, TraesCS4D02G096300 and TraesCS4D02G093400 do not show any evidence of being expressed and have no Cadenza TILLING mutants whatsoever, which would suggest they may not be real genes (Ramírez-González *et al.*, 2018, Borrill *et al.*, 2016, Winter *et al.*, 2007).

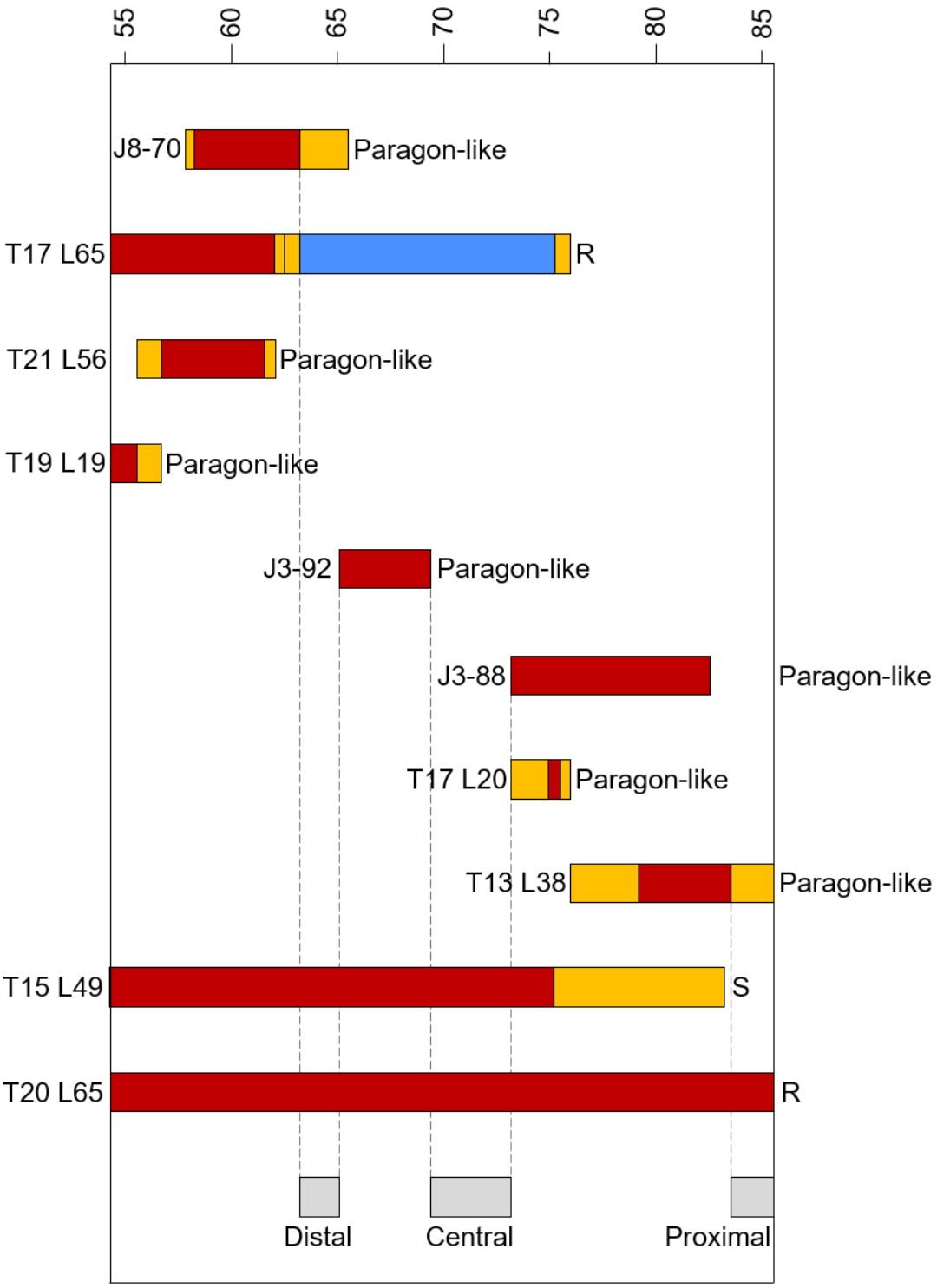

Figure 3.16 Gamma-irradiated lines containing deletions across the FHB susceptibility interval on 4DS. Line name to the left of the deletion diagram and FHB phenotype to the right of the diagram. R= more resistant compared with Paragon; S= more susceptible compared with Paragon. Physical position (Mbp) on 4DS is provided above the diagrams. Red bar indicates a deletion. Blue bar indicates a duplication. Yellow bar indicates an interval in which a deletion ends. Three intervals containing candidate genes are displayed as grey bars and contain the FHB susceptibility factor.

Table 3.5 FHB susceptibility factor genes candidates and their functional annotations extracted from Ensembl Plants. Genes are split across three intervals referred to as the distal, central and proximal intervals based on their physical positions on 4DS.

Gene	Interval	Functional annotation
TraesCS4D02G088200	Distal	Sucrose-phosphate synthase
TraesCS4D02G088300	Distal	Alpha/beta hydrolase
TraesCS4D02G088400	Distal	Protein kinase, leucine rich repeat domains
TraesCS4D02G088500	Distal	Protein kinase, leucine rich repeat domains
TraesCS4D02G088600	Distal	Peptidase/ protease
TraesCS4D02G088700	Distal	Leucine rich repeat domain
TraesCS4D02G088800	Distal	No information
TraesCS4D02G088900	Distal	NB-ARC, leucine rich repeat domains
TraesCS4D02G089000	Distal	Major sperm protein, WD40 repeat domains
TraesCS4D02G089100	Distal	Protein kinase domain
TraesCS4D02G089200	Distal	Protein kinase domain
TraesCS4D02G089300	Distal	Protein kinase, major sperm protein, WD40 repeat domains
TraesCS4D02G089400	Distal	NB-ARC, leucine rich repeat, Rx domains
TraesCS4D02G089500	Distal	No information
TraesCS4D02G089600	Distal	Protein kinase domain
TraesCS4D02G089700LC	Distal	Low confidence gene
TraesCS4D02G089800	Distal	NB-ARC, leucine rich repeat, Rx domains

Table 3.5 (continued) FHB susceptibility factor genes candidates and their functional annotations extracted from Ensembl Plants. Genes are split across three intervals referred to as the distal, central and proximal intervals based on their physical positions on 4DS.

Gene	Interval	Functional annotation
TraesCS4D02G093100	Central	Major facilitator transporter
TraesCS4D02G093200	Central	MLO-like protein
TraesCS4D02G093300	Central	Fe-S cluster assembly domain
TraesCS4D02G093400	Central	No information
TraesCS4D02G093500	Central	NAD(P)-binding short-chain dehydrogenase
TraesCS4D02G093600	Central	Fatty acid dehydroxylase
TraesCS4D02G093700	Central	Unknown function (DUF688)
TraesCS4D02G093800	Central	F-box, WD40-repeat domains
TraesCS4D02G093900	Central	Homeobox-like, SWIRM, SANT/Myb-like domains
TraesCS4D02G094000	Central	Armadillo domain
TraesCS4D02G094100	Central	Heavy metal-associated domain
TraesCS4D02G094200	Central	Peptidase/ protease
TraesCS4D02G094300	Central	Peptidase/ protease
TraesCS4D02G094400	Central	NAC domain
TraesCS4D02G094500	Central	Aldehyde dehydrogenase
TraesCS4D02G094600	Central	S-adenosyl-L-methionine-dependent methyltransferase
TraesCS4D02G094700	Central	DNA polymerase
TraesCS4D02G094800	Central	Tetratricopeptide-like helical domain

Table 3.5 (continued) FHB susceptibility factor genes candidates and their functional annotations extracted from Ensembl Plants. Genes are split across three intervals referred to as the distal, central and proximal intervals based on their physical positions on 4DS.

Gene	Interval	Functional annotation
TraesCS4D02G094900	Central	Tetratricopeptide-like helical domain
TraesCS4D02G095000	Central	Protein kinase domain
TraesCS4D02G095100	Central	Proteasome subunit beta
TraesCS4D02G095200	Central	No information
TraesCS4D02G095300	Central	BURP domain
TraesCS4D02G095400	Central	NAD kinase domain
TraesCS4D02G095500	Central	Iron-dependent dioxygenase
TraesCS4D02G095600	Central	WD40 repeat domain
TraesCS4D02G095700	Central	Zinc finger (GATA-type)
TraesCS4D02G095800	Central	Zinc finger (RING-type)
TraesCS4D02G095900	Central	Fatty acid dehydroxylase
TraesCS4D02G096000	Central	BRCT domain
TraesCS4D02G096100	Central	Protein kinase domain
TraesCS4D02G096200	Central	Protein translocase subunit SecA
TraesCS4D02G096300	Central	No information
TraesCS4D02G096400	Central	Alpha/beta hydrolase, fungal lipase-like domains
TraesCS4D02G096500	Central	No information

Table 3.5 (continued) FHB susceptibility factor genes candidates and their functional annotations extracted from Ensembl Plants. Genes are split across three intervals referred to as the distal, central and proximal intervals based on their physical positions on 4DS.

Gene	Interval	Functional annotation
TraesCS4D02G105400	Proximal	TLDc domain
TraesCS4D02G105500	Proximal	ATPase (AAA-type)
TraesCS4D02G105600	Proximal	Ribosomal protein L10e
TraesCS4D02G105700	Proximal	Auxin-responsive protein
TraesCS4D02G105800	Proximal	Auxin-responsive protein
TraesCS4D02G105900LC	Proximal	Low confidence gene
TraesCS4D02G106000	Proximal	Regulator of chromosome condensation 1/beta-lactamase-inhibitor protein II, protein kinase domain
TraesCS4D02G106100	Proximal	Serpin domain
TraesCS4D02G106200	Proximal	FRIGIDA-like protein
TraesCS4D02G106300	Proximal	60S acidic ribosomal protein P0
TraesCS4D02G106400	Proximal	Unknown function (DUF1677)
TraesCS4D02G106500	Proximal	Unknown function (DUF1677)
TraesCS4D02G106600	Proximal	Leucine rich repeat domain
TraesCS4D02G106700	Proximal	Protein kinase domain
TraesCS4D02G106800	Proximal	Shortage in chiasmata 1-like
TraesCS4D02G106900	Proximal	Protein kinase, leucine rich repeat domains
TraesCS4D02G107000	Proximal	Protein kinase, leucine rich repeat domains
TraesCS4D02G107100	Proximal	Forkhead-associated, PIN domains
TraesCS4D02G107200	Proximal	Protein kinase, EF-hand domain

3.3.11 Homoeologous deletions of 4A and 4B

There is a clear effect on FHB susceptibility when 4DS is deleted but little is known about whether the susceptibility factor possesses homoeologues that also influence FHB susceptibility.

The homoeologue nonspecific markers used in the initial screen of the gamma-irradiated Paragon population were capable of detecting deletions of homoeologous regions on chromosomes 4A and 4B. These data were used to select lines containing 4A and 4B deletions across the susceptibility interval, and additional lines with 4A and 4B deletions were identified from the skim sequencing data (**Table 3.6**). The deletions in these lines have good coverage of the 4A and 4B intervals homoeologous to the FHB susceptibility interval on 4D (**Figure 3.17**). 4A deletions entirely cover the regions homoeologous to both the central and proximal FHB susceptibility intervals on 4D (**Figure 3.17**). All lines containing 4B deletions were identified using homoeologue nonspecific markers, with the exception of J7-28. For this reason, the positions of the deletion breakpoints are not certain in these lines. The coverage of 4B deletions is likely to be more fragmented across the interval but this depends upon how far the deletions extend (**Figure 3.17**).

The lines containing 4A and 4B deletions were point inoculated to assess the FHB levels in the lines (FHBpt_PGhom_Poly_19). With the exception of J1-50, all lines were similar in FHB susceptibility to wild type Paragon ($p > 0.05$) (**Figure 3.18**). J1-50 was significantly more resistant to the spread of FHB than Paragon (mean= 0.601, $p < 0.001$) (**Figure 3.18**).

Table 3.6 Lines containing deletion on 4A and 4B chromosomes, homoeologous to the FHB susceptibility interval on 4D. Deletion start and end (Mbp) is provided for lines that were skim sequenced. For lines identified from the initial marker screen using homoeologue nonspecific markers, the physical positions of markers showing a deletion signal are listed.

Line	Chromosome	Deletion position (Mbp)	Source
J6-31	4A	474.4-508.1	Skim sequencing
J1-50	4A	501.2-511.9	Skim sequencing
J6-19	4A	508.0-529.6	Skim sequencing
J5-67	4A	521.9-532.2	Skim sequencing
J7-28	4B	59.8-81.8	Skim sequencing
T15 L72	4B	Marker at 89.5	Initial marker screen
T16 L73	4B	Marker at 89.5	Initial marker screen
T19 L93	4B	Markers at 107.6, 118.3, 112.6	Initial marker screen
T15 L26	4B	Markers at 118.3, 112.6	Initial marker screen

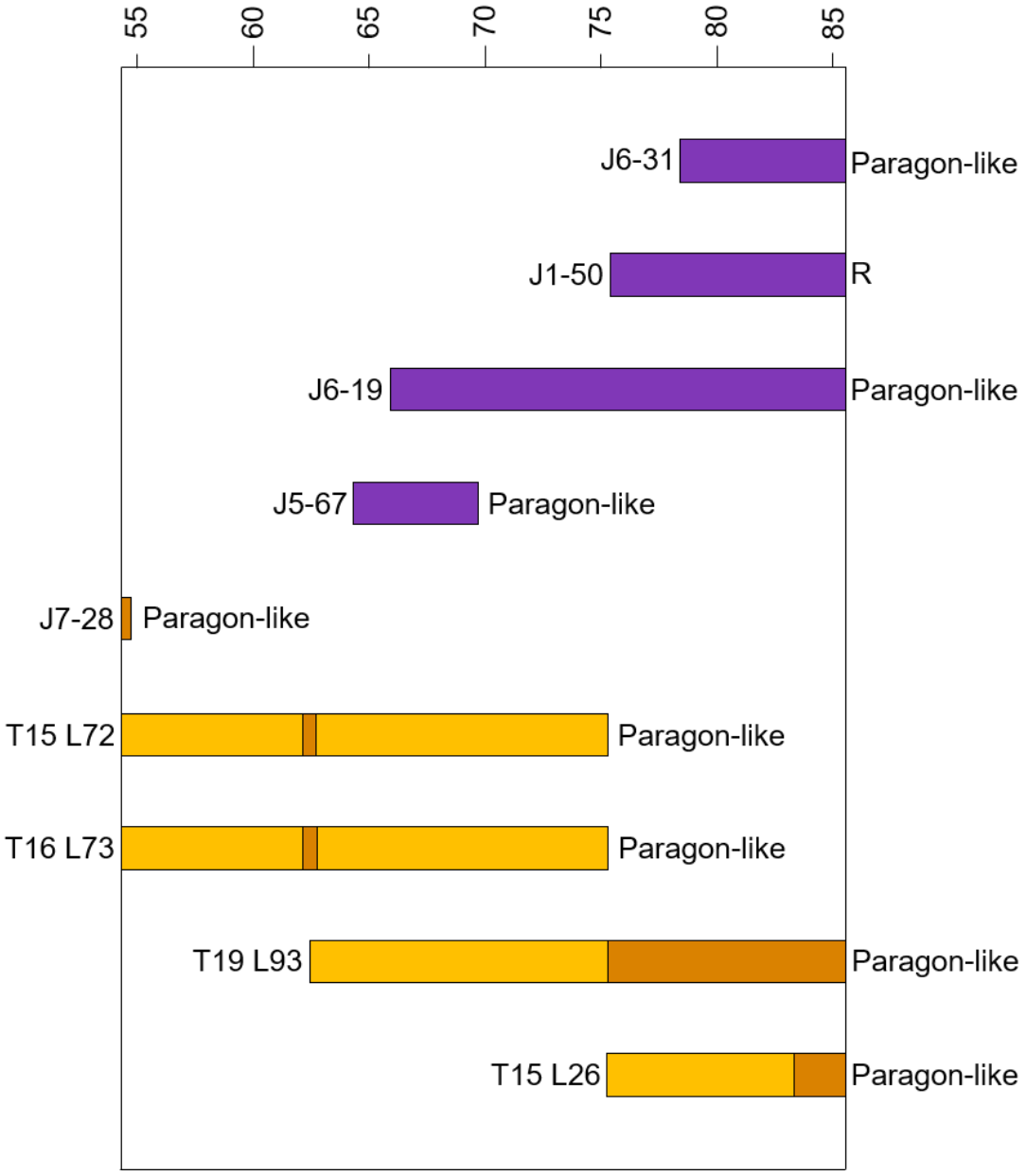

Figure 3.17 Gamma-irradiated Paragon lines containing 4A and 4B deletions across the intervals homoeologous to the FHB susceptibility factor on 4D. Line name is provided to the left of the deletion diagram and FHB phenotype to the right of the diagram: R= more resistant compared with Paragon. The physical position (Mbp) on 4D is provided above the diagrams. Purple bar indicates 4A deletion. Orange bar indicates a 4B deletion. Yellow bar indicates an interval in which a deletion ends.

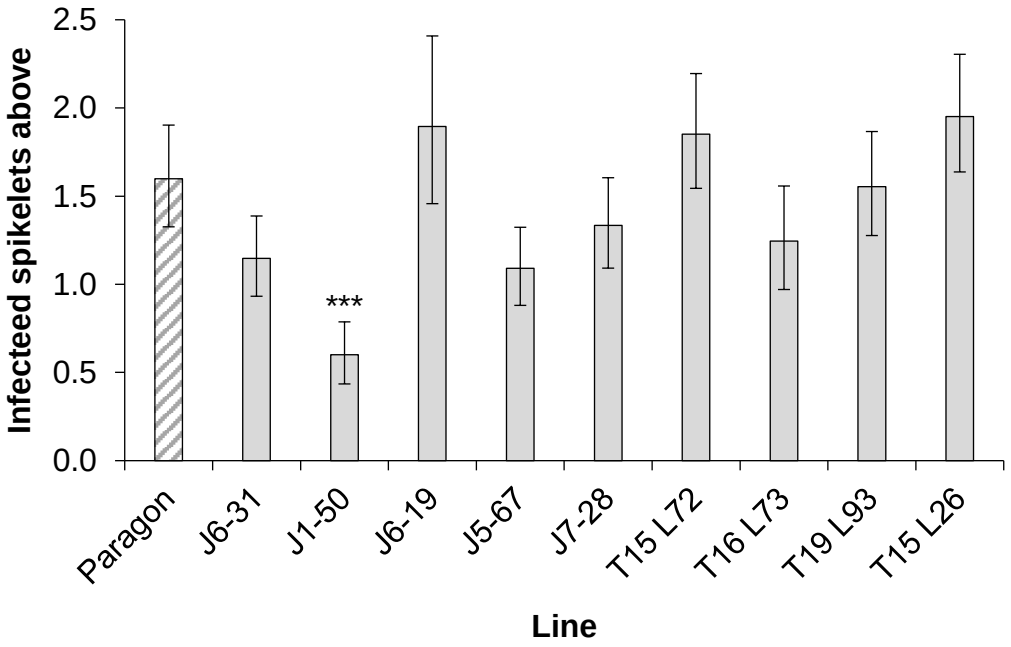

Figure 3.18 FHB point inoculation experiment of gamma-irradiated Paragon lines with 4A and 4B deletions across homoeologous intervals to the FHB susceptibility factor on chromosome 4D. Predicted means were generated using a linear mixed model, accounting for line as a fixed effect and replicate as a random effect. Statistical analyses were conducted using Log10 transformed values. Predicted means and standard error bars have been back transformed for presentation. Error bars are ± standard error. *** p< 0.001 compared with Paragon.

3.4 Discussion

3.4.1 Deletion mapping in wheat

EMS mutagenesis, as utilised in the generation of the tetraploid and hexaploid wheat TILLING populations, generally produces single base substitutions; usually G to A, or C to T (Uauy *et al.*, 2009). In contrast, gamma irradiation typically generates deletions of varying size across the genome. This is induced by the production of reactive oxygen species (ROS) which lead to single- or double-strand breaks of DNA (Roldan-Arjona and Ariza, 2009). In the event of a double-strand break, DNA is most commonly repaired by non-homologous end-joining (NHEJ) (Puchta, 2005). NHEJ is an error-prone DNA repair mechanism, which can result in deletions, in addition to duplications, insertions and inversions (Puchta, 2005).

Gamma-irradiated populations, such as that generated in the UK spring wheat variety Paragon, provide a tool for dissecting a region of interest (Shaw *et al.*, 2013, Wheat Genetic Improvement Network, 2019). Identifying lines containing deletions that form a tiling path across an interval, followed by phenotyping of the deletion lines, provides a method of refining a genetic factor to a much smaller physical interval. This is invaluable where the number of gene candidates are too numerous to practically utilise the wheat TILLING populations. It is necessary to be mindful that background deletions (or other alterations such as duplications) may also alter the phenotype in question. One or more rounds of crossing lines of interest to wild type Paragon, followed by self-fertilisation of progeny, whilst using markers to track the deletion of interest, can be used to remove background deletions. However, this is a time-consuming process and doing so was impractical in the timescale of this PhD project.

A deletion mapping method was employed to refine the position of an FHB susceptibility factor. An initial screen of the gamma-irradiated Paragon population was performed using five homoeologue nonspecific markers spanning the FHB

susceptibility interval. This 31.7 Mbp susceptibility interval was identified following the genotyping and FHB phenotyping of four 4DS terminal deletion lines in Chinese Spring (Chapter 2).

Six lines were identified with deletions across the FHB susceptibility interval (T17 L65, T19 L19, T15 L49, T17 L20, T13 L38 and T20 L65). The identified lines were bulked, during which the plants were genotyped to confirm the 4D deletions were present in a homozygous state. However, T20 L65 was of immediate interest because it contained a deletion spanning the entire susceptibility interval. Hence, the line could be used to confirm that the susceptibility factor is retained in the Paragon genetic background.

An FHB point inoculation experiment was conducted on Paragon and T20 L65. The plants were genotyped and the 4D deletion was still segregating in T20 L65. T20 L65 plants containing a homozygous 4D deletion were highly resistant to the spread of infection compared with Paragon, whilst T20 L65 plants containing a hemizygous 4D deletion showed an intermediate level of FHB resistance. The effect of dosage of the 4D deletion on FHB susceptibility demonstrates that the susceptibility factor is present in Paragon and that the enhanced resistance is associated with the 4D deletion in T20 L65.

T17 L65 had similarly high levels of FHB resistance to T20 L65 and was significantly more resistant than wild type Paragon. T15 L49 was significantly more susceptible than Paragon but this is presumably due to one or more unknown background deletions that would otherwise be contributing towards resistance. These background deletions may be masking the effect of the loss of the 4D susceptibility factor, which would be the case assuming the 4D deletion in T17 L65 has indeed resulted in the loss of the FHB susceptibility factor. To confirm this, it is necessary to cross T15 L49 to Paragon, to isolate the 4D deletion. Phenotyping the cleaned line will confirm to what extent the 4D deletion in T15 L49 is responsible for the altered

FHB susceptibility. It is also possible that the 4D deletion in T15 L49 is not a single deletion a series of smaller deletions with interstitial portions of the deleted regions retained between adjacent markers. This phenomenon was relatively common in the skim sequencing data (Ramirez-Gonzalez *et al.*, unpublished). No evidence of this could be detected in T15 L49, using a higher density of KASP markers focussing on the deletion present in T17 L65. However, proximal to this, no additional genotyping has been performed since the initial screen of the gamma-irradiated Paragon population. Further genotyping is necessary to confirm this possibility. Skim sequencing T15 L49 would allow genome-wide deletions in the line to be detected, allowing the identification of which background deletions may be responsible for altered FHB susceptibility.

3.4.2 Focussed screen of the gamma-irradiated Paragon population

T17 L65 contains a distal deletion of the susceptibility interval and is highly resistant to spread of FHB. Hence, the line appeared to have lost the FHB susceptibility factor. KASP markers were designed that are capable of detecting deletions and used to saturate the interval spanning the 4D deletion in T17 L65 with markers. The markers were used to screen the gamma-irradiated Paragon population, which identified fourteen lines containing 4D deletions. However, because only a single DNA sample per line was used in the screen, it was necessary to confirm that the deletions could be reliably detected in the identified lines. These lines required disease phenotyping and hence plants grown for experimental use were genotyped to confirm the expected deletions were present. The seed for these lines came directly from the M4B1 and M4B2 stocks. The six newly identified lines containing deletions visible across more than one marker were all confirmed as true deletions. All deletions were fixed in these lines. However, all lines in which a deletion appeared to be present at a single marker could not be found and these lines were discounted as false positives. This suggests that the KASP markers are reliable in detecting larger deletions that can be detected across several markers. However, in

cases where a deletion is characterised using only a single marker, there is a higher chance of a false positive result. Hence, it is essential to confirm the deletions are real in such lines.

The line J4-50 showed a more complex deletion pattern, that appeared to alternate between a 4D deletion and a 4B deletion. It is likely that regions of both 4B and 4D contain overlapping homoeologous deletions that make deletion detection using these KASP markers unreliable. As the markers rely on annealing to at least one of either the 4B or 4D homoeologue, if deletions are present on both chromosomes, the marker will not be able to anneal correctly and hence the sample is likely to lack any fluorescence. Analysis of the skim sequencing data detected deletions on 4B (approximately 85.6- 89.6 Mbp) and 4D (approximately 61.1- 61.2 Mbp) in J4-50 (Ramirez-Gonzalez *et al.*, unpublished). These regions are indeed homoeologous with each other, which explains the unclear KASP results in the line.

The point inoculation experiment of selected deletion lines indicated that the FHB susceptibility factor is not present in the interval covered by the T17 L65 deletion. The lines containing deletions across the interval were not resistant. Furthermore, T17 L65 was highly resistant to FHB, regardless of whether the deletion was present in a homozygous state, or in a likely hemizygous state. As a result, the 4D deletion in T17 L65 is unlikely to be responsible for the FHB resistance in this line.

Interrogation of the genotyping data of T17 L65 provides evidence that homoeologue dosage of the group 4 chromosomes influences FHB susceptibility. Initially, a 4B deletion at marker BH0010.2 (targeting TraesCS4D02G098400) had been noted in line T17 L65. However, when returning to the capillary electrophoresis output data, it became apparent that the 4B deletion had been mischaracterised and it was in fact a 4D duplication present at marker BH0010.2. If the 4D duplication is indeed responsible for the resistance in T17 L65, this would suggest that dosage is critical to the outcome of manipulating the susceptibility factor. This is supported by previous

observations in Chinese Spring nullisomic-tetrasomic lines that alluded to the importance of dosage (Steed and Nicholson, unpublished-a). N4A T4D has two pairs of chromosome 4D, and hence a double dose of the susceptibility factor. However, N4A T4D was significantly more resistant to infection than euploid Chinese Spring (**Figure 3.19**). N4D T4B was significantly more susceptible than euploid Chinese Spring (**Figure 3.19**). In this line, 4D has been lost and hence a resistant phenotype is to be expected, unless the 4D susceptibility factor does have homoeologues (at least on 4B) and dosage of these homoeologues also have an influence on FHB susceptibility.

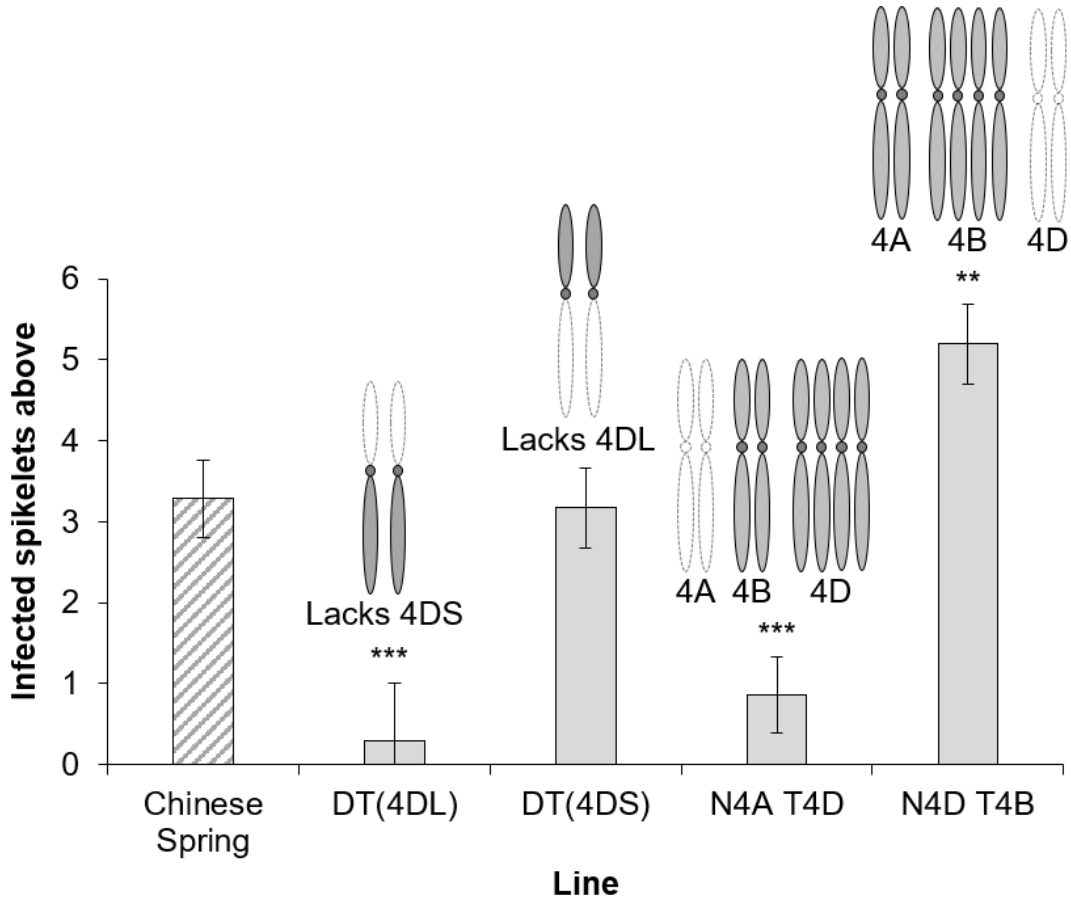

Figure 3.19 FHB disease at 17 dpi in euploid Chinese Spring, 4D ditelosomic lines DT(4DL) and DT(4DS), missing 4DS and 4DL, respectively, and nullisomic-tetrasomic lines N4A T4D and N4D T4B. Diagrams of relevant chromosomes are included above each aneuploid line to illustrate their genetic state. Predicted means were generated using a general linear model. Error bars are ± standard error. ** p< 0.01; *** p< 0.001 compared with Chinese Spring. Experiment was conducted by Steed and Nicholson (unpublished-a).

Recent developments regarding *Fhb1* suggest that this important FHB resistance QTL may also operate in a dosage dependent manner. Su *et al.* (2018) found that a deletion in a gene encoding a histidine-rich calcium-binding protein (*TaHRC*) in the *Fhb1* interval could be used to diagnose the presence of *Fhb1*. Su *et al.* (2019) have since confirmed that the deletion within *TaHRC* in the FHB QTL was associated with FHB resistance. Using RNAi and CRISPR Cas9-derived mutations of *TaHRC* in the FHB-susceptible Bobwhite, they demonstrated that the loss of function of *TaHRC* results in enhanced FHB resistance (Su *et al.*, 2019, Lagudah and Krattinger, 2019). Furthermore, overexpression of *TaHRC-R* under the maize ubiquitin promoter did not alter FHB susceptibility and hence Su *et al.* (2019) concluded that *TaHRC* is a susceptibility factor that has been knocked out in *Fhb1*-containing wheat varieties. Li *et al.* (2019) also identified *TaHRC* as the gene responsible for FHB resistance in the *Fhb1* QTL. Using three mapping populations, they fine-mapped *Fhb1* to a 23.8 kb physical interval, the only gene in which was *TaHRC* (Li *et al.*, 2019, Lagudah and Krattinger, 2019). Li *et al.* (2019) also identified the deletion in *TaHRC-R* to be responsible for the FHB resistance but claimed that the deletion still produced a functional protein that acts as a resistance factor (TaHRC-R). *TaHRC-R* was transformed into susceptible ND183 under the native promoter and overexpressed in Yangmai158 under the maize ubiquitin promoter: both resulted in enhanced FHB resistance (Li *et al.*, 2019, Lagudah and Krattinger, 2019).

Lagudah and Krattinger (2019) propose that the contradictory results of Su *et al.* (2019) and Li *et al.* (2019) may be the result of interaction of protein products of *TaHRC* on 3B and its homoeologous copies on 3A and 3D. They suggest that heteromultimers are formed from homoeologous copies of TaHRC, which are used by *Fusarium* spp. in some as-yet unknown way to aid infection (Lagudah and Krattinger, 2019). Hence, knocking out TaHRC would prevent formation of the multimers, whilst TaHRC-R may still be forming multimers but preventing correct

function. Both outcomes would prevent the fungus from exploiting the multimeric protein structures.

Further study is required to verify how *Fhb1* is operating but the model proposed by Lagudah and Krattinger (2019) possesses similarities with how the 4D susceptibility appears to be functioning in the present study. Whilst the 4D susceptibility factor is certainly not resulting in the generation of a functional resistance allele, the interaction between the 4D-encoded protein and its homoeologues (if it possesses them) appear to be dosage sensitive. Increasing or decreasing the dosage of a particular homoeologue may result in different changes in FHB susceptibility by disrupting the balance of protein products in favour of either host or pathogen. Additional experiments are necessary to verify this dosage sensitive FHB factor. Once the gene has been identified, Cadenza TILLING lines containing mutations of the 4D susceptibility factor and its homoeologues can be crossed to generate lines containing different combinations of the mutated genes. The effect of these combinations of knock-out mutations can then be confirmed by performing FHB point inoculation experiments. If available, FHB experiments using Chinese Spring isosomic lines may be informative. Isosomic lines possess two identical chromosome arms on a particular chromosome, which effectively results in a doubling of dosage of the present chromosome arm. Observing the effect of isosomic lines of 4DS, 4BS and 4AL, if available, may provide further support for the dosage effect of the susceptibility factor.

3.4.3 Gamma-irradiated Paragon lines identified from skim sequencing further refined the susceptibility factor to one of three small intervals

Deletions of the distal region of the FHB susceptibility factor were found not to be associated with enhanced FHB resistance. However, only T13 L38 and T17 L20 are known to contain small deletions of the remaining 23.1 Mbp. Two additional lines were identified from the approximately 650 gamma-irradiated Paragon lines that

were skim sequenced. The skim sequenced lines, J3-88 and J3-92, in addition to T13 L38 and T17 L20, were point inoculated to confirm the FHB phenotype of the lines. None of the lines exhibited significantly different disease levels compared to Paragon, confirming that the deletions in all four lines are unlikely to contain the susceptibility factor.

The deletion in line J8-70 extends into the remaining FHB susceptibility interval. Furthermore, it was not known how large the duplication in T17 L65 is. The sizes of the deletions in T13 L38 and T17 L20 were also quite poorly characterised. Hence, ten additional homoeologue nonspecific markers were designed across the remaining FHB susceptibility interval and used to genotype the lines. The available genotyping and phenotyping data were then interrogated to identify three small intervals that are likely to contain the FHB susceptibility factor. In these intervals are a total of 66 genes that remain candidates for the effect.

3.4.4 4A and 4B deletions homoeologous to the FHB susceptibility interval

Deletion of the FHB susceptibility factor on 4DS alone is sufficient to confer FHB resistance. This would suggest that the FHB susceptibility factor may be 4D specific or is preferentially expressed on 4D. However, if dosage is important, it remains possible that 4A and 4B homoeologues may also influence FHB susceptibility.

This is impossible to test using resources developed in Chinese Spring. The short arm of 4B contains a factor that results in sterility when deleted (Endo and Gill, 1996). Hence, the ditelosomic line missing 4BS and terminal deletion lines of 4BS are not available. Chromosome 4A has undergone substantial restructuring, including translocations from 5AL and 7BS located distally on 4AL (Hernandez *et al.*, 2012). Furthermore, a pericentric inversion has resulted in the majority of the ancestral short arm of 4A being present on the long arm (Hernandez *et al.*, 2012). Endo and Gill (1996) were unable to generate large terminal deletions of 4AL, although the reason for this is not known. The ditelosomic line lacking 4AL also does

not appear to be available. Together, this would suggest that sterility may also be associated with deletions of 4AL.

The gamma-irradiated Paragon population contains lines with small deletions. Hence, regions on 4A and 4B can be deleted without disturbing genes that confer sterility when knocked out. Lines were identified that contain deletions on 4A and 4B that span the homoeologous intervals to the 31.7 Mbp FHB susceptibility interval on 4D. The deletions do not saturate the homoeologous intervals. However, 4A deletions have complete coverage of the regions equivalent to the central and proximal FHB susceptibility intervals, in addition to part of the distal FHB susceptibility interval. Most 4B deletions were identified from the initial screen of the gamma-irradiated Paragon population. For this reason, it is unknown how far the deletions extend between markers flanking a deletion. Time limitations have prevented additional genotyping, but this should be considered for future work.

Only one line, J1-50, was significantly more resistant than wild type Paragon. However, the 4A deletion is unlikely to be responsible for resistance in J1-50, because line J6-19 contains a larger deletion, spanning the entire deletion of J1-50, but has similar disease levels to Paragon. The available deletions on 4A and 4B regions homoeologous to the FHB susceptibility interval did not show evidence of altered FHB resistance as a result of these deletions. This provides additional support to the hypothesis that the FHB susceptibility factor is present only on 4D, or the 4D copy is preferentially expressed.

3.4.5 4D specific gene candidates for the FHB susceptibility factor

No evidence was found that homoeologous 4A and 4B deletions alters FHB susceptibility. Hence, it is likely that the susceptibility factor is 4D specific or is preferentially expressed from 4D. Five genes across the distal, central and proximal FHB susceptibility intervals do not have homoeologues but show evidence of being

expressed. Hence, these five genes can be considered 4D specific and are the best candidates for the FHB susceptibility factor.

TraesCS4D02G089300 is present in the distal FHB susceptibility interval and encodes a protein with several annotated domains, including protein kinase, major sperm protein and WD40 repeat domains. VAP27, a protein with a major sperm protein-like domain, was found to interact with the tomato resistance protein Cf-9 (Laurent *et al.*, 2000). Furthermore, protein kinase domains are often present in resistance genes and are involved in downstream resistance signalling (Corrion and Day, 2015). Hence, it is possible that TraesCS4D02G089300 is a component of a disease-induced signalling cascade that the fungus has exploited to compromise plant resistance.

There is no functional information available for TraesCS4D02G095200, which is present in the central FHB susceptibility interval. This gene may be responsible for increased FHB susceptibility through the action of previously uncharacterised domains.

TraesCS4D02G095300 encodes a BURP protein and is located in the central FHB susceptibility interval. Such proteins are plant specific and are involved in responding to abiotic stresses, such as drought and salinity (Sun *et al.*, 2019, Li *et al.*, 2016). Furthermore, *BURP* genes have been implicated in phytohormone signalling, particularly abscisic acid (ABA) (Sun *et al.*, 2019, Li *et al.*, 2016). Increased abscisic acid concentrations are associated with increased susceptibility to FHB (Gordon *et al.*, 2016, Buhrow *et al.*, 2016). Hence, a *BURP* gene could feasibly be responsible for increased FHB susceptibility.

TraesCS4D02G106600 and TraesCS4D02G107000 are both present in the proximal FHB susceptibility interval and encode LRR and LRR-RK proteins, respectively. If one of these genes is implicated in promoting FHB susceptibility, they may be functioning similarly to host sensitivity genes important in the interaction of

necrotrophic pathogens, such as *Parastagonospora nodorum* and *Pyrenophora tritici-repentis* (Francki, 2013, Faris *et al.*, 2013). An LRR gene has been found to be associated with increased susceptibility to *F. graminearum* in soybean (Zhang *et al.*, 2019).

It remains possible that a gene that does have homoeologues on 4A and/ or 4B is responsible for the effect. The effect on FHB susceptibility being isolated to 4D may be due to preferential expression of the 4D copy, or due to diverged function of the homoeologous genes.

Perhaps the most interesting gene with 4A and 4B homoeologues is TraesCS4D02G093200, which encodes an Mlo-like protein. *Mlo* is a known powdery mildew susceptibility gene originally identified in barley (Jorgensen, 1992). Mutations of *mlo* results in durable mildew resistance but has also been demonstrated to compromise resistance to hemibiotrophic and necrotrophic pathogens under certain conditions (Kusch and Panstruga, 2017). *Mlo-like* genes have not been implicated in susceptibility to other fungal pathogens but their function in plants remains elusive.

Aranyi *et al.* (2014) performed powdery mildew experiments on the same Martonvasari9 wheat-barley introgressions that identified the FHB susceptibility factor (Giovannelli, 2012). Their data appeared to show mildew resistance in the 4H(4D) substitution but not the 4H addition line (Aranyi *et al.*, 2014). Surprisingly, this would suggest that deleting the FHB susceptibility factor also confers resistance to powdery mildew. To confirm this, a powdery mildew experiment was conducted on 4H(4D) substitution and 4H addition lines, in addition to Chinese Spring 4D ditelosomic lines (with appropriate wild type control lines). However, none of the lines tested showed increased resistance to any of the four wheat powdery mildew isolates tested (data not shown). Hence, the results of Aranyi *et al.* (2014) could not be verified and, furthermore, no evidence was found that the FHB susceptibility factor has any influence on powdery mildew susceptibility. If *Mlo-like* is confirmed as

the FHB susceptibility factor, this gene does not appear to alter powdery mildew susceptibility.

Another gene in the FHB susceptibility intervals, with homoeologues and a function less implicated in host-pathogen interactions, may also be involved. Cadenza TILLING lines have been acquired for 4D specific genes where mutants are available. Additional genotyping of lines J8-70 and T13 L38, to more precisely characterise the proximal deletion breakpoints in these lines, will allow for the elimination of additional genes from the distal and proximal FHB susceptibility intervals, respectively.

3.4.6 Concluding remarks

In this chapter, a deletion mapping approach using a gamma-irradiated Paragon population, has been successfully utilised to significantly refine a 31.7 Mbp interval on 4DS associated with FHB susceptibility. The number of gene candidates has been reduced from 274 to 66 genes (IWGSC, 2018). Furthermore, only five of these genes are specific to 4D and they will be prioritised for verification using TILLING. This advance makes the next steps in identifying the gene, or genes, responsible for the FHB susceptibility much more achievable.

Chapter 4: Mapping a DON resistance factor on chromosome 4D in wheat

4.1 Introduction

Many studies have demonstrated that plants are capable of detoxifying DON by glucosylation. In *Arabidopsis thaliana*, a UDP glucosyltransferase (UGT) protein, encoded by *AtUGT73C5* (also known as *DOGT1*), was found that chemically modifies DON to the less toxic DON-3-*O*-glucoside (D3G) (Poppenberger *et al.*, 2003). Furthermore, Poppenberger *et al.* (2003) demonstrated that overexpression of *AtUGT73C5* resulted in improved resistance to DON. The barley UGT, *HvUGT13248*, is more highly upregulated in response to trichothecene producing *F. graminearum*, than following inoculation with the *tri5* mutant that is unable to synthesise trichothecenes (Boddu *et al.*, 2007). Further study identified the same gene to be upregulated following application of purified DON (Gardiner *et al.*, 2010). Expression of *HvUGT13248* in both *Arabidopsis thaliana* and yeast confirmed that the gene improved DON resistance by converting DON to D3G (Schweiger *et al.*, 2010, Shin *et al.*, 2012). Transforming wheat with *HvUGT13248*, under the maize ubiquitin promoter, resulted in high levels of resistance to FHB (Li *et al.*, 2015). In addition to work on the barley UGT, it has been demonstrated that overexpression of the native wheat UGT, $TaUGT_3$, also results in high levels of FHB resistance (Xing *et al.*, 2018).

Whilst glucosylation appears to be the primary metabolization pathway for detoxifying DON in wheat, there is evidence that wheat utilises more diverse means of DON detoxification. Kluger *et al.* (2013) used an untargeted metabolomics approach to detect metabolised forms of DON from wheat heads of the susceptible cultivar Remus. Unmodified DON, D3G, and an additional eight distinct metabolised forms of DON, were detected (Kluger *et al.*, 2013). Of these, a DON-glutathione conjugate was identified, in addition to two glutathione-related metabolites, DON-*S*-

cysteine and DON-*S*-cysteinyl-glycine (Kluger *et al.*, 2013). The remaining five DON metabolites have since been putatively annotated as DON-hexitol, DON-di-hexoside, DON-malonylglucoside, “DON-2H”-glutathione and 15-acetyl-DON-3-β-D-glucoside (Kluger *et al.*, 2015).

Bacteria are capable of detoxifying DON by different means, including epimerisation, de-epoxidation and acetylation. In *Devosia mutans*, a two-step epimerisation pathway converts DON to 3-*epi*-DON (Carere *et al.*, 2018a). A dehydrogenase protein, DepA, oxidises DON to 3-*keto*-DON, which is then converted to 3-*epi*-DON by an aldo-keto reductase, DepB (Carere *et al.*, 2018a, Carere *et al.*, 2018b). In *Sphingomonas* sp., however, an aldo-keto reductase protein appears to be responsible for the conversion of DON to 3-*keto*-DON (He *et al.*, 2017).

Bacteria extracted from chicken intestine have been demonstrated to be capable of both de-epoxidation and acetylation of trichothecene mycotoxins under anaerobic conditions (Young *et al.*, 2007). Several bacterial isolates were identified that could de-epoxidise DON to de-epoxy-4-DON (Yu *et al.*, 2010).

A trichothecene-3-acetylase protein, encoded by *Tri101*, was identified in *F. sporotrichioides* that can acetylate trichothecene mycotoxins, including DON (Kimura *et al.*, 1998, McCormick *et al.*, 1999). Transgenic wheat plants containing *Tri101* were partially resistant to the spread of FHB (Okubara *et al.*, 2002).

Experiments described in Chapter 2, in the variety Chinese Spring, identified a possible DON resistance factor on the short arm of chromosome 4D. In this chapter, the 4.2 Mbp interval is interrogated to attempt to identify the gene responsible for the effect.

4.2 Materials and Methods

4.2.1 Plant material

Lines containing deletions across the DON resistance factor were identified from a gamma-irradiated population of the UK spring wheat variety Paragon, produced by Shaw *et al.* (2013). Further development of the population, described in Chapter 3, resulted in the generation of 1860 lines of bulked seed at the M4 generation.

Four Cadenza TILLING lines were obtained from the Germplasm Resource Unit, John Innes Centre, Norwich, UK. CZ1140 possesses a homozygous premature stop codon within TraesCS4D02G078200. CZ0320 contains a homozygous premature stop codon in the gene TraesCS4D02G078600. In addition, two randomly selected lines, CZ0346A and CS0479B, were used as controls to observe the effect of random mutations on DON susceptibility.

4.2.2 Gene expression and sequence variation of candidate genes

The expression of genes within the DON resistance interval were examined in an RNA-seq dataset of genes that showed altered expression in response to purified DON at 6 h and 24 h post application in root tissue of the wheat variety Hobbit Sib. Access to the dataset was kindly provided by Santos *et al.* (unpublished). The wheat RNA-seq database, expVIP, was used to search for any altered expression of genes in the DON resistance interval to FHB infection (Ramírez-González *et al.*, 2018, Borrill *et al.*, 2016).

Sequences of candidate genes from the IWGSC Refseq v1.1 assembly were retrieved from Ensembl Plants (EMBL-EBI, 2019, IWGSC, 2018). BLAST searches were made to the UK spring wheat varieties, Paragon and Cadenza, (Earlham Institute, 2019, 10+ Wheat Genomes Project, 2019).

4.2.3 Genotyping of the gamma-irradiated Paragon population

Eleven gene-based KASP markers were designed, as described in Chapters 2 and 3, to detect deletions at the position of homoeologous genes on 4DS and 4BS (**Table 4.1** and **Table 4.2**). Markers are split into two tables to distinguish between the homoeologues annealing to the HEX and FAM fluorophores. The 4A homoeologue was prevented from amplifying using a SNP in the common marker, which enabled the markers to function as on a pseudotetraploid. Three markers (BH_4D076100, BH_4D076500 and BH_4D077700) were designed across the DON resistance interval, with an additional eight genes used in Chapter 3 to characterise the 4D deletions in T19 L19 and T17 L65. KASP markers were designed and utilised, as described in Chapter 2 (p. 34-5).

Table 4.1 Primer sequences for the KASP markers designed to detect deletions on the short arm of chromosome 4D across the DON resistance interval, including the genes targeted on 4D and their corresponding physical positions (bp). the HEX tail was attached to the primer corresponding to the 4D homoeologues and the FAM tail to the 4B homoeologues.

Marker	Sequence (HEX 4D, FAM 4B, Common)	4D gene	Physical position (bp)
BH_4D076100	GAAGGTCGGAGTCAACGGATTTGCTCTTCAGCACAAGACAC	TraesCS4D02G076100	50,757,331-50,759,427
	GAAGGTGACCAAGTTCATGCTTGCTCTTCAGCACAAGACAA		
	GGAAGTCGGTCATTTGATGC		
BH_4D076500	GAAGGTCGGAGTCAACGGATTTCGGTGCCGTAAAACCCTTTC	TraesCS4D02G076500	50,974,621-50,978,309
	GAAGGTGACCAAGTTCATGCTTCGGTGCCGTAAAACCCTTTT		
	GGTGGTGCCCTTCATGATAA		
BH_4D077700	GAAGGTCGGAGTCAACGGATTTGAAGCATATGAAGCTTGGC	TraesCS4D02G077700	51,793,621-51,799,330
	GAAGGTGACCAAGTTCATGCTTGAAGCATATGAAGCTTGGG		
	TATTGCTGCCCTCTGTCTG		
BH_4D078800	GAAGGTCGGAGTCAACGGATTGCAAGAAGACGAAAAGACTCGA	TraesCS4D02G078800	52,763,212-52,765,266
	GAAGGTGACCAAGTTCATGCTGCAAGAAGACGAAAAGACTCGT		
	TCACGGTTTCTTTGATGTTCA		
BH_4D081100	GAAGGTCGGAGTCAACGGATTGCACTAAATCGCCTTAAAACTGTA	TraesCS4D02G081100	55,046,522-55,052,757
	GAAGGTGACCAAGTTCATGCTGCACTAAATCGCCTTAAAACTGTC		
	GATCAACCCAAGAAGCAAGTGT		
BH_4D082100	GAAGGTCGGAGTCAACGGATTCAAGAGATGACAAGTGCACATTC	TraesCS4D02G082100	55,559,928-55,564,146
	GAAGGTGACCAAGTTCATGCTCAAGAGATGACAAGTGCACATTT		
	CTTGGCATAATAGGAGGCTATG		

Table 4.1 (continued) Primer sequences for the KASP markers designed to detect deletions on the short arm of chromosome 4D across the DON resistance interval, including the genes targeted on 4D and their corresponding physical positions (bp). the HEX tail was attached to the primer corresponding to the 4D homoeologues and the FAM tail to the 4B homoeologues.

Marker	Sequence (HEX 4D, FAM 4B, Common)	4D gene	Physical position (bp)
BH_4D082800	GAAGGTCGGAGTCAACGGATTTATCAACCTTATCAGCACTACCT	TraesCS4D02G082800	56,716,994-56,723,032
	GAAGGTGACCAAGTTCATGCTTATCAACCTTATCAGCACTACCA		
	GCAAAGTAGTTGCTACCCC		

Table 4.2 Primer sequences for the KASP markers designed to detect deletions on the short arm of chromosome 4D across the DON resistance interval, including the genes targeted on 4D and their corresponding physical positions (bp). the FAM tail was attached to the primer corresponding to the 4D homoeologues and the HEX tail to the 4B homoeologues.

Marker	Sequence (FAM 4D, HEX 4B, Common)	4D gene	Physical position (bp)
BH_4D078200	GAAGGTGACCAAGTTCATGCTGACCGCCCTTTCACAGCA	TraesCS4D02G078200	52,492,099-52,496,665
	GAAGGTCGGAGTCAACGGATTGACCGCCCTTTCACAGCT		
	ACTGATCCATGGTGGTTGCTC		
BH_4D078600	GAAGGTGACCAAGTTCATGCTCATTCAGTGCTGCAATGGAGC	TraesCS4D02G078600	52,751,281-52,754,472
	GAAGGTCGGAGTCAACGGATTCATTCAGTGCTGCAATGGAGT		
	CGTCAGTGTATATCATTGTTCTGG		
BH_4D079900	GAAGGTGACCAAGTTCATGCTTGGAAGGAGGTGTTCGACA	TraesCS4D02G079900	53,862,557-53,864,923
	GAAGGTCGGAGTCAACGGATTTGGAAGGAGGTGTTCGACC		
	CAGGTCCTCGGGCCACTT		
BH_4D080200	GAAGGTGACCAAGTTCATGCTGAAGCCATCCAACTCGAAGCC	TraesCS4D02G080200	54,261,815-54,266,356
	GAAGGTCGGAGTCAACGGATTGAAGCCATCCAACTCGAAGCA		
	ACCAGGATGTAATGCCCTTTC		

4.2.4 DON application experiments

A DON application experiment on Cadenza TILLING mutant lines was conducted in the summer of 2018 in a polytunnel (DON_CZ_Poly_18). Plants were arranged in a randomised complete block design with four replicates, each containing four plants per line. A DON application experiment was performed in spring 2019 under controlled conditions, on gamma-irradiated Paragon lines (DON_PG_CER_19). Plants were organised in a randomised complete block design consisting of three replicates, containing five or six plants per line.

DON was applied to the primary wheat head of each plant at mid-anthesis, using a protocol modified from Lemmens *et al.* (2005). DON (> 98 % pure) was kindly provided by Dr Marc Lemmens, which was was purified at IFA-Tulln, Austria, as described by Altpeter and Posselt (1994). The DON application protocol is described in detail in Chapter 2 (p. 40). Each treated wheat head received a total application of 0.8 mg DON. At regular intervals post-application, bleaching damage was assessed on each treated head. In both experiments, the number of DON damaged spikelets was recorded above and below the application point.

4.2.5 Dissection of DON treated heads

Following the DON experiment of the gamma-irradiated Paragon lines (DON_PG_CER_19), DON treated heads were harvested. Grain was removed above and below the DON application point. Spikelets to which DON was applied were discounted but invariably did not produce seed. The grain obtained from above and below the point of application were separately counted and weighed.

4.2.6 Statistical analysis

DON bleaching data were analysed using a linear mixed model using GenStat software (18th edition, VSN International). ANOVA tables for all statistical analyses are presented in the appendix (p. 195-7). Residuals of DON bleaching data were visually checked for conformation to a normal distribution and that residuals were

largely independent of the fitted values. Where this was not the case, data were log10 transformed prior to statistical analysis, which was successful in correcting for the necessary assumptions. In the model, line was included as a fixed term and replicate as a random term. During model construction, application date and the interaction between application date and line were included as fixed terms and plant number nested within replicate was included as a random term. However, the terms did not have a significant effect on the model and hence were omitted for clarity. In all cases, the final model included line as a fixed term and replicate as a random term. Predicted means and standard errors were generated for the lines included in the linear mixed model and were back transformed for presentation. Pairwise differences between the wild type line and mutant/ deletion lines were tested by Fisher's Protected Least Significant Difference.

For grain data, average grain weights were calculated for grain obtained from each head above and below the application point (grain weight/ grain number). For each head, the ratio of average grain weight above and below the application point was calculated (average grain weight above/ average grain weight below). Hence, a ratio value of 1.0 indicates no difference in grain weight above and below the application point. A ratio value above or below 1.0 indicates an imbalance in the grain weight above the application point compared to the grain weight below the application point.

Residuals of the DON grain ratio data were normally distributed and largely independent of fitted values. Hence, transformation of these data was not necessary. Grain ratio values were analysed using a linear mixed model, using the same model construction procedure as described above. The model accounted for line as a fixed term and replicate as a random term. Predicted means and standard errors were calculated for lines included in the linear mixed model. Pairwise comparisons between wild type Paragon and deletion lines were tested by Fisher's Protected Least Significant Difference.

4.3 Results

4.3.1 Interrogating genes within the DON resistance interval

The DON resistance interval lies between TraesCS4D02G076000 (4D: 50,641,002-50,644,244 bp) and TraesCS4D02G081000 (4D: 54,808,771-54,812,009 bp). Excluding these genes, which lie immediately outside the interval, there are an estimated 49 high confidence genes in this region (IWGSC RefSeq v1.1; **Table 4.3**).

There are no glucosyltransferase genes within the DON resistance interval. However, there are two genes annotated as aldo-keto reductase genes (TraesCS4D02G078200 and TraesCS4D02G078600, designated *TaAKR-D1* and *TaAKR-D2*, respectively). Aldo-keto reductase genes have been demonstrated to be capable of detoxifying DON in bacteria and are hence interesting gene candidates for the DON resistance factor (He *et al.*, 2017, Carere *et al.*, 2018b).

TaAKR-D1 and *TaAKR*-D2 genes were codon-optimised for expression in *E. coli* and synthesised. The synthesised *TaAKR-D1* and *TaAKR*-D2 genes in pET plasmids were sent to collaborators at Guelph Research and Development Centre, Agriculture and Agri-Food Canada, Canada, to confirm whether either gene encodes a protein capable of epimerising DON or 3-*keto*-DON. They transformed *E. coli* with *TaAKR-D1* and *TaAKR*-D2 but neither gene was expressed and hence they were unable to purify either protein (Carere and Zhou, unpublished).

Table 4.3 List of the forty-nine genes in the DON resistance interval. The physical positions (bp) and functional annotations are provided for each gene, which were extracted from Ensembl Plants (EMBL-EBI, 2019).

Gene	Position (bp)	Functional annotation
TraesCS4D02G076100	50,757,723-50,758,993	Zinc finger (RING-type)
TraesCS4D02G076200	50,769,402-50,771,961	Protein of unknown function (DUF620)
TraesCS4D02G076300	50,792,297-50,792,620	Zinc finger (CCHC-type)
TraesCS4D02G076400	50,888,586-50,889,461	Gibberellin regulated protein
TraesCS4D02G076500	50,974,900-50,977,709	NRAMP family
TraesCS4D02G076600	50,990,222-51,006,711	Methyltransferase
TraesCS4D02G076700	51,007,653-51,010,870	Myb/SANT-like domain
TraesCS4D02G076800	51,071,696-51,077,502	Protein of unknown function (DUF760)
TraesCS4D02G076900	51,286,599-51,288,866	Cyclin
TraesCS4D02G077000	51,295,762-51,296,753	Zinc finger (C2H2-type)
TraesCS4D02G077100	51,314,635-51,315,295	No annotation
TraesCS4D02G077200	51,347,689-51,348,336	No annotation
TraesCS4D02G077300	51,455,328-51,455,990	No annotation
TraesCS4D02G077400	51,554,004-51,558,494	Fumarylacetoacetase-like
TraesCS4D02G077500	51,608,464-51,609,747	AP2/ERF domain
TraesCS4D02G077600	51,615,420-51,616,874	Lateral organ boundaries
TraesCS4D02G077700	51,793,934-51,800,093	BTB/POZ and NPH3 domains

Table 4.3 (continued) List of the forty-nine genes in the DON resistance interval. The physical positions (bp) and functional annotations are provided for each gene , which were extracted from Ensembl Plants (EMBL-EBI, 2019).

Gene	Position (bp)	Functional annotation
TraesCS4D02G077800	52,014,023-52,014,534	Cysteine proteinase inhibitor
TraesCS4D02G077900	52,215,095-52,216,001	Zinc finger (C2H2-type)
TraesCS4D02G078000	52,467,388-52,470,105	Serpin superfamily
TraesCS4D02G078100	52,470,433-52,473,315	SNF1-type serine-threonine protein kinase
TraesCS4D02G078200	52,492,099-52,496,665	NADP-dependent oxidoreductase, aldo-keto reductase
TraesCS4D02G078300	52,496,892-52,497,366	No annotation
TraesCS4D02G078400	52,620,984-52,623,428	NAD kinase
TraesCS4D02G078500	52,748,593-52,749,372	No annotation
TraesCS4D02G078600	52,751,281-52,754,472	NADP-dependent oxidoreductase, aldo-keto reductase
TraesCS4D02G078700	52,753,957-52,756,579	ssDNA-binding protein
TraesCS4D02G078800	52,762,678-52,766,546	Lateral organ boundaries
TraesCS4D02G078900	52,775,740-52,779,092	Ribosomal protein L25
TraesCS4D02G079000	52,779,401-52,780,851	F-box
TraesCS4D02G079100	53,231,602-53,237,375	DNA polymerase IV
TraesCS4D02G079200	53,237,605-53,242,400	Calcium-transporting ATPase
TraesCS4D02G079300	53,242,266-53,248,192	Condensin-2 complex subunit, armadilo-like motif

Table 4.3 (continued) List of the forty-nine genes in the DON resistance interval. The physical positions (bp) and functional annotations are provided for each gene.

Gene	Position (bp)	Functional annotation
TraesCS4D02G079400	53,493,887-53,496,177	Cyclin
TraesCS4D02G079500	53,750,729-53,752,656	Helix-loop-helix (Myc-type)
TraesCS4D02G079600	53,758,442-53,762,789	Semialdehyde dehydrogenase, N-acetyl-gamma-glutamyl-phosphate reductase (type-1)
TraesCS4D02G079700	53,772,857-53,775,601	Transcription termination factor (mitochondrial/ chloroplastic)
TraesCS4D02G079800	53,777,911-53,778,865	Protein glutamine dumper
TraesCS4D02G079900	53,862,639-53,864,410	Oxoglutarate/ iron-dependent dioxygenase
TraesCS4D02G080000	54,052,706-54,055,530	No annotation
TraesCS4D02G080100	54,126,623-54,127,674	Zinc finger (Dof-type)
TraesCS4D02G080200	54,261,815-54,266,356	B3 DNA-binding domain
TraesCS4D02G080300	54,407,216-54,408,847	Zinc finger (GRF-type)
TraesCS4D02G080400	54,474,398-54,476,568	B3 DNA-binding domain
TraesCS4D02G080500	54,604,350-54,605,788	B3 DNA-binding domain
TraesCS4D02G080600	54,620,793-54,622,251	Protein of unknown function (DUF1685)
TraesCS4D02G080700	54,678,101-54,684,917	ATP-dependent (S)-NAD(P)H-hydrate dehydratase
TraesCS4D02G080800	54,787,728-54,802,178	Exocyst complex component Sec3
TraesCS4D02G080900	54,805,532-54,807,867	Ribosomal protein S27e

4.3.2 Variation of *TaAKR-D1* and *TaAKR-D2* in Chinese Spring, Paragon and Cadenza

BLAST searches of *TaAKR-D1* and *TaAKR-D2* genomic sequences were made against the genome assemblies of Paragon and Cadenza. *TaAKR-D1* was identical between Chinese Spring, Paragon and Cadenza. *TaAKR-D2* was identical between Chinese Spring and Paragon. *TaAKR-D2* was identical between Chinese Spring and Cadenza after nucleotide 1489 of the query sequence. This apparent difference is likely to be due to the fragmented nature of the Cadenza assembly.

4.3.3 DON application to TILLING lines containing mutations of *TaAKR-D1* and *TaAKR-D2* do not show altered response to DON

Cadenza TILLING lines were obtained, which contain homozygous mutations resulting in premature stop codons in *TaAKR-D1* (CZ1140) and *TaAKR-D2* (CZ0320). Wild type Cadenza, in addition to two randomly selected Cadenza TILLING lines (CZ0346A and CS0479B), were used as control lines. These lines were included in a DON application experiment performed in a polytunnel in summer 2018 (DON_CZ_Poly_18). Cadenza did not respond to DON application in the same way as Chinese Spring. Very few bleaching symptoms were observed in response to DON and symptoms were generally limited to spikelets immediately above the application point. Hence, data are presented as the number of DON damaged spikelets above the point of DON application. Wild type Cadenza (mean= 0.84) showed similar levels of DON damage to both control TILLING lines, CZ0346A (mean= 1.10, p=0.370) and CZ0479B (mean= 1.13, p=0.283) (**Figure 4.1**). Neither CZ0320 (mean= 0.54, p= 0.253), nor CZ1140 (mean= 0.73, p= 0.693), were significantly different from wild type Cadenza (**Figure 4.1**).

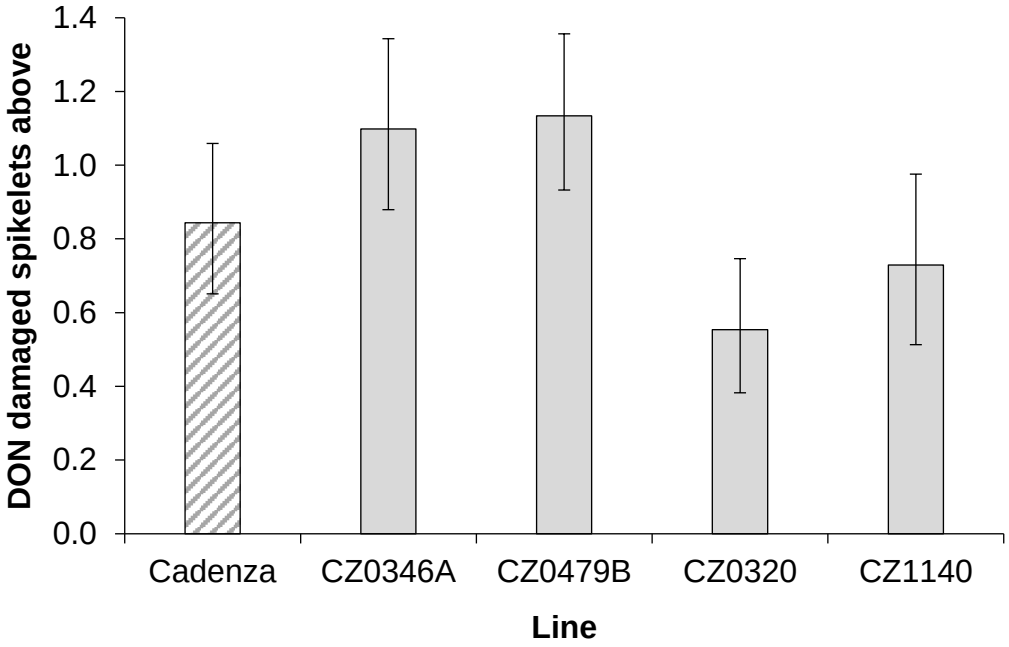

Figure 4.1 Number of DON damaged spikelets above application at 15 days post DON application. The experiment was conducted in a polytunnel in summer 2018. Lines CZ0320 and CZ1140 contain premature stop codons in aldo-keto reductase genes *TaAKR-D2* and *TaAKR-D1*, respectively. CZ0346A and CZ0479B were randomly selected from the Cadenza TILLING mutants as control lines, in addition to wild type Cadenza. Statistical analyses were conducted using log10 transformed values. Predicted means were generated using a linear mixed model. Presented data were back transformed. Error bars are ± standard error. No significant difference was found compared with Cadenza in any of the mutant lines.

4.3.4 Screening the gamma-irradiated Paragon population for lines containing deletions within the DON resistance interval

Eleven KASP markers, spanning the DON resistance interval, were used to screen the gamma-irradiated Paragon population (**Figure 4.2**). J3-51 contains a small deletion at 51.79 Mbp, which does not extend further than the adjacent markers, at 50.95 Mbp and 52.49 Mbp (**Figure 4.2**). T19 L19 and T17 L65 were both previously identified in the first screen of the gamma-irradiated Paragon population for the FHB susceptibility factor (Chapter 3). The 4D deletion in T19 L19 begins between 52.49 Mbp and 52.75 Mbp and extends beyond the proximal flank of the DON resistance interval (**Figure 4.2**). The line T19 L19 retains 2.11 Mbp of the DON resistance interval. T17 L65 is deleted across all markers spanning the DON resistance interval (**Figure 4.2**). A marker obtained from RAGT Seeds, targeting 16.53 Mbp on 4DS, confirmed that the 4D deletion in T17 L65 extends well beyond the distal flank of the DON resistance interval (data not shown).

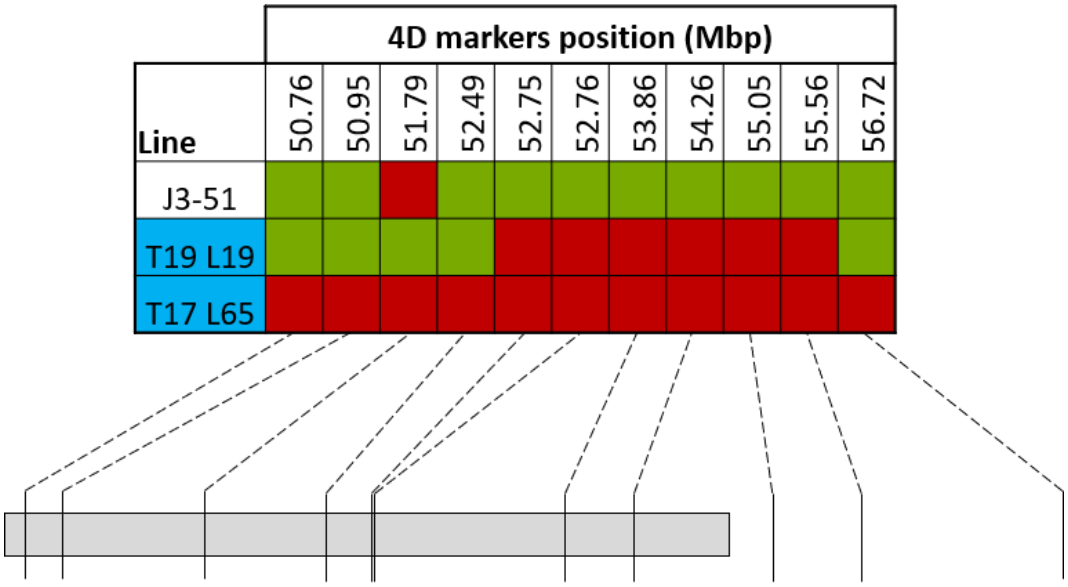

Figure 4.2 Eleven KASP markers were used to screen for deletions across the DON resistance interval in a gamma-irradiated Paragon population. The lines highlighted in blue were detected in a previous screen of the population. Red boxes indicate a 4D deletion at the position of the marker. Green boxes indicate a wild type signal. The physical distance between markers is indicated below the genotyping diagram. The interval inferred to contain the DON resistance factor is indicated by the grey bar.

4.3.5 DON application to Paragon lines containing deletions in the DON resistance interval on 4DS

Gamma-irradiated Paragon lines, containing deletions within the DON resistance interval, were used in a DON application experiment performed under controlled conditions in spring 2019 (DON_PG_CER_19). Paragon responded to DON application in a similar way to Cadenza. Bleaching symptoms were very limited, with most treated heads showing little damage in response to DON application. For this reason, treated heads were scored in the same way as Cadenza and data are presented as the number of DON damaged spikelets above the application point. For all lines, there was no significant difference compared with wild type Paragon (**Figure 4.3A**).

To confirm whether DON application had any effect on grain filling, the grain of DON treated heads were harvested after senescence. A ratio was calculated between average grain weight above/ below the DON application point. Paragon showed a small difference in grain weight above versus below the application point (mean= 0.774; **Figure 4.3B**). Furthermore, all three deletion lines, J3-51 (mean= 0.822, p= 0.511), T19 L19 (mean= 0.780, p= 0.925) and T17 L65 (mean= 0.730, p= 0.564), had very similar ratio values to Paragon, and none were significantly different than that of Paragon (**Figure 4.3B**). Therefore, it was not possible to use this information to further refine the DON resistance interval.

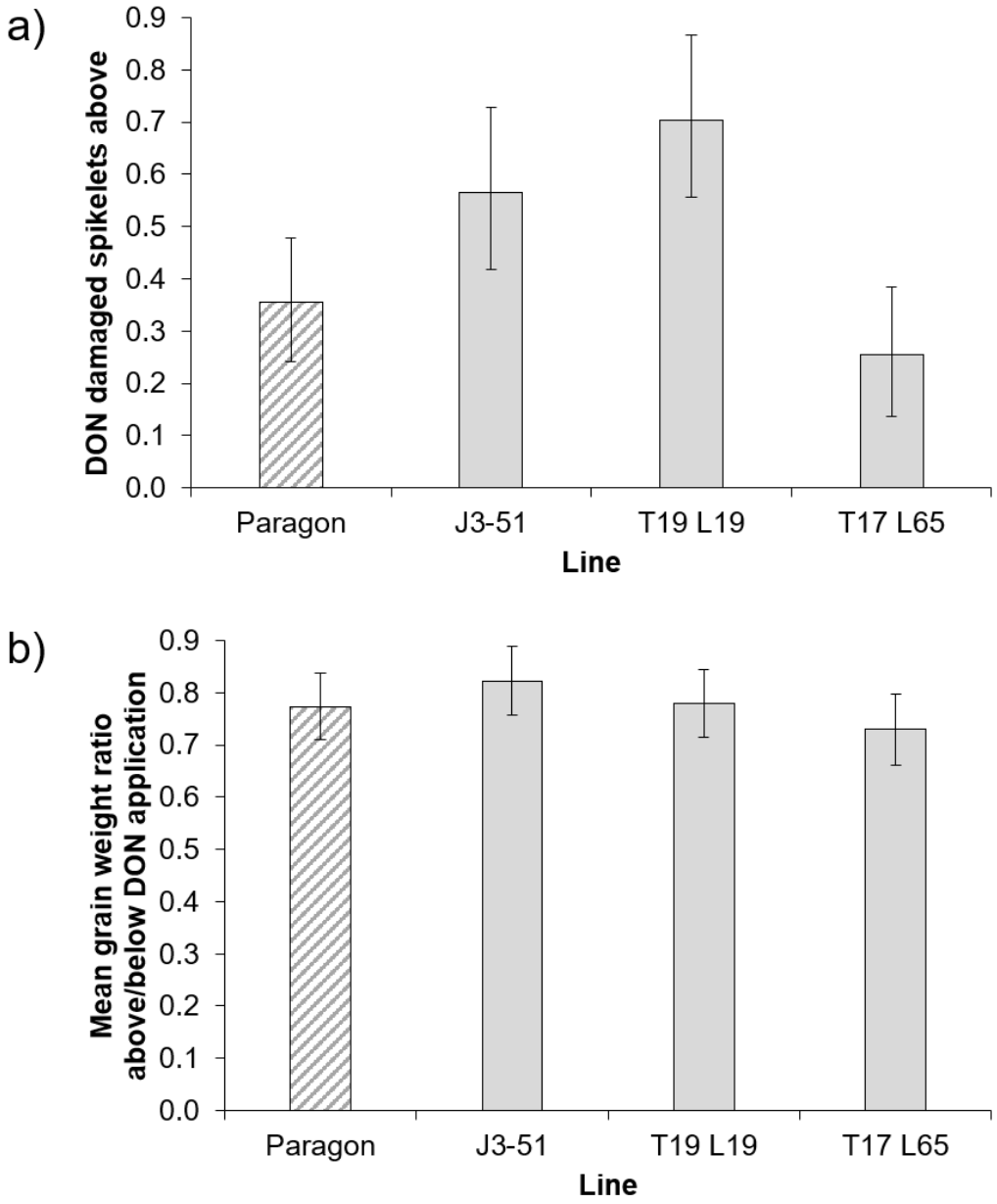

Figure 4.3 DON application experiment of Paragon and three deletion lines, conducted under controlled conditions. a) Percentage of DON damaged spikelets above application 10 days post DON application, and b) mean grain weight ratio above/ below DON application point. Statistical analyses of grain weight data were log10 transformed and presented values have been back transformed. In both cases, predicted means were calculated using a linear mixed model. Error bars are ± standard error. No significant difference was found compared with Paragon in any of the deletion lines.

4.3.6 Expression of genes in the DON resistance interval

The wheat RNA-seq database expVIP was used to search for genes that are upregulated in response to FHB (Ramírez-González *et al.*, 2018, Borrill *et al.*, 2016). Specifically, RNA-seq data from Gou *et al.* (2016) were used. They point inoculated wheat heads, of the cultivar Chinese Spring, with either water (mock) or *F. graminearum* and rachis tissue samples were taken at 4 dpi. RNA was extracted from the samples, which was used for the RNA-seq. Most genes in the DON resistance interval showed no evidence of differential expression in response to FHB infection (**Table 4.4**). Neither *AKR-D1* (TraesCS4D02G078200) nor *AKR-D2* (TraesCS4D02G078600) show evidence of upregulation in response to FHB (**Table 4.4**). However, TraesCS4D02G079900 is highly upregulated following FHB infection (151.18 ± 18.92 tpm) compared to mock treatment (6.19 ± 3.13 tpm, **Table 4.4**). Homoeologues of TraesCS4D02G079900 (TraesCS4A02G234100 and TraesCS4B02G081200) are also strongly upregulated in the same dataset (**Table 4.5**). TraesCS4D02G079900, at 53.86 Mbp on 4D, encodes an iron-dependent dioxygenase (**Table 4.3**). TraesCS4D02G079900 was also modestly upregulated at both 6 h (log2(fold change)= 0.551, p= 0.0016) and 24 h (log2(fold change)= 0.838, p< 0.001) in response to DON application in root tissue of wheat variety Hobbit Sib (Santos *et al.*, unpublished). TraesCS4A02G234100 (log2(fold change)= 0.577, p< 0.001) and TraesCS4B02G081200 (log2(fold change)= 0.802, p< 0.001) are also slightly upregulated in response to DON at 24 h post application. A BLAST search confirmed that the Chinese Spring genomic sequence of TraesCS4D02G079900 is identical to both Paragon and Cadenza.

Table 4.4 Gene expression (tpm) ± standard error of the mean (s.e.) of genes in the DON resistance interval in the rachis of mock inoculated and FHB inoculated Chinese Spring heads. Data from Gou *et al.* (2016).

	Gene expression (tpm) ± s.e.	
Gene	**Mock**	**FHB**
TraesCS4D02G076100	0.96 ± 0.17	0.07 ± 0.12
TraesCS4D02G076200	0.59 ± 0.23	0.04 ± 0.07
TraesCS4D02G076300	No data	No data
TraesCS4D02G076400	0.45 ± 0.35	No data
TraesCS4D02G076500	No data	No data
TraesCS4D02G076600	1.18 ± 0.14	0.17 ± 0.11
TraesCS4D02G076700	2.05 ± 0.18	0.88 ± 0.41
TraesCS4D02G076800	32.78 ± 2.52	29.05 ± 3.29
TraesCS4D02G076900	0.06 ± 0.01	No data
TraesCS4D02G077000	22.32 ± 10.30	4.03 ± 2.56
TraesCS4D02G077100	0.09 ± 0.16	No data
TraesCS4D02G077200	No data	0.15 ± 0.25
TraesCS4D02G077300	No data	No data
TraesCS4D02G077400	4.84 ± 0.99	1.05 ± 0.97
TraesCS4D02G077500	No data	No data
TraesCS4D02G077600	4.78 ± 1.24	No data
TraesCS4D02G077700	12.86 ± 3.67	0.67 ± 0.20
TraesCS4D02G077800	No data	No data
TraesCS4D02G077900	0.43 ± 0.19	0.39 ± 0.45
TraesCS4D02G078000	7.68 ± 1.77	3.33 ± 1.14
TraesCS4D02G078100	8.67 ± 2.06	0.44 ± 0.53
TraesCS4D02G078200	3.82 ± 0.55	0.58 ± 0.57
TraesCS4D02G078300	1.02 ± 1.10	0.38 ± 0.66
TraesCS4D02G078400	No data	No data
TraesCS4D02G078500	2.10 ± 1.12	0.44 ± 0.76
TraesCS4D02G078600	0.44 ± 0.12	0.20 ± 0.34
TraesCS4D02G078700	7.08 ± 0.61	1.89 ± 0.67
TraesCS4D02G078800	No data	No data
TraesCS4D02G078900	6.55 ± 1.14	2.17 ± 0.37
TraesCS4D02G079000	No data	No data
TraesCS4D02G079100	1.95 ± 0.40	0.64 ± 0.60
TraesCS4D02G079200	2.46 ± 0.66	0.33 ± 0.05
TraesCS4D02G079300	0.05 ± 0.04	No data
TraesCS4D02G079400	0.38 ± 0.03	0.05 ± 0.08
TraesCS4D02G079500	No data	No data
TraesCS4D02G079600	40.90 ± 13.47	29.02 ± 10.91
TraesCS4D02G079700	2.30 ± 0.85	0.35 ± 0.26

Table 4.4 (continued) Gene expression (tpm) ± standard error of the mean (s.e.) of genes in the DON resistance interval in the rachis of mock inoculated and *F. graminearum* inoculated Chinese Spring heads. Data from Gou *et al.* (2016).

	Gene expression (tpm) ± s.e.	
Gene	**Mock**	**FHB**
TraesCS4D02G079800	6.48 ± 2.23	No data
TraesCS4D02G079900	6.19 ± 3.13	151.18 ± 18.92
TraesCS4D02G080000	No data	No data
TraesCS4D02G080100	No data	No data
TraesCS4D02G080200	2.82 ± 0.70	0.30 ± 0.27
TraesCS4D02G080300	No data	No data
TraesCS4D02G080400	No data	No data
TraesCS4D02G080500	No data	No data
TraesCS4D02G080600	36.66 ± 11.25	16.43 ± 1.89
TraesCS4D02G080700	17.80 ± 1.59	12.72 ± 3.12
TraesCS4D02G080800	0.25 ± 0.03	0.08 ± 0.07
TraesCS4D02G080900	45.66 ± 11.68	20.02 ± 7.43

Table 4.5 Expression of homoeologous genes TraesCS4A02G234100, TraesCS4B02G081200 and TraesCS4D02G079900 in the rachis of mock inoculated and *F. graminearum* inoculated Chinese Spring. Expression presented as transcripts per kilobase million (TPM) with standard error of the mean (s.e.). Data from Gou *et al.* (2016).

	Mock		**FHB inoculated**	
Gene	TPM	s.e.	TPM	s.e.
TraesCS4A02G234100	32.68	19.44	698.47	78.85
TraesCS4B02G081200	19.65	8.43	65.87	6.93
TraesCS4D02G079900	6.19	3.13	151.18	18.92

4.3.7 There are fifteen DON responsive genes on the distal region of 4DS

DON bleaching data of Chinese Spring 4DS terminal deletion lines suggested that the DON resistance factor was present in a 4.2 Mbp interval (Chapter 2). However, the grain weight data from the same experiment suggested that the DON resistance factor was distal to 51.6 Mbp. There are 775 genes in this distal interval but only fifteen of these genes were upregulated in response to DON application in an RNA-seq experiment conducted by Santos *et al.* (unpublished) (**Table 4.6**). TraesCS4D02G003700LC has been classified as a low confidence gene in IWGSC Refseq v1.1 and a BLAST search to NCBI suggests that this is because it is a retrotransposon (U.S. National Library of Medicine and National Centre for Biotechnology Information, 2019). TraesCS4D02G003700LC, TraesCS4D02G026600 and TraesCS4D02G075500 do not have homoeologues. Homoeologues of TraesCS4D02G049300, TraesCS4D02G055600 and TraesCS4D02G071000 do not show any evidence of differential expression. The genes TraesCS4D02G056000, TraesCS4D02G056100, TraesCS4D02G063900, TraesCS4D02G064400, TraesCS4D02G064800 and TraesCS4D02G081300 all have relatively uniform upregulation in response to DON across all three homoeologous genes. The remaining genes, TraesCS4D02G053000, TraesCS4D02G055000 and TraesCS4D02G059200, show the strongest upregulation to DON in the 4D copy and one or both other homoeologues show weaker upregulation in response to DON application. Most of the upregulated genes have been functionally annotated on Ensembl Plants (**Table 4.7**).

Table 4.6 Differential expression [log2(fold change)] of genes in the distal 51.6 Mbp region of 4DS that are upregulated in response to DON 6 h post application in root tissue of Hobbit Sib. Homoeologous genes on 4A and 4B are provided with their respective expression under the same conditions. RNA-seq data from Santos *et al.* (unpublished).

4D gene	Differential expression [log2(fold change)]	4B homoeologue	Differential expression [log2(fold change)]	4A homoeologue	Differential expression [log2(fold change)]
TraesCS4D02G003700LC	4.136	None	N/A	None	N/A
TraesCS4D02G026600	1.729	None	N/A	None	N/A
TraesCS4D02G049300	2.140	None	N/A	TraesCS4A02G265700	0.000
TraesCS4D02G053000	2.610	TraesCS4B02G052800	0.951	TraesCS4A02G262100	1.677
TraesCS4D02G055000	6.848	TraesCS4B02G054900	3.338	TraesCS4A02G259800	0.000
TraesCS4D02G055600	2.780	TraesCS4B02G055300	0.000	TraesCS4A02G259400	0.000
TraesCS4D02G056000	6.571	TraesCS4B02G056000	6.834	TraesCS4A02G258500	5.657
TraesCS4D02G056100	4.486	TraesCS4B02G055900	3.338	TraesCS4A02G258600	3.976
TraesCS4D02G059200	2.200	TraesCS4B02G059800	0.939	TraesCS4A02G255500	0.000
TraesCS4D02G063900	2.726	TraesCS4B02G065000	1.860	TraesCS4A02G249700	2.750
TraesCS4D02G064400	2.566	TraesCS4B02G065400	2.464	TraesCS4A02G249300	2.468
TraesCS4D02G064800	5.383	TraesCS4B02G065700	5.295	TraesCS4A02G248900	5.253
TraesCS4D02G071000	4.098	TraesCS4B02G072100	0.000	TraesCS4A02G242900	0.000
TraesCS4D02G075500	3.275	None	N/A	None	N/A
TraesCS4D02G081300	3.657	TraesCS4B02G083200	2.980	TraesCS4A02G232600	3.188

Table 4.7 DON responsive genes distal to 51.6 Mbp on 4DS, with functional annotations of each gene extracted from Ensembl Plants.

Gene	Functional annotation
TraesCS4D02G026600	pollen maturation gametophyte development
TraesCS4D02G049300	no known function
TraesCS4D02G053000	DUF569 actin cross-linking
TraesCS4D02G055000	alanine tRNA ligase
TraesCS4D02G055600	acyl-transferase activity
TraesCS4D02G056000	hydrolase activity, acting on acid anhydrides
TraesCS4D02G056100	no known function
TraesCS4D02G059200	peroxiredoxin-like
TraesCS4D02G063900	no known function
TraesCS4D02G064400	protein binding membrane bounded organelle
TraesCS4D02G064800	eukaryotic translation initiation factor 3 subunit G
TraesCS4D02G071000	protein binding WD40 motif
TraesCS4D02G075500	transferase activity integral component of membrane
TraesCS4D02G081300	translation initiation factor binding WD40 motif protein binding

4.4 Discussion

In Chinese Spring, the loss of the short arm of chromosome 4D was associated with increased susceptibility to DON. Furthermore, Chinese Spring lines containing larger terminal deletions of 4DS also appeared to be more susceptible to the bleaching symptoms induced by DON. This was especially striking between the lines del4DS-2 (slightly susceptible) and del4DS-4 (susceptible). These data were used to infer that a DON resistance factor is located between the deletion breakpoints of del4DS-2 and del4DS-4. Genotyping was used to more precisely characterise the deletion breakpoints in the terminal deletion lines, thereby refining the putative DON resistance factor to a 4.2 Mbp interval.

This interval was considered relatively easy to confirm whether any genes in the interval were indeed involved in DON resistance. Containing only 49 genes, it was possible to use gene functional annotations to identify the most promising gene candidates and select Cadenza TILLING mutants to attempt to verify the candidates. Furthermore, the DON resistance and FHB susceptibility intervals are adjacent and hence distal deletions of the FHB susceptibility factor in the gamma-irradiated Paragon population were also likely to extend into the DON resistance interval.

4.4.1 Functional annotation of genes in the DON resistance interval

The DON resistance interval contains 49 genes, which was considered a sufficiently small number to identify candidate genes based on their functional annotations. The glucosylation of DON to D3G by UGT proteins is well documented in plants (Schweiger *et al.*, 2010, Poppenberger *et al.*, 2003, Xing *et al.*, 2018). However, no UGT-encoding genes are present within the DON resistance interval.

Two genes encoding aldo-keto reductase proteins were particularly interesting candidates from the gene list. Epimerisation of DON by aldo-keto reductase proteins is well documented in bacteria (Carere *et al.*, 2018b, He *et al.*, 2017). An aldo-keto reductase from a strain of *Sphingomonas* sp. is capable of converting DON to 3-

keto-DON (He *et al.*, 2017). Furthermore, an aldo-keto reductase from *Devosia mutans* converts 3-*keto*-DON to 3-*epi*-DON (Carere *et al.*, 2018b). However, no such method of DON detoxification has been demonstrated in plants. The potential involvement of one or both aldo-keto reductase genes in wheat would offer a novel source of resistance to DON accumulation that may also contribute towards Type II FHB resistance.

TILLING lines with mutations resulting in premature stop codons in *TaAKR-D1* and *TaAKR-D2* were used in DON application experiments. However, no significant difference in DON-induced symptoms was observed in either line compared to wild type Cadenza. There are several reasons why mutation of the aldo-keto reductase genes may not have altered DON resistance in Cadenza. Due to time restrictions, no attempts were made to remove background mutations and hence the high number of background mutations may be disruptive enough to mask the effect. Alternatively, it may be that both aldo-keto reductase genes are involved in DON detoxification and a mutation of one gene is insufficient to observe an effect. The 4D aldo-keto reductase genes and their homoeologues may contribute differently to DON resistance in Cadenza, compared with Chinese Spring. Cadenza was far less sensitive to bleaching induced by DON, compared with experiments conducted in Chinese Spring. Hence, Cadenza may have an inherently higher tolerance to DON than Chinese Spring. This would make a higher concentration of DON necessary to induce sufficient bleaching symptoms to be able to detect any differential between lines. Finally, it is possible that neither of the aldo-keto reductase genes in the interval are responsible for the enhanced DON resistance and that another gene in the interval is responsible for the DON resistance.

In an attempt to confirm whether TaAKR-D1 and TaAKR-D2 proteins possess DON epimerisation activity, constructs containing *TaAKR-D1* and *TaAKR-D2* that had been codon optimised for expression in *E. coli* were sent to collaborators. *E. coli* was

transformed by collaborators using the provided constructs, but neither gene was expressed, which made it impossible to proceed using this approach (Carere and Zhou, unpublished).

Gamma-irradiated Paragon lines were identified with deletions across the DON resistance interval, including a line containing a deletion of the entire interval (T17 L65). A DON application experiment was conducted on these lines (DON_PG_CER_19) with the aim of further refining the DON resistance interval. However, none of the deletion lines showed any significant difference in bleaching or grain weight compared to wild type Paragon and therefore it was not possible to dissect the region beyond the 4.2 Mbp interval. The line T17 L65 lacks the entire DON resistance interval, including both *TaAKR-D1* and *TaAKR-D2*. This indicates that deleting both genes does not increase DON susceptibility in Paragon and hence mutating only one of the genes in the Cadenza TILLING lines is unlikely to be the reason for not observing an effect in Cadenza. Paragon and Cadenza are both UK spring wheat varieties with a high level of relatedness as they are both derived from a cross between the varieties Axona and Tonic (Dobrotvorskaya *et al.*, 2017a, Dobrotvorskaya *et al.*, 2017b). Hence, similar reasons for the lack of effect in Cadenza are also possible in Paragon. There may be altered expression of the responsible 4D aldo-keto reductase gene and its homoeologous copies in Paragon compared with Chinese Spring. Alternatively, it appears that Paragon, like Cadenza, is less sensitive to DON than Chinese Spring and hence a higher concentration of DON may be necessary to detect the effect of deleting the DON resistance factor. It is also possible that Paragon does not possess a functional copy of the DON resistance factor, or it is not expressed.

Both Paragon and Cadenza appear to be inherently less sensitive to DON and this will need to be considered when conducting further experiments. It is likely that a higher concentration of DON solution will need to be applied to each treated head.

Furthermore, the A and/ or B homoeologues of the DON resistance factor may be more influential in these varieties compared with Chinese Spring, which may be masking the effect in lines where only the 4D copy has been mutated or deleted.

4.4.2 Gene expression in the DON resistance interval

Expression levels of most genes in the DON resistance interval were very low and did not show any noticeable change following *F. graminearum* infection (Ramírez-González *et al.*, 2018, Gou *et al.*, 2016, Borrill *et al.*, 2016). This is with the exception of one gene, TraesCS4D02G079900, which encodes an iron-dependent dioxygenase and is strongly upregulated in response to *F. graminearum* infection and, to a lesser extent, following DON application (Santos *et al.*, unpublished, Gou *et al.*, 2016). The RNA-seq data of Santos *et al.* (unpublished) was conducted on root tissue and in a different wheat genetic background (Hobbit Sib). However, TraesCS4D02G079900 was still found to be upregulated in the dataset, albeit weakly (Santos *et al.*, unpublished). This gene and its homoeologues, which are both also upregulated in response to *F. graminearum* infection, present the most convincing gene candidate within the DON resistance interval. Lines containing premature stop codons in 4A and 4B homoeologues (TraesCS4A02G234100 and TraesCS4B02G081200, respectively) of TraesCS4D02G079900 were identified in the Kronos TILLING population. These lines, containing the mutated 4A and 4B copies, will be crossed and then treated with DON to confirm whether these homoeologous genes are responsible for enhanced resistance to DON.

If indeed these genes are found to be responsible for the effect, the mechanism of the iron-dependent dioxygenase is most likely to be by chemical modification of DON. Iron-dependent dioxygenases are a large family of proteins that catalyse a diverse array of oxidative chemical modifications, including hydroxylation and epimerisation (Martinez and Hausinger, 2015). Hence, the protein may be modifying DON by one of these mechanisms.

The primary response to DON by the plant host appears to be through metabolising DON to a less toxic form. Hence, the function of the DON resistance factor is most likely to be through directly detoxifying DON or by increasing the expression of such a gene. Whilst there are several transcription factors in the DON resistance interval, none are upregulated in response to infection by DON-producing *F. graminearum* and hence the DON resistance factor is more likely to be metabolising DON directly.

Resistance to DON can also be achieved through increased tolerance of DON. Trichothecene mycotoxins, including DON, disrupt protein synthesis in eukaryotic organisms. Single amino acid changes to the DON target, ribosomal protein L3 (RPL3), have been demonstrated to improve tolerance to DON in yeast, and orthologues have been identified in wheat (Mitterbauer *et al.*, 2004, Lucyshyn *et al.*, 2007). There are two ribosomal proteins in the DON resistance interval. It is possible that an allele of one of these proteins may result in altered protein folding that prevents DON from binding to the ribosome. However, both ribosomal proteins show very low expression and do not appear to be upregulated in response to FHB. An ATP-binding cassette (ABC) transporter protein has also been demonstrated to be involved in improved tolerance to DON by pumping DON out of the plant cell (Walter *et al.*, 2015). However, no genes encoding an ABC transporter are present in the DON resistance interval.

4.4.3 DON resistance factor candidates in the distal interval of 4DS

The 4.2 Mbp DON resistance interval was identified from DON-induced bleaching data of Chinese Spring 4DS terminal deletion lines (Chapter 2). However, grain data from DON-treated and untreated heads of Chinese Spring 4DS terminal deletion lines indicated that there may be a DON resistance factor distal to this small interval. This distal region contains a daunting 775 genes. However, based on the RNA-seq dataset of Santos *et al.* (unpublished), only fifteen of these genes show differential regulation in response to DON application. The functional annotations of differentially

regulated genes provided further insight, with genes encoding an acyl-transferase (TraesCS4D02G055600) and a peroxiredoxin-like protein (TraesCS4D02G059200) looking the most interesting in terms of function, as they could feasibly be involved in DON detoxification.

Chapter 5: General Discussion

Fusarium head blight resistance has been a major challenge in wheat research. FHB resistance is quantitative and influenced by many genes dispersed throughout the wheat genome. Furthermore, FHB resistance QTL are often environmentally sensitive and may only be effective under certain climatic conditions. QTL mapping studies have identified many FHB resistance QTL but only a few of these are commonly used in wheat breeding (Buerstmayr *et al.*, 2009).

The elimination of susceptibility factors has the potential to offer a novel source of disease resistance. However, such susceptibility factors cannot be detected in conventional mapping studies unless natural mutations are present. Whilst the cause of the resistance underlying the *Fhb1* QTL remains controversial, some evidence suggests that a deletion resulting in the loss-of-function of a gene encoding a calcium-dependent histidine-rich protein (*TaHRC*) may be responsible for the resistance (Su *et al.*, 2019, Su *et al.*, 2018). This would make *TaHRC* an FHB susceptibility factor that has undergone natural mutation, thereby resulting in FHB resistance.

Other FHB susceptibility factors are likely to be present in the wheat genome but cannot be detected unless artificially induced deletion lines are utilised in FHB disease experiments. This was evident in a study conducted by Ma *et al.* (2006). Point inoculation of the available Chinese Spring ditelosomic lines, in which entire chromosome arms have been deleted, identified lines with significantly improved FHB resistance (Ma *et al.*, 2006). In particular, the loss of chromosome arms 7AS, 3BL, 7BS and 4DS were particularly effective in increasing FHB resistance and therefore they are likely to contain FHB susceptibility factors.

Since then, unpublished research from the research group of Prof. Paul Nicholson have independently observed the effect of deleting 4D on FHB resistance. The effect was originally observed in wheat-barley introgression lines, in which barley chromosome 4H was either introgressed as an addition line, or substituted for 4D (Steed and Nicholson, unpublished-b, Giovannelli, 2012). The addition of 4H had little effect on FHB susceptibility, whilst the 4H(4D) substitution resulted in a potent resistance (Steed and Nicholson, unpublished-b, Giovannelli, 2012). Surprisingly, this demonstrated that addition of barley chromosome 4H was not responsible for the increased FHB resistance, and it was the loss of wheat chromosome 4D that was implicated. FHB experiments using Chinese Spring ditelosomic lines, lacking 4DS or 4DL, clearly demonstrated that the FHB susceptibility is associated with the short arm (Steed and Nicholson, unpublished-a).

5.1 Project aims

Following compelling evidence for the presence of an FHB susceptibility factor on the short arm of wheat chromosome 4D, the aim of this PhD research project was to characterise and refine the physical position of the FHB susceptibility factor, with the ultimate aim of identifying the underlying gene, or genes.

In characterising the FHB susceptibility factor, a DON resistance factor and a Type I FHB resistance factor were also identified on the short arm and long arm of 4D, respectively. A secondary aim was to physically map and identify gene candidates for the DON resistance factor.

5.2 Deletion mapping

The wheat TILLING populations in tetraploid Kronos and hexaploid Cadenza have become an invaluable wheat community resource. However, it is impractical to validate a gene responsible for a trait of interest where there is a large number of gene candidates. Hence, an approach whereby the number of candidate genes can

be reduced prior to use of the wheat TILLING populations would be highly complementary.

As part of this PhD project, a pre-existing gamma-irradiated population in the variety Paragon has undergone further development, resulting in 1860 bulked lines at the M4 generation. In addition to ensuring that sufficient seed and DNA samples from all lines were available for this PhD project, it also provided an opportunity to make the population useful to other wheat researchers. Paragon is a closely related variety to Cadenza, used to generate the hexaploid TILLING population (Dobrotvorskaya *et al.*, 2017a, Dobrotvorskaya *et al.*, 2017b). In addition, both Cadenza and Paragon have been sequenced (Earlham Institute, 2019).

A subset of 650 gamma-irradiated Paragon lines were skim sequenced, which has been successful in revealing genome wide deletions in each of the lines (Ramirez-Gonzalez *et al.*, unpublished). This work is in preparation for publication and these data will soon be made available to wheat researchers, along with access to the germplasm. Parts of the genome are not yet saturated with deletions in the 650 lines so it is intended to skim sequence the additional 1210 lines from the gamma-irradiated Paragon population to produce a full genome-wide saturated panel for use by the wheat research community.

Genetic markers are essential for tracking a deletion of interest, but it is more challenging to design markers for deletions than it is for SNPs. This becomes yet more complex when attempting to detect hemizygous deletions. Two methods for designing markers were used during this PhD project.

Homoeologue nonspecific markers exploit triplets of homoeologous genes to reliably detect deletions. Identical sequences between homoeologues were used in primer design that produced PCR products differing in size for each homoeologue, which allowed them to be distinguished. Capillary electrophoresis was necessary to resolve the generally small size differences between homoeologue PCR products. For a

marker used on DNA lacking a deletion at any of the homoeologues, three peaks should be evident on the output graph, corresponding to each of the three homoeologous genes on the A, B and D genomes. When a deletion is present, the signal corresponding to the deleted homoeologue will be lost but the remaining two peaks will be maintained. Hence, the assay contains two internal controls that confirm that the primers are functioning correctly, even in the presence of a deletion. Chia *et al.* (2017) used similar techniques to track deletions of homoeologous regions during crossing. However, this PhD project utilises such an approach to genotype deletion lines across an entire chromosome arm (4DS) and its homoeologues.

The relative signals corresponding to individual homoeologues are usually very consistent between replicate samples. Hence, it is often possible to identify altered copy number of individual homoeologues if the fluorescence strength in one homoeologue increases or decreases relative to the other two peaks, when compared with wild type samples. Biological replication is essential to diagnose copy number variation in both wild type and copy number variation lines. However, it can be more reliably diagnosed where altered fluorescence strength is evident across several markers.

The second assay used KASP markers designed to detect deletions. In this case, a homoeologue specific SNP is used to distinguish between two homoeologous genes. In the case of the KASP markers used in this PhD project, SNPs between the 4B and 4D copies were used. The third homoeologue (4A in this case) was prevented from amplifying because of an A genome specific SNP in the common primer. Where both 4B and 4D copies are present, a heterozygous-like signal is observed because both FAM- and HEX-tagged homoeologues are amplified. Where a deletion is present at the position of the marker on either 4B or 4D, only the retained copy will be amplified and the fluorescence corresponding to the deleted copy is lost. This

allows homozygous deletions of either copy to be detected. This method is unreliable at detecting hemizygous deletions, but it does seem to be possible where only a few lines (with replication) are tested.

5.3 FHB susceptibility factor

The FHB susceptibility factor was refined to a 31.7 Mbp interval using Chinese Spring lines containing terminal deletions of 4DS. Following this, the gamma-irradiated Paragon population was used to map the FHB susceptibility factor using deletions spanning the FHB susceptibility interval. A total of ten lines were identified that contain deletions across the FHB susceptibility interval and these were phenotyped for FHB susceptibility. The majority of lines exhibited similar disease levels to wild type Paragon. The physical regions that have been deleted in these lines can be excluded from the investigation, as they do not appear to have lost the FHB susceptibility factor.

The line T20 L65 has the entire FHB susceptibility interval deleted and it shows consistent resistance to the spread of FHB in all experiments in which it was tested. Furthermore, plants containing a hemizygous 4D deletion possessed a weaker resistance than plants containing a homozygous deletion. This provides evidence that the FHB susceptibility factor is present in Paragon and that the effect on FHB susceptibility is likely to be semi-dominant.

T17 L65 contains a 4D deletion covering the distal region of the FHB susceptibility interval. In addition, a 4D duplication of the central region of the FHB susceptibility interval was later identified in T17 L65. The 4D deletion was found to be hemizygous in five plants, whilst the duplication was fixed, regardless of whether the 4D deletion was homozygous or hemizygous. Hence, the deletion and the duplication appear to segregate independently but the duplicated region is very close to the deletion. This would suggest the duplicated segment is located elsewhere to 4DS in the genome of line T17 L65.

T17 L65 is highly resistant to FHB but the deletion on 4D does not appear to be responsible. Plants containing the hemizygous 4D deletion and those containing a homozygous deletion are equally resistant to the spread of FHB. I hypothesise that the 4D duplication is responsible for the resistance of T17 L65 and the FHB susceptibility factor is sensitive to an increase, as well as decrease in dosage. To confirm this, T17 L65 will require crossing to Paragon, to remove both the 4D deletion and background deletions, leaving only the 4D duplication. The progeny will need to be allowed to self, to retrieve seed with a homozygous duplication. This can then be used in a Type II FHB disease experiment to confirm whether the 4D duplication is indeed responsible for the increased resistance in the line.

Line T15 L49 has a large deletion covering the majority of the FHB susceptibility interval. However, this line is significantly more susceptible to FHB than Paragon. Due to the increased disease levels associated with this line, it is likely that background deletions are masking the effect of deleting the FHB susceptibility factor. To confirm this, T15 L49 also requires backcrossing to Paragon to remove background deletions. Point inoculating the self-fertilised progeny (which will require screening to identify plants containing the homozygous 4D deletion) will confirm how the 4D deletion in this line is influencing FHB susceptibility in isolation. Plant material to cross both T17 L65 and T15 L49 to Paragon have been set up, in order to answer these questions.

Whilst excluding the results from susceptible T15 L49, this leaves three relatively small intervals that remain the subject of additional investigation. There are 66 genes distributed across these three intervals. Gene expression data were relatively uninformative, especially because the expression pattern of an FHB susceptibility factor is unknown. However, there are only five genes that are 4D specific and lack homoeologues. Deletions of homoeologous regions of 4A and 4B had no effect on FHB susceptibility and hence 4D specific genes are the strongest candidates for the

FHB susceptibility factor. Of these 4D specific genes, four possess functional annotations. They encode a protein kinase with major sperm protein domain, a BURP protein, an LRR protein and an LRR-RK protein. Cadenza TILLING lines have been obtained for these genes, where available, and will be used to confirm whether mutating any of these genes results in enhanced FHB resistance. Otherwise, where no suitable TILLING mutants are available, CRISPR-Cas9-derived gene knockouts, or transient gene silencing such as VIGS, may be necessary.

It is important to be aware of any pleiotropic effects that may be associated with the knockout of the FHB susceptibility factor. Assessing this will be easier once the gene, or genes, have been identified, as crosses can be made to ensure that background deletions are not influencing plant phenotype. Whilst no morphological effects were noticeably associated with deleting the FHB susceptibility factor, it will be important to confirm that important traits such as yield, quality and flowering time are maintained in the absence of the FHB susceptibility factor. It will also be necessary to test how mutation of the FHB susceptibility factor influences susceptibility to other economically important diseases.

5.4 DON resistance factor

Upon applying DON to Chinese Spring ditelosomic lines, it was evident that the loss of 4DS increased susceptibility to DON. If the FHB susceptibility factor was increasing sensitivity to DON, the opposite result is to be expected. Therefore, it is unlikely the FHB susceptibility factor is influenced by DON, but there may be an independent resistance factor to DON on the same chromosome arm. Chinese Spring 4DS terminal deletion lines showed the clearest increase in DON-induced visual symptoms (above the point of application) between del4DS-2 and del4DS-4. This was used to infer that the DON resistance factor was located in a 4.2 Mbp interval. This interval contains 49 genes.

Whilst no glucosyltransferase genes are present in this interval, two aldo-keto genes are present in the DON resistance interval. Several studies have demonstrated that bacteria are capable of detoxifying DON by epimerisation using aldo-keto reductases (Carere *et al.*, 2018b, He *et al.*, 2017). These two aldo-keto reductase genes were the most obvious genes that may be responsible for resistance to DON. Hence, Cadenza TILLING lines were obtained with homozygous premature stop mutations in the aldo-keto reductase genes. However, all lines, including wild type Cadenza, showed very low sensitivity to DON compared with Chinese Spring. No increase in DON bleaching was evident in the aldo-keto reductase knockout mutants.

Several gamma-irradiated Paragon lines were identified with deletions spanning all or part of the DON resistance interval. However, following DON application to these lines, no line showed increased DON-induced bleaching or any significant change in grain weight. The experiment confirmed that Paragon, like Cadenza, is substantially less sensitive to DON than Chinese Spring. Paragon and Cadenza are likely to require a higher concentration of DON to induce the necessary bleaching symptoms and to sufficiently inhibit grain filling to detect a differential between lines. This ought to be considered if work on the DON resistance factor is continued beyond this PhD project.

Based on gene expression data, only one gene in the DON resistance interval is highly upregulated in response to FHB (Ramírez-González *et al.*, 2018, Borrill *et al.*, 2016). Furthermore, modest upregulation in response to DON was also evident in roots of wheat (Santos *et al.*, unpublished). The gene encodes an iron-dependent dioxygenase, which is the best candidate for the DON resistance factor in this interval. Dioxygenase genes are able to perform a diverse range of oxidative chemical modifications, such as hydroxylation, halogenation, desaturation, epimerization and epoxidation (Martinez and Hausinger, 2015). Hence, the protein encoded by this gene may be modifying DON by one of these mechanisms.

In order to confirm the results of the DON bleaching experiment, grain data from the DON and mock treated terminal deletion lines were collected. However, collecting these data is time-consuming, as grain must be carefully dissected separately from above and below the application point of both DON and mock treated heads per plant. For this reason, only grain data from wild type Chinese Spring, del4DS-2 and del4DS-4 were collected and this was carried out over a year after the DON bleaching was scored.

The grain weight data did not agree with the DON-induced bleaching data. Both del4DS-2 and del4DS-4 were similarly susceptible to DON-induced inhibition of grain filling, which suggested that the most potent DON resistance factor is located distally on 4DS. This distal interval contains 775 genes. However, only fifteen of these genes are upregulated in response to DON application (Santos *et al.*, unpublished). Assuming TILLING mutants are available, it will be possible to confirm whether any of these genes are involved in resistance to DON.

5.5 Type I FHB resistance factor on long arm of 4D

Spray inoculation of Chinese Spring 4D ditelosomic lines suggested that there is a Type I resistance factor on the long arm of chromosome 4D. Unfortunately, the results of spray inoculating the 4DL terminal deletion lines were inconclusive, making refinement of the FHB resistance factor impossible. Two of the seven terminal deletion lines were more susceptible to initial infection, but it is necessary to repeat the experiment before any conclusions can be drawn. A recent report underlines the importance of head morphology, and particularly anther retention, in Type I resistance (Steiner *et al.*, 2019). Hence, observing differences in such morphological traits may be informative when repeating the experiment.

5.6 Concluding remarks

The study of FHB is notoriously challenging, and this is partly due to the highly polygenic nature underlying the strictly quantitative trait. In this PhD project,

utilisation of Chinese Spring aneuploid material to test Type I and Type II FHB resistance, in addition to DON resistance, has identified three factors that influence FHB susceptibility on chromosome 4D alone. In addition to providing compelling evidence for the presence of an FHB susceptibility factor on the short arm of 4D, an independent DON resistance factor was identified. The DON resistance factor is positioned distally, relative to the FHB susceptibility factor. Evidence of a Type I FHB resistance factor on the long arm of 4D was also found, although additional experiments are necessary to confirm this.

These data reiterate that FHB resistance is influenced by many genes that are likely to span every chromosome of the wheat genome. However, the underlying effects of individual factors may not be clear unless a combination of FHB and DON phenotyping methods are used. This, in part, may explain why FHB resistance has been so challenging to study using QTL mapping approaches, as FHB susceptibility is likely to be influenced by a number of genes within an interval of interest. This also makes the use of aneuploid lines, such as nullisomic-tetrasomic lines, impractical for use in FHB studies. Altered dosage of several homoeologous chromosomes in the same line is likely to make results from FHB disease experiments very difficult to interpret.

A population containing relatively small deletions is likely to offer a useful method of mapping both disease resistance and susceptibility factors to smaller physical intervals. Buerstmayr *et al.* (2018) utilised a gamma irradiated population to overcome the lack of recombination in a pericentromeric interval on chromosome 5A containing a Type I FHB resistance QTL. Steiner *et al.* (2019) have since found two independent Type I FHB resistance QTL in the interval that are contributing to resistance to initial infection. This PhD project has also successfully demonstrated the power of utilising gamma-irradiated deletion mutants in the study of FHB. In this instance, a deletion population was necessary to delete the FHB susceptibility factor,

given the apparent lack of natural variation. Whilst background mutations may influence the FHB phenotype, crossing any lines possessing an unexpected phenotype to wild type Paragon can be used to remove background deletions and thereby confirm the effect of the deletion of interest in isolation from confounding effects.

References

10+ Wheat Genomes Project. 2019. *The wheat 'pan genome'* [Online]. 10+ Wheat Genomes Project. Available: http://www.10wheatgenomes.com/ [Accessed 21 May 2019].

Acevedo-Garcia, J., Kusch, S., Panstruga, R. 2014. Magical mystery tour: MLO proteins in plant immunity and beyond. *New Phytologist,* **204**, 273-281.

Acevedo-Garcia, J., Spencer, D., Thieron, H., Reinstadler, A., Hammond-Kosack, K., Phillips, A.L., Panstruga, R. 2017. mlo-based powdery mildew resistance in hexaploid bread wheat generated by a non-transgenic TILLING approach. *Plant Biotechnology Journal,* **15**, 367-378.

Albrecht, C., Boutrot, F., Segonzac, C., Schwessinger, B., Gimenez-Ibanez, S., Chinchilla, D., Rathjen, J.P., de Vries, S.C., Zipfel, C. 2012. Brassinosteroids inhibit pathogen-associated molecular pattern-triggered immune signaling independent of the receptor kinase BAK1. *Proceedings of the National Academy of Sciences of the United States of America,* **109**, 303-308.

Altpeter, F., Posselt, U.K. 1994. Production of high quantities of 3-acetyldeoxynivalenol and deoxynivalenol. *Applied Microbiology and Biotechnology,* **41**, 384-387.

Aranyi, N.R., Varga, I., Poczai, P., Cernak, I., Vida, G., Molnar-Lang, M., Hoffmann, B. 2014. What types of powdery mildew can infect wheat-barley introgression lines? *European Journal of Plant Pathology,* **139**, 19-25.

Bai, G.H., Plattner, R., Desjardins, A., Kolb, F. 2001. Resistance to Fusarium head blight and deoxynivalenol accumulation in wheat. *Plant Breeding,* **120**, 1-6.

Bari, R., Jones, J. 2009. Role of plant hormones in plant defence responses. *Plant Molecular Biology,* **69**, 473-488.

Boddu, J., Cho, S.H., Muehlbauer, G.J. 2007. Transcriptome analysis of trichothecene-induced gene expression in barley. *Molecular Plant-Microbe Interactions,* **20**, 1364-1375.

Borrill, P., Adamski, N., Uauy, C. 2015. Genomics as the key to unlocking the polyploid potential of wheat. *New Phytologist,* **208**, 1008-22.

Borrill, P., Ramirez-Gonzalez, R., Uauy, C. 2016. expVIP: a Customizable RNA-seq Data Analysis and Visualization Platform. *Plant Physiology,* **170**, 2172-2186.

Boutigny, A.L., Richard-Forget, F., Barreau, C. 2008. Natural mechanisms for cereal resistance to the accumulation of Fusarium trichothecenes. *European Journal of Plant Pathology,* **121**, 411-423.

Brauer, E.K., Rocheleau, H., Balcerzak, M., Pan, Y., Fauteux, F., Liu, Z., Wang, L., Zheng, W., Ouellet, T. 2019. Transcriptional and hormonal profiling of Fusarium graminearum-infected wheat reveals an association between auxin and susceptibility. *Physiological and Molecular Plant Pathology,* **107**, 33-39.

Brenchley, R., Spannagl, M., Pfeifer, M., Barker, G.L.A., D'Amore, R., Allen, A.M., McKenzie, N., Kramer, M., Kerhornou, A., Bolser, D., Kay, S., Waite, D., Trick, M., Bancroft, I., Gu, Y., Huo, N., Luo, M.C., Sehgal, S., Gill, B., Kianian, S., Anderson, O., Kersey, P., Dvorak, J., McCombie, W.R., Hall, A., Mayer, K.F.X., Edwards, K.J., Bevan, M.W., Hall, N. 2012. Analysis of the breadwheat genome using whole-genome shotgun sequencing. *Nature,* **491**, 705-710.

Brown, N.A., Urban, M., Van De Meene, A.M.L., Hammond-Kosack, K.E. 2010. The infection biology of Fusarium graminearum: Defining the pathways of spikelet to spikelet colonisation in wheat ears. *Fungal Biology,* **114**, 555-571.

Buerstmayr, H., Ban, T., Anderson, J.A. 2009. QTL mapping and marker-assisted selection for Fusarium head blight resistance in wheat: a review. *Plant Breeding,* **128**, 1-26.

Buerstmayr, H., Steiner, B., Hartl, L., Griesser, M., Angerer, N., Lengauer, D., Miedaner, T., Schneider, B., Lemmens, M. 2003. Molecular mapping of QTLs for Fusarium head blight resistance in spring wheat. II. Resistance to fungal penetration and spread. *Theoretical and Applied Genetics,* **107**, 503-508.

Buerstmayr, M., Buerstmayr, H. 2016. The Semidwarfing Alleles Rht-D1b and Rht-B1b Show Marked Differences in Their Associations with Anther-Retention in Wheat Heads and with Fusarium Head Blight Susceptibility. *Phytopathology,* **106**, 1544-1552.

Buerstmayr, M., Steiner, B., Wagner, C., Schwarz, P., Brugger, K., Barabaschi, D., Volante, A., Vale, G., Cattivelli, L., Buerstmayr, H. 2018. High-resolution mapping of the pericentromeric region on wheat chromosome arm 5AS harbouring the Fusarium head blight resistance QTL Qfhs.ifa-5A. *Plant Biotechnology Journal,* **16**, 1046-1056.

Buhrow, L.M., Cram, D., Tulpan, D., Foroud, N.A., Loewen, M.C. 2016. Exogenous Abscisic Acid and Gibberellic Acid Elicit Opposing Effects on Fusarium graminearum Infection in Wheat. *Phytopathology,* **106**, 986-996.

Carere, J., Hassan, Y.I., Lepp, D., Zhou, T. 2018a. The enzymatic detoxification of the mycotoxin deoxynivalenol: identification of DepA from the DON epimerization pathway. *Microbial Biotechnology,* **11**, 1106-1111.

Carere, J., Hassan, Y.I., Lepp, D., Zhou, T. 2018b. The Identification of DepB: An Enzyme Responsible for the Final Detoxification Step in the Deoxynivalenol Epimerization Pathway in Devosia mutans 17-2-E-8. *Frontiers in Microbiology,* **9**, 9.

Carere, J., Zhou, T. unpublished. Attempts to obtain purified TaAKR-D1 and TaARK-D2 proteins from transformed E. coli for use in interaction assays with DON.

Chapman, J.A., Mascher, M., Buluc, A., Barry, K., Georganas, E., Session, A., Strnadova, V., Jenkins, J., Sehgal, S., Oliker, L., Schmutz, J., Yelick, K.A., Scholz, U., Waugh, R., Poland, J.A., Muehlbauer, G.J., Stein, N., Rokhsar, D.S. 2015. A whole-genome shotgun approach for assembling and anchoring the hexaploid bread wheat genome. *Genome Biology,* **16**, 17.

Chen, X., Steed, A., Travella, S., Keller, B., Nicholson, P. 2009. Fusarium graminearum exploits ethylene signalling to colonize dicotyledonous and monocotyledonous plants. *New Phytologist,* **182**, 975-983.

Chia, T., Adamski, N.M., Saccomanno, B., Greenland, A., Nash, A., Uauy, C., Trafford, K. 2017. Transfer of a starch phenotype from wild wheat to bread wheat by deletion of a locus controlling B-type starch granule content. *Journal of Experimental Botany,* **68**, 5497-5509.

Choulet, F., Alberti, A., Theil, S., Glover, N., Barbe, V., Daron, J., Pingault, L., Sourdille, P., Couloux, A., Paux, E., Leroy, P., Mangenot, S., Guilhot, N., Le Gouis, J., Balfourier, F., Alaux, M., Jamilloux, V., Poulain, J., Durand, C., Bellec, A., Gaspin, C., Safar, J., Dolezel, J., Rogers, J., Vandepoele, K., Aury, J.M., Mayer, K., Berges, H., Quesneville, H., Wincker, P., Feuillet, C. 2014. Structural and functional partitioning of bread wheat chromosome 3B. *Science,* **345**, 7.

Clavijo, B.J., Venturini, L., Schudoma, C., Accinelli, G.G., Kaithakottil, G., Wright, J., Borrill, P., Kettleborough, G., Heavens, D., Chapman, H., Lipscombe, J., Barker, T., Lu, F.H., McKenzie, N., Raats, D., Ramirez-Gonzalez, R.H., Coince, A., Peel, N., Percival-Alwyn, L., Duncan, O., Trosch, J., Yu, G.T., Bolser, D.M., Namaati, G., Kerhornou, A., Spannagl, M., Gundlach, H., Haberer, G., Davey, R.P., Fosker, C., Di Palma, F., Phillips, A.L., Millar, A.H., Kersey, P.J., Uauy, C., Krasileva, K.V., Swarbreck, D., Bevan, M.W., Clark, M.D. 2017. An improved assembly and annotation of the allohexaploid wheat genome identifies complete families of agronomic genes and provides genomic evidence for chromosomal translocations. *Genome Research,* **27**, 885-896.

Corrion, A., Day, B. 2015. Pathogen Resistance Signalling in Plants. *eLS.* John Wiley & Sons, Ltd.

Cuthbert, P.A., Somers, D.J., Brule-Babel, A. 2007. Mapping of Fhb2 on chromosome 6BS: a gene controlling Fusarium head blight field resistance in bread wheat (Triticum aestivum L.). *Theoretical and Applied Genetics,* **114**, 429-437.

Dean, R., Van Kan, J.A.L., Pretorius, Z.A., Hammond-Kosack, K.E., Di Pietro, A., Spanu, P.D., Rudd, J.J., Dickman, M., Kahmann, R., Ellis, J., Foster, G.D. 2012. The Top 10 fungal pathogens in molecular plant pathology. *Molecular Plant Pathology,* **13**, 414-430.

Department for Environment Food and Rural Affairs. 2018a. *Farming Statistics - Provisional crop areas, yields and livestock populations - at June 2018 - United Kingdom* [Online]. Department for Environment Food and Rural Affairs. Available: https://assets.publishing.service.gov.uk/government/uploads/system/uploads/attachment_data/file/747210/structure-jun2018prov-UK-11oct18.pdf [Accessed 26 Apr 2019].

Department for Environment Food and Rural Affairs. 2018b. *Farming Statistics – First estimates of 2018 UK wheat and barley production* [Online]. Department for Environment Food and Rural Affairs. Available: https://assets.publishing.service.gov.uk/government/uploads/system/uploads/attachment_data/file/746084/structure_jun18_wheatandbarleyUK_08oct18.pdf [Accessed 26 Apr 2019].

Desjardins, A.E., Proctor, R.H., Bai, G.H., McCormick, S.P., Shaner, G., Buechley, G., Hohn, T.M. 1996. Reduced virulence of trichothecene-nonproducing mutants of Gibberella zeae in wheat field tests. *Molecular Plant-Microbe Interactions,* **9**, 775-781.

Devoto, A., Piffanelli, P., Nilsson, I., Wallin, E., Panstruga, R., von Heijne, G., Schulze-Lefert, P. 1999. Topology, subcellular localization, and sequence diversity of the Mlo family in plants. *Journal of Biological Chemistry,* **274**, 34993-35004.

Dobrotvorskaya, T., Dobrotvorskiy, D., Martynov, S. 2017a. *Pedigree of Cadenza* [Online]. Available: http://wheatpedigree.net/sort/show/9638 [Accessed 19 Jun 2019].

Dobrotvorskaya, T., Dobrotvorskiy, D., Martynov, S. 2017b. *Pedigree of Paragon* [Online]. Available: http://wheatpedigree.net/sort/show/79390 [Accessed 19 Jun 2019].

Draeger, R., Gosman, N., Steed, A., Chandler, E., Thomsett, M., Srinivasachary, Schondelmaier, J., Buerstmayr, H., Lemmens, M., Schmolke, M., Mesterhazy, A., Nicholson, P. 2007. Identification of QTLs for resistance to Fusarium head blight, DON accumulation and associated traits in the winter wheat variety Arina. *Theoretical and Applied Genetics,* **115**, 617-625.

Earlham Institute. 2019. *Grassroots Genomics BLAST Search* [Online]. Available: https://wheatis.tgac.ac.uk/grassroots-portal/blast [Accessed 19 Jun 2019].

Effertz, R.J., Meinhardt, S.W., Anderson, J.A., Jordahl, J.G., Francl, L.J. 2002. Identification of a chlorosis-inducing toxin from Pyrenophora tritici-repentis and the chromosomal location of an insensitivity locus in wheat. *Phytopathology,* **92**, 527-533.

EMBL-EBI. 2019. *Ensembl Plants release 43* [Online]. Available: http://plants.ensembl.org/Triticum_aestivum/Info/Index [Accessed 19 Jun 2019].

Endo, T.R., Gill, B.S. 1996. The deletion stocks of common wheat. *Journal of Heredity,* **87**, 295-307.

Faris, J.D., Anderson, J.A., Francl, L.J., Jordahl, J.G. 1996. Chromosomal location of a gene conditioning insensitivity in wheat to a necrosis-inducing culture filtrate from Pyrenophora tritici-repentis. *Phytopathology,* **86**, 459-463.

Faris, J.D., Liu, Z.H., Xu, S.S. 2013. Genetics of tan spot resistance in wheat. *Theoretical and Applied Genetics,* **126**, 2197-2217.

Faris, J.D., Zhang, Z.C., Lu, H.J., Lu, S.W., Reddy, L., Cloutier, S., Fellers, J.P., Meinhardt, S.W., Rasmussen, J.B., Xu, S.S., Oliver, R.P., Simons, K.J., Friesen, T.L. 2010. A unique wheat disease resistance-like gene governs effector-triggered susceptibility to necrotrophic pathogens. *Proceedings of the National Academy of Sciences of the United States of America,* **107**, 13544-13549.

Food and Agricultural Organisation. 2014. *Wheat - the largest primary commodity* [Online]. Available: http://www.fao.org/resources/infographics/infographics-details/en/c/240943/ [Accessed 17 Jul 2019].

Food and Agricultural Organisation. 2019. *FAO Cereal Supply and Demand Brief* [Online]. Food and Agricultural Organisation. Available: http://www.fao.org/worldfoodsituation/csdb/en/ [Accessed 26 Apr 2019].

Food Standards Agency. 2007. *The UK code of good agricultural practice to reduce Fusarium mycotoxins in cereals* [Online]. Available: http://www.food.gov.uk/sites/default/files/multimedia/pdfs/fusariumcop.pdf [Accessed 22 Feb 2016].

Foroud, N.A., Eudes, F. 2009. Trichothecenes in Cereal Grains. *International Journal of Molecular Sciences,* **10**, 147-173.

Francki, M.G. 2013. Improving Stagonospora nodorum Resistance in Wheat: A Review. *Crop Science,* **53**, 355-365.

Friesen, T.L., Chu, C.G., Xu, S.S., Faris, J.D. 2012. SnTox5-Snn5: a novel Stagonospora nodorum effector-wheat gene interaction and its relationship with the SnToxA-Tsn1 and SnTox3-Snn3-B1 interactions. *Molecular Plant Pathology,* **13**, 1101-1109.

Friesen, T.L., Faris, J.D. 2004. Molecular mapping of resistance to Pyrenophora tritici-repentis race 5 and sensitivity to Ptr ToxB in wheat. *Theoretical and Applied Genetics,* **109**, 464-471.

Friesen, T.L., Faris, J.D. 2010. Characterization of the wheat-Stagonospora nodorum disease system: what is the molecular basis of this quantitative necrotrophic disease interaction? *Canadian Journal of Plant Pathology-Revue Canadienne De Phytopathologie,* **32**, 20-28.

Fung, F., Clark, R.F. 2004. Health effects of mycotoxins: A toxicological overview. *Journal of Toxicology-Clinical Toxicology,* **42**, 217-234.

Gao, Y., Faris, J.D., Liu, Z., Kim, Y.M., Syme, R.A., Oliver, R.P., Xu, S.S., Friesen, T.L. 2015. Identification and Characterization of the SnTox6-Snn6 Interaction in the Parastagonospora nodorum-Wheat Pathosystem. *Molecular Plant-Microbe Interactions,* **28**, 615-625.

Gardiner, S.A., Boddu, J., Berthiller, F., Hametner, C., Stupar, R.M., Adam, G., Muehlbauer, G.J. 2010. Transcriptome Analysis of the Barley-Deoxynivalenol Interaction: Evidence for a Role of Glutathione in Deoxynivalenol Detoxification. *Molecular Plant-Microbe Interactions,* **23**, 962-976.

Giovannelli, V., Nicholson, P., Burt, C. 2012. *Investigation of type II Fusarium head blight (FHB) resistance in wheat and barley.* MSc, John Innes Centre.

Goddard, R., Peraldi, A., Ridout, C., Nicholson, P. 2014. Enhanced Disease Resistance Caused by BRI1 Mutation Is Conserved Between Brachypodium distachyon and Barley (Hordeum vulgare). *Molecular Plant-Microbe Interactions,* **27**, 1095-1106.

Gordon, C.S., Rajagopalan, N., Risseeuw, E.P., Surpin, M., Ball, F.J., Barber, C.J., Buhrow, L.M., Clark, S.M., Page, J.E., Todd, C.D., Abrams, S.R., Loewen, M.C. 2016. Characterization of Triticum aestivum Abscisic Acid Receptors and a Possible Role for These in Mediating Fusairum Head Blight Susceptibility in Wheat. *Plos One,* **11**, 23.

Gosman, N., Chandler, E., Thomsett, M., Draeger, R., Nicholson, P. 2005. Analysis of the relationship between parameters of resistance to Fusarium head blight and in vitro tolerance to deoxynivalenol of the winter wheat cultivar WEK0609 (R). *European Journal of Plant Pathology,* **111**, 57-66.

Goswami, R.S., Kistler, H.C. 2004. Heading for disaster: Fusarium graminearum on cereal crops. *Molecular Plant Pathology,* **5**, 515-525.

Gou, L., Hattori, J., Fedak, G., Balcerzak, M., Sharpe, A., Visendi, P., Edwards, D., Tinker, N., Wei, Y.M., Chen, G.Y., Ouellet, T. 2016. Development and Validation of Thinopyrum elongatum-Expressed Molecular Markers Specific for the Long Arm of Chromosome 7E. *Crop Science,* **56**, 354-363.

Grewal, S., Hubbart-Edwards, S., Yang, C.Y., Scholefield, D., Ashling, S., Burridge, A., Wilkinson, P.A., King, I.P., King, J. 2018. Detection of T. urartu Introgressions in Wheat and Development of a Panel of Interspecific Introgression Lines. *Frontiers in Plant Science,* **9**, 10.

Griffiths, S., Sharp, R., Foote, T.N., Bertin, I., Wanous, M., Reader, S., Colas, I., Moore, G. 2006. Molecular characterization of Ph1 as a major chromosome pairing locus in polyploid wheat. *Nature,* **439**, 749-752.

Gunupuru, L.R., Perochon, A., Doohan, F.M. 2017. Deoxynivalenol resistance as a component of FHB resistance. *Tropical Plant Pathology,* **42**, 175-183.

Hassan, Y.I., He, J.W., Perilla, N., Tang, K.J., Karlovsky, P., Zhou, T. 2017. The enzymatic epimerization of deoxynivalenol by Devosia mutans proceeds through the formation of 3-keto-DON intermediate. *Scientific Reports,* **7**, 11.

He, W.J., Zhang, L.M., Yi, S.Y., Tang, X.L., Yuan, Q.S., Guo, M.W., Wu, A.B., Qu, B., Li, H.P., Liao, Y.C. 2017. An aldo-keto reductase is responsible for Fusarium toxin-degrading activity in a soil Sphingomonas strain. *Scientific Reports,* **7**, 13.

Hedden, P. 2003. The genes of the Green Revolution. *Trends in Genetics,* **19**, 5-9.

Hernandez, P., Martis, M., Dorado, G., Pfeifer, M., Galvez, S., Schaaf, S., Jouve, N., Simkova, H., Valarik, M., Dolezel, J., Mayer, K.F.X. 2012. Next-generation sequencing and syntenic integration of flow-sorted arms of wheat chromosome 4A exposes the chromosome structure and gene content. *Plant Journal,* **69**, 377-386.

Hofer, K., Linkmeyer, A., Textor, K., Huckelhoven, R., Hess, M. 2015. MILDEW LOCUS O mutation does not affect resistance to grain infections with Fusarium spp. and Ramularia collo-cygni. *Phytopathology,* **105**, 1214-1219.

IWGSC 2018. Shifting the limits in wheat research and breeding using a fully annotated reference genome. *Science,* **361**.

Jansen, C., von Wettstein, D., Schafer, W., Kogel, K.H., Felk, A., Maier, F.J. 2005. Infection patterns in barley and wheat spikes inoculated with wild-type and trichodiene synthase gene disrupted Fusarium graminearum. *Proceedings of the National Academy of Sciences of the United States of America,* **102**, 16892-16897.

Jarosch, B., Kogel, K.H., Schaffrath, U. 1999. The ambivalence of the barley Mlo locus: Mutations conferring resistance against powdery mildew (Blumeria graminis f. sp, hordei) enhance susceptibility to the rice blast fungus Magnaporthe grisea. *Molecular Plant-Microbe Interactions,* **12**, 508-514.

Jia, H.Y., Zhou, J.Y., Xue, S.L., Li, G.Q., Yan, H.S., Ran, C.F., Zhang, Y.D., Shi, J.X., Jia, L., Wang, X., Luo, J., Ma, Z.Q. 2018. A journey to understand wheat Fusarium head blight resistance in the Chinese wheat landrace Wangshuibai. *Crop Journal,* **6**, 48-59.

Jorgensen, J.H. 1992. Discovery, characterization and exploitation of Mlo powdery mildew resistance in barley. *Euphytica,* **63**, 141-152.

Kang, Z.S., Buchenauer, H. 2000. Cytology and ultrastructure of the infection of wheat spikes by Fusarium culmorum. *Mycological Research,* **104**, 1083-1093.

Kim, T.W., Wang, Z.Y. 2010. Brassinosteroid Signal Transduction from Receptor Kinases to Transcription Factors. *In:* Merchant, S., Briggs, W.R., Ort, D. (eds.) *Annual Review of Plant Biology, Vol 61.* Palo Alto: Annual Reviews.

Kimura, M., Kaneko, I., Komiyama, M., Takatsuki, A., Koshino, H., Yoneyama, K., Yamaguchi, I. 1998. Trichothecene 3-O-acetyltransferase protects both the producing organism and transformed yeast from related mycotoxins - Cloning and characterization of Tri101. *Journal of Biological Chemistry,* **273**, 1654-1661.

Kluger, B., Bueschl, C., Lemmens, M., Berthiller, F., Haubl, G., Jaunecker, G., Adam, G., Krska, R., Schuhmacher, R. 2013. Stable isotopic labelling-assisted untargeted metabolic profiling reveals novel conjugates of the mycotoxin deoxynivalenol in wheat. *Analytical and Bioanalytical Chemistry,* **405**, 5031-5036.

Kluger, B., Bueschl, C., Lemmens, M., Michlmayr, H., Malachova, A., Koutnik, A., Maloku, I., Berthiller, F., Adam, G., Krska, R., Schuhmacher, R. 2015. Biotransformation of the Mycotoxin Deoxynivalenol in Fusarium Resistant and Susceptible Near Isogenic Wheat Lines. *Plos One,* **10**, 19.

Kusch, S., Panstruga, R. 2017. mlo-Based Resistance: An Apparently Universal "Weapon" to Defeat Powdery Mildew Disease. *Molecular Plant-Microbe Interactions,* **30**, 179-189.

Kusch, S., Pesch, L., Panstruga, R. 2016. Comprehensive Phylogenetic Analysis Sheds Light on the Diversity and Origin of the MLO Family of Integral Membrane Proteins. *Genome Biology and Evolution,* **8**, 878-895.

Lagudah, E.S., Krattinger, S.G. 2019. A new player contributing to durable Fusarium resistance. *Nature Genetics,* **51**, 1070-1071.

Langevin, F., Eudes, F., Comeau, A. 2004. Effect of trichothecenes produced by Fusarium graminearum during Fusarium head blight development in six cereal species. *European Journal of Plant Pathology,* **110**, 735-746.

Laurent, F., Labesse, G., de Wit, P. 2000. Molecular cloning and partial characterization of a plant VAP33 homologue with a major sperm protein domain. *Biochemical and Biophysical Research Communications,* **270**, 286-292.

Law, C.N., Snape, J.W., Worland, A.J. 1987. *Aneuploidy in wheat and its uses in genetic analysis*, Springer Netherlands.

Lemmens, M., Scholz, U., Berthiller, F., Dall'Asta, C., Koutnik, A., Schuhmacher, R., Adam, G., Buerstmayr, H., Mesterhazy, A., Krska, R., Ruckenbauer, P. 2005. The ability to detoxify the mycotoxin deoxynivalenol colocalizes with a major quantitative trait locus for fusarium head blight resistance in wheat. *Molecular Plant-Microbe Interactions,* **18**, 1318-1324.

Li, G., Zhou, J., Jia, H., Gao, Z., Fan, M., Luo, Y., Zhao, P., Xue, S., Li, N., Yuan, Y., Ma, S., Kong, Z., Jia, L., An, X., Jiang, G., Liu, W., Cao, W., Zhang, R., Fan, J., Xu, X., Liu, Y., Kong, Q., Zheng, S., Wang, Y., Qin, B., Cao, S., Ding, Y., Shi, J., Yan, H., Wang, X., Ran, C., Ma, Z. 2019. Mutation of a histidine-rich calcium-binding-protein gene in wheat confers resistance to Fusarium head blight. *Nature Genetics,* **51**, 1106-1112.

Li, X., Shin, S., Heinen, S., Dill-Macky, R., Berthiller, F., Nersesian, N., Clemente, T., McCormick, S., Muehlbauer, G.J. 2015. Transgenic Wheat Expressing a Barley UDP-Glucosyltransferase Detoxifies Deoxynivalenol and Provides High Levels of Resistance to Fusarium graminearum. *Molecular Plant-Microbe Interactions,* **28**, 1237-1246.

Li, Y., Chen, X., Chen, Z., Cai, R.H., Zhang, H.M., Xiang, Y. 2016. Identification and Expression Analysis of BURP Domain-Containing Genes in Medicago truncatula. *Frontiers in Plant Science,* **7**, 16.

Lin, F., Xue, S.L., Zhang, Z.Z., Zhang, C.Q., Kong, Z.X., Yao, G.Q., Tian, D.G., Zhu, H.L., Li, C.J., Cao, Y., Wei, J.B., Luo, Q.Y., Ma, Z.Q. 2006. Mapping QTL associated with resistance to Fusarium head blight in the Nanda2419 x Wangshuibai population. II: Type I resistance. *Theoretical and Applied Genetics,* **112**, 528-535.

Liu, W.X., Koo, D.H., Friebe, B., Gill, B.S. 2016. A set of Triticum aestivum-Aegilops speltoides Robertsonian translocation lines. *Theoretical and Applied Genetics,* **129**, 2359-2368.

Lucyshyn, D., Busch, B.L., Abolmaali, S., Steiner, B., Chandler, E., Sanjarian, F., Mousavi, A., Nicholson, P., Buerstmayr, H., Adam, G. 2007. Cloning and characterization of the ribosomal protein L3 (RPL3) gene family from Triticum aestivum. *Molecular Genetics and Genomics,* **277**, 507-517.

Lyngkjaer, M.F., Carver, T.L.W. 2000. Conditioning of cellular defence responses to powdery mildew in cereal leaves by prior attack. *Molecular Plant Pathology,* **1**, 41-49.

Ma, H.X., Bai, G.H., Gill, B.S., Hart, L.P. 2006. Deletion of a chromosome arm altered wheat resistance to Fusarium head blight and deoxynivalenol accumulation in Chinese Spring. *Plant Disease,* **90**, 1545-1549.

Ma, Z., Li, G., Zhou, J., Jia, H., Xue, S., Li, N., Gao, Z., Fan, M., Zhang, R., Ding, Y., Kong, Z., Yuan, Y., Ma, S., Jia, L., Ran, C. 2017. Map-based cloning of Fhb1 revealed unique mutation of a well-conserved gene resulting in resistance to wheat Fusarium head blight *In:* Buerstmayr, H., Lang-Mladek, C., Steiner, B., Michel, S., Buerstmayr, M., Lemmens, M., Vollmann, J., Grausgruber, H., eds. 13th International Wheat Genetics Symposium, 2017 Tulln, Austria. Vienna, Austria: BOKU - University of Natural Resources and Life Sciences, Vienna, 68.

Madeira, F., Park, Y.M., Lee, J., Buso, N., Gur, T., Madhusoodanan, N., Basutkar, P., Tivey, A.R.N., Potter, S.C., Finn, R.D., Lopez, R. 2019. The EMBL-EBI search and sequence analysis tools APIs in 2019. *Nucleic acids research,* **47**, W636-W641.

Magan, N., Aldred, D., Mylona, K., Lambert, R.J.W. 2010. Limiting mycotoxins in stored wheat. *Food Additives and Contaminants Part a-Chemistry Analysis Control Exposure & Risk Assessment,* **27**, 644-650.

Maier, F.J., Miedaner, T., Hadeler, B., Felk, A., Salomon, S., Lemmens, M., Kassner, H., Schafer, W. 2006. Involvement of trichothecenes in fusarioses of wheat, barley and maize evaluated by gene disruption of the trichodiene synthase (Tri5) gene in three field isolates of different chemotype and virulence. *Molecular Plant Pathology,* **7**, 449-461.

Martinez, S., Hausinger, R.P. 2015. Catalytic mechanisms of Fe(II)-and 2-oxoglutarate-dependent oxygenases. *Journal of Biological Chemistry,* **290**, 20702-20711.

McCormick, S.P., Alexander, N.J., Trapp, S.E., Hohn, T.M. 1999. Disruption of TRI101, the gene encoding trichothecene 3-O-acetyltransferase, from Fusarium sporotrichioides. *Applied and Environmental Microbiology,* **65**, 5252-5256.

McGrann, G.R.D., Stavrinides, A., Russell, J., Corbitt, M.M., Booth, A., Chartrain, L., Thomas, W.T.B., Brown, J.K.M. 2014. A trade off between mlo resistance to powdery mildew and increased susceptibility of barley to a newly important disease, Ramularia leaf spot. *Journal of Experimental Botany,* **65**, 1025-1037.

McMullen, M., Jones, R., Gallenberg, D. 1997. Scab of wheat and barley: A re-emerging disease of devastating impact. *Plant Disease,* **81**, 1340-1348.

Mesterhazy, A. 1995. Types and components of resistance to Fusarium head blight of wheat. *Plant Breeding,* **114**, 377-386.

Mitterbauer, R., Poppenberger, B., Raditschnig, A., Lucyshyn, D., Lemmens, M., Glossl, J., Adam, G. 2004. Toxin-dependent utilization of engineered ribosomal protein L3 limits trichothecene resistance in transgenic plants. *Plant Biotechnology Journal,* **2**, 329-340.

Nalam, V.J., Alam, S., Keereetaweep, J., Venables, B., Burdan, D., Lee, H., Trick, H.N., Sarowar, S., Makandar, R., Shah, J. 2015. Facilitation of Fusarium graminearum Infection by 9-Lipoxygenases in Arabidopsis and Wheat. *Molecular Plant-Microbe Interactions,* **28**, 1142-1152.

Nazari, L., Pattori, E., Manstretta, V., Terzi, V., Morcia, C., Somma, S., Moretti, A., Ritieni, A., Rossi, V. 2018. Effect of temperature on growth, wheat head infection, and nivalenol production by Fusarium poae. *Food Microbiology,* **76**, 83-90.

Nganje, W.E., Kaitibie, S., Wilson, W.W., Leistritz, F.L., Bangsund, D.A. 2004. Economic impacts of fusarium head blight in wheat and barley: 1993-2001. *Agribusiness & Applied Economics Report - Department of Agribusiness and Applied Economics, North Dakota State University*, 62 pp.

Ni, F., Qi, J., Hao, Q.Q., Lyu, B., Luo, M.C., Wang, Y., Chen, F.J., Wang, S.Y., Zhang, C.Z., Epstein, L., Zhao, X.Y., Wang, H.G., Zhang, X.S., Chen, C.X., Sun, L.Z., Fu, D.L. 2017. Wheat Ms2 encodes for an orphan protein that confers male sterility in grass species. *Nature Communications,* **8**, 12.

Niwa, S., Kubo, K., Lewis, J., Kikuchi, R., Alagu, M., Ban, T. 2014. Variations for Fusarium head blight resistance associated with genomic diversity in different sources of the resistant wheat cultivar 'Sumai 3'. *Breeding Science,* **64**, 90-96.

Okubara, P.A., Blechl, A.E., McCormick, S.P., Alexander, N.J., Dill-Macky, R., Hohn, T.M. 2002. Engineering deoxynivalenol metabolism in wheat through the expression of a fungal trichothecene acetyltransferase gene. *Theoretical and Applied Genetics,* **106**, 74-83.

Pallotta, M., Warner, P., Fox, R.L., Kuchel, H., Jefferies, S.J., Langridge, P. 2003. Marker assisted wheat breeding in the southern region of Australia. *In:* Pogna, N., Mcintosh, R. (eds.) *Proceedings of the 10th international wheat genetics symposium* Paestum, Italy: Istituto Sperimentale per per la Cerealicoltura

Parry, D.W., Jenkinson, P., McLeod, L. 1995. Fusarium ear blight (scab) in small-grain cereals - a review. *Plant Pathology,* **44**, 207-238.

Peng, J.R., Richards, D.E., Hartley, N.M., Murphy, G.P., Devos, K.M., Flintham, J.E., Beales, J., Fish, L.J., Worland, A.J., Pelica, F., Sudhakar, D., Christou, P., Snape, J.W., Gale, M.D., Harberd, N.P. 1999. 'Green revolution' genes encode mutant gibberellin response modulators. *Nature,* **400**, 256-261.

Pestka, J.J. 2010. Deoxynivalenol: mechanisms of action, human exposure, and toxicological relevance. *Archives of Toxicology,* **84**, 663-679.

Petersen, G., Seberg, O., Yde, M., Berthelsen, K. 2006. Phylogenetic relationships of Triticum and Aegilops and evidence for the origin of the A, B, and D genomes of common wheat (Triticum aestivum). *Molecular Phylogenetics and Evolution,* **39**, 70-82.

Poppenberger, B., Berthiller, F., Lucyshyn, D., Sieberer, T., Schuhmacher, R., Krska, R., Kuchler, K., Glossl, J., Luschnig, C., Adam, G. 2003. Detoxification of the Fusarium mycotoxin deoxynivalenol by a UDP-glucosyltransferase from Arabidopsis thaliana. *Journal of Biological Chemistry,* **278**, 47905-47914.

Puchta, H. 2005. The repair of double-strand breaks in plants: mechanisms and consequences for genome evolution. *Journal of Experimental Botany,* **56**, 1-14.

Qi, L.L., Pumphrey, M.O., Friebe, B., Chen, P.D., Gill, B.S. 2008. Molecular cytogenetic characterization of alien introgressions with gene Fhb3 for resistance to Fusarium head blight disease of wheat. *Theoretical and Applied Genetics,* **117**, 1155-1166.

Rahmatov, M., Rouse, M.N., Steffenson, B.J., Andersson, S.C., Wanyera, R., Pretorius, Z.A., Houben, A., Kumarse, N., Bhavani, S., Johansson, E. 2016. Sources of Stem Rust Resistance in Wheat-Alien Introgression Lines. *Plant Disease,* **100**, 1101-1109.

Ramirez-Gonzalez, R., Adamski, N.M., Hales, B., Nicholson, P., Uauy, C. unpublished. Skim sequencing of gamma-irradiated Paragon lines to detect genome-wide deletion profiles. John Innes Centre.

Ramírez-González, R.H., Borrill, P., Lang, D., Harrington, S.A., Brinton, J., Venturini, L., Davey, M., Jacobs, J., van Ex, F., Pasha, A., Khedikar, Y., Robinson, S.J., Cory, A.T., Florio, T., Concia, L., Juery, C., Schoonbeek, H., Steuernagel, B., Xiang, D., Ridout, C.J., Chalhoub, B., Mayer, K.F.X., Benhamed, M., Latrasse, D., Bendahmane, A., Wulff, B.B.H., Appels, R., Tiwari, V., Datla, R., Choulet, F., Pozniak, C.J., Provart, N.J., Sharpe, A.G., Paux, E., Spannagl, M., Bräutigam, A., Uauy, C. 2018. The transcriptional landscape of polyploid wheat. *Science,* **361**.

Rawat, N., Pumphrey, M.O., Liu, S., Zhang, X., Tiwari, V.K., Ando, K., Trick, H.N., Bockus, W.W., Akhunov, E., Anderson, J.A., Gill, B.S. 2016. Wheat Fhb1 encodes a chimeric lectin with agglutinin domains and a pore-forming toxin-like domain conferring resistance to Fusarium head blight. *Nature Genetics,* **48**, 1576–1580.

Rawat, N., Pumphrey, M.O., Liu, S., Zhang, X., Tiwari, V.K., Trick, H.N., Akhunov, E., Anderson, J.A., Gill, B.S. 2017. Pore-forming toxin-like gene provides resistance against Fusarium head blight in wheat *In:* Buerstmayr, H., Lang-Mladek, C., Steiner, B., Michel, S., Buerstmayr, M., Lemmens, M., Vollmann, J., Grausgruber, H., eds. 13th International Wheat Genetics Symposium, 2017 Tulln, Austria. Vienna, Austria: BOKU - University of Natural Resources and Life Sciences, Vienna, 67.

Reddy, L., Friesen, T.L., Meinhardt, S.W., Chao, S.A.M., Faris, J.D. 2008. Genomic Analysis of the Snn1 Locus on Wheat Chromosome Arm 1BS and the Identification of Candidate Genes. *Plant Genome,* **1**, 55-66.

Ribichich, K.F., Lopez, S.E., Vegetti, A.C. 2000. Histopathological spikelet changes produced by Fusarium graminearum in susceptible and resistant wheat cultivars. *Plant Disease,* **84**, 794-802.

Riley, R., Chapman, V. 1958. Genetic control of the cytologically diploid behaviour of hexaploid wheat. *Nature,* **182**, 713-715.

Robert-Seilaniantz, A., Navarro, L., Bari, R., Jones, J.D. 2007. Pathological hormone imbalances. *Current Opinion in Plant Biology,* **10**, 372-379.

Roldan-Arjona, T., Ariza, R.R. 2009. Repair and tolerance of oxidative DNA damage in plants. *Mutation Research-Reviews in Mutation Research,* **681**, 169-179.

Santos, M.A., Gongalez-Penades, L., Nicholson, P. unpublished. RNA-seq dataset of DON responsive genes at 6 h and 24 h post application in root tissue of wheat variety Hobbit Sib. John Innes Centre.

Saville, R.J., Gosman, N., Burt, C.J., Makepeace, J., Steed, A., Corbitt, M., Chandler, E., Brown, J.K.M., Boulton, M.I., Nicholson, P. 2012. The 'Green Revolution' dwarfing genes play a role in disease resistance in Triticum aestivum and Hordeum vulgare. *Journal of Experimental Botany,* **63**, 1271-1283.

Schmale, D.G., Bergstrom, G.C. 2003. *Fusarium head blight (FHB) or scab* [Online]. The American Phytopathological Society. Available: http://www.apsnet.org/edcenter/intropp/lessons/fungi/ascomycetes/Pages/Fusarium.aspx [Accessed 25 Nov 2015].

Schoneberg, T., Kibler, K., Wettstein, F.E., Bucheli, T.D., Forrer, H.R., Musa, T., Mascher, F., Bertossa, M., Keller, B., Vogelgsang, S. 2019. Influence of temperature, humidity duration and growth stage on the infection and mycotoxin production by Fusarium langsethiae and Fusarium poae in oats. *Plant Pathology,* **68**, 173-184.

Schroeder, H.W., Christensen, J.J. 1963. Factors affecting resistance of wheat to scab caused by *Gibberella zeae*. *Phytopathology,* **53**, 831-838.

Schuelke, M. 2000. An economic method for the fluorescent labeling of PCR fragments. *Nature Biotechnology,* **18**, 233-234.

Schweiger, W., Boddu, J., Shin, S., Poppenberger, B., Berthiller, F., Lemmens, M., Muehlbauer, G.J., Adam, G. 2010. Validation of a Candidate Deoxynivalenol-Inactivating UDP-Glucosyltransferase from Barley by Heterologous Expression in Yeast. *Molecular Plant-Microbe Interactions,* **23**, 977-986.

Schweiger, W., Steiner, B., Vautrin, S., Nussbaumer, T., Siegwart, G., Zamini, M., Jungreithmeier, F., Gratl, V., Lemmens, M., Mayer, K.F.X., Berges, H., Adam, G., Buerstmayr, H. 2016. Suppressed recombination and unique candidate genes in the

divergent haplotype encoding Fhb1, a major Fusarium head blight resistance locus in wheat. *Theoretical and Applied Genetics,* **129**, 1607-1623.

Sears, E.R. 1954. The aneuploids of common wheat. *Missouri Agricultural Experiment Station Research Bulletin,* **572**, 1-58.

Sears, E.R., Sears, L.M.S. The telocentric chromosomes of common wheat. 5th International Wheat Genetics Symposium, 1978 New Delhi. 389–407.

Shaw, L.M., Turner, A.S., Herry, L., Griffiths, S., Laurie, D.A. 2013. Mutant Alleles of Photoperiod-1 in Wheat (Triticum aestivum L.) That Confer a Late Flowering Phenotype in Long Days. *Plos One,* **8**, 11.

Shen, X.R., Ittu, M., Ohm, H.W. 2003. Quantitative trait loci conditioning resistance to Fusarium head blight in wheat line F201R. *Crop Science,* **43**, 850-857.

Shi, G.J., Friesen, T.L., Saini, J., Xu, S.S., Rasmussen, J.B., Faris, J.D. 2015. The Wheat Snn7 Gene Confers Susceptibility on Recognition of the Parastagonospora nodorum Necrotrophic Effector SnTox7. *Plant Genome,* **8**, 10.

Shin, S., Torres-Acosta, J.A., Heinen, S.J., McCormick, S., Lemmens, M., Paris, M.P.K., Berthiller, F., Adam, G., Muehlbauer, G.J. 2012. Transgenic Arabidopsis thaliana expressing a barley UDP-glucosyltransferase exhibit resistance to the mycotoxin deoxynivalenol. *Journal of Experimental Botany,* **63**, 4731-4740.

Smith, W.G. 1884. *Diseases of Field and Garden Crops,* London, MacMillan and Co.

Srinivasachary, Gosman, N., Steed, A., Hollins, T.W., Bayles, R., Jennings, P., Nicholson, P. 2009. Semi-dwarfing Rht-B1 and Rht-D1 loci of wheat differ significantly in their influence on resistance to Fusarium head blight. *Theoretical and Applied Genetics,* **118**, 695-702.

Steed, A., Chandler, E., Thomsett, M., Gosman, N., Faure, S., Nicholson, P. 2005. Identification of type I resistance to Fusarium head blight controlled by a major gene located on chromosome 4A of Triticum macha. *Theoretical and Applied Genetics,* **111**, 521-529.

Steed, A., Nicholson, P. unpublished-a. Fusarium head blight point-inoculation experiments of ditelosomic and nulli-tetrasomic Chinese Spring. John Innes Centre.

Steed, A., Nicholson, P. unpublished-b. Fusarium head blight point inoculation of wheat-barley introgression lines. John Innes Centre.

Steiner, B., Buerstmayr, M., Wagner, C., Danler, A., Eshonkulov, B., Ehn, M., Buerstmayr, H. 2019. Fine-mapping of the Fusarium head blight resistance QTL Qfhs.ifa-5A identifies two resistance QTL associated with anther extrusion. *Theoretical and Applied Genetics,* **132**, 2039-2053.

Steiner, B., Lemmens, M., Griesser, M., Scholz, U., Schondelmaier, J., Buerstmayr, H. 2004. Molecular mapping of resistance to Fusarium head blight in the spring wheat cultivar Frontana. *Theoretical and Applied Genetics,* **109**, 215-224.

Steiner, B., Zimmerl, S., Polzer, R., Mühl, S., Lemmens, M., Adam, G., Till, B., Schweiger, W., Buerstmayr, H. 2017. Functional identification of the wheat gene enhancing mycotoxin detoxification of the major Fusarium resistance QTL Fhb1. *In:* Buerstmayr, H., Lang-Mladek, C., Steiner, B., Michel, S., Buerstmayr, M., Lemmens, M., Vollmann, J., Grausgruber, H., eds. 13th International Wheat Genetics Symposium, 2017 Tulln, Austria. Vienna, Austria: BOKU - University of Natural Resources and Life Sciences, Vienna, 70.

Su, Z., Bernardo, A., Li, C., Lu, P., Cai, S., Bai, G. 2017. TaHRC is the key gene underlying Fhb1 resistance to Fusarium head blight in wheat *In:* Buerstmayr, H., Lang-Mladek, C., Steiner, B., Michel, S., Buerstmayr, M., Lemmens, M., Vollmann, J., Grausgruber, H., eds. 13th International Wheat Genetics Symposium, 2017 Tulln, Austria. Vienna, Austria: BOKU - University of Natural Resources and Life Sciences, Vienna, 69.

Su, Z., Bernardo, A., Tian, B., Chen, H., Wang, S., Ma, H., Cai, S., Liu, D., Zhang, D., Li, T., Trick, H., St. Amand, P., Yu, J., Zhang, Z., Bai, G. 2019. A deletion mutation in TaHRC confers Fhb1 resistance to Fusarium head blight in wheat. *Nature Genetics,* **51**, 1099–1105.

Su, Z.Q., Jin, S.J., Zhang, D.D., Bai, G.H. 2018. Development and validation of diagnostic markers for Fhb1 region, a major QTL for Fusarium head blight resistance in wheat. *Theoretical and Applied Genetics,* **131**, 2371-2380.

Sun, H.R., Wei, H.L., Wang, H.T., Hao, P.B., Gu, L.J., Liu, G.Y., Ma, L., Su, Z.Z., Yu, S.X. 2019. Genome-wide identification and expression analysis of the BURP domain-containing genes in Gossypium hirsutum. *BMC Genomics,* **20**, 19.

Toronto International Data Release Workshop Authors 2009. Prepublication data sharing. *Nature,* **461**, 168.

U.S. National Library of Medicine, National Centre for Biotechnology Information. 2019. *NCBI Basic Local Alignment Search Tool* [Online]. Available: https://blast.ncbi.nlm.nih.gov/Blast.cgi [Accessed 16 Aug 2019].

Uauy, C., Paraiso, F., Colasuonno, P., Tran, R.K., Tsai, H., Berardi, S., Comai, L., Dubcovsky, J. 2009. A modified TILLING approach to detect induced mutations in tetraploid and hexaploid wheat. *BMC Plant Biology,* **9**, 14.

United Nations. 2013. *World population projected to reach 9.6 billion by 2050* [Online]. United Nations. Available: https://www.un.org/development/desa/en/news/population/un-report-world-population-projected-to-reach-9-6-billion-by-2050.html [Accessed 25 Nov 2015].

United States Department of Agriculture. 2019. *World Agricultural Production* [Online]. Available: https://apps.fas.usda.gov/psdonline/circulars/production.pdf [Accessed 26 Apr 2019].

van der Lee, T., Zhang, H., van Diepeningen, A., Waalwijk, C. 2015. Biogeography of Fusarium graminearum species complex and chemotypes: a review. *Food Additives and Contaminants Part a-Chemistry Analysis Control Exposure & Risk Assessment,* **32**, 453-460.

Walter, S., Kahla, A., Arunachalam, C., Perochon, A., Khan, M.R., Scofield, S.R., Doohan, F.M. 2015. A wheat ABC transporter contributes to both grain formation and mycotoxin tolerance. *Journal of Experimental Botany,* **66**, 2583-2593.

Walter, S., Nicholson, P., Doohan, F.M. 2010. Action and reaction of host and pathogen during Fusarium head blight disease. *New Phytologist,* **185**, 54-66.

Wang, Y.P., Cheng, X., Shan, Q.W., Zhang, Y., Liu, J.X., Gao, C.X., Qiu, J.L. 2014. Simultaneous editing of three homoeoalleles in hexaploid bread wheat confers heritable resistance to powdery mildew. *Nature Biotechnology,* **32**, 947-951.

Wheat Genetic Improvement Network. 2019. *Wheat Genetic Improvement Network* [Online]. Rothamsted Research. Available: http://www.wgin.org.uk/ [Accessed 08 Mar 2019 2019].

Wilson, W., Dahl, B., Nganje, W. 2018. Economic costs of Fusarium Head Blight, scab and deoxynivalenol. *World Mycotoxin Journal,* **11**, 291-302.

Winter, D., Vinegar, B., Nahal, H., Ammar, R., Wilson, G.V., Provart, N.J. 2007. An "Electronic Fluorescent Pictograph" Browser for Exploring and Analyzing Large-Scale Biological Data Sets. *Plos One,* **2**, 12.

Xia, C., Zhang, L.C., Zou, C., Gu, Y.Q., Duan, J.L., Zhao, G.Y., Wu, J.J., Liu, Y., Fang, X.H., Gao, L.F., Jiao, Y.N., Sun, J.Q., Pan, Y.H., Liu, X., Jia, J.Z., Kong, X.Y. 2017. A TRIM insertion in the promoter of Ms2 causes male sterility in wheat. *Nature Communications,* **8**, 9.

Xing, L.P., Gao, L., Chen, Q.G., Pei, H.Y., Di, Z.C., Xiao, J., Wang, H.Y., Ma, L.L., Chen, P.D., Cao, A.Z., Wang, X.E. 2018. Over-expressing a UDP-glucosyltransferase gene (Ta-UGT (3)) enhances Fusarium Head Blight resistance of wheat. *Plant Growth Regulation,* **84**, 561-571.

Xu, X.M., Parry, D.W., Nicholson, P., Thomsett, M.A., Simpson, D., Edwards, S.G., Cooke, B.M., Doohan, F.M., Monaghan, S., Moretti, A., Tocco, G., Mule, G., Hornok, L., Beki, E., Tatnell, J., Ritieni, A. 2008. Within-field variability of Fusarium head blight pathogens and their associated mycotoxins. *European Journal of Plant Pathology,* **120**, 21-34.

Young, J.C., Zhou, T., Yu, H., Zhu, H.H., Gong, J.H. 2007. Degradation of trichothecene mycotoxins by chicken intestinal microbes. *Food and Chemical Toxicology,* **45**, 136-143.

Yu, H., Zhou, T., Gong, J.H., Young, C., Su, X.J., Li, X.Z., Zhu, H.H., Tsao, R., Yang, R. 2010. Isolation of deoxynivalenol-transforming bacteria from the chicken intestines using the approach of PCR-DGGE guided microbial selection. *Bmc Microbiology,* **10**, 9.

Zhang, C.J., Zhao, X., Qu, Y.F., Teng, W.L., Qiu, L.J., Zheng, H.K., Wang, Z.H., Han, Y.P., Li, W.B. 2019. Loci and candidate genes in soybean that confer resistance to Fusarium graminearum. *Theoretical and Applied Genetics,* **132**, 431-441.

Zhu, J.Y., Sae-Seaw, J., Wang, Z.Y. 2013. Brassinosteroid signalling. *Development,* **140**, 1615-1620.

Zhuang, Y.B., Gala, A., Yen, Y. 2013. Identification of Functional Genic Components of Major Fusarium Head Blight Resistance Quantitative Trait Loci in Wheat Cultivar Sumai 3. *Molecular Plant-Microbe Interactions,* **26**, 442-450.

Appendix

ANOVA tables presented for all statistical analyses performed as part of the thesis.

Associated figures and experiment codes are provided above each table.

Figure 2.1a, FHBpt_CSditelo_Poly_16					
Source	**d.f.**	**s.s.**	**m.s.**	**v.r.**	**F pr.**
Regression	5	1.006	0.20114	2.06	0.088
Residual	46	4.492	0.09765		
Total	51	5.498	0.1078		

Figure 2.1b, DON_ CSditelo_Poly_16					
Source	**d.f.**	**s.s.**	**m.s.**	**v.r.**	**F pr.**
Regression	5	1.2078	0.24157	13.23	<.001
Residual	49	0.8946	0.01826		
Total	54	2.1025	0.03893		

Figure 2.1c, FHBsp_CSditelo_Poly_17					
Source	**d.f.**	**s.s.**	**m.s.**	**v.r.**	**F pr.**
Regression	5	29.07	5.8147	19.81	<.001
Residual	296	86.88	0.2935		
Total	301	115.95	0.3852		

Figure 2.2a, DON_ CSditelo_Poly_16					
Fixed term	**Wald statistic**	**n.d.f.**	**F statistic**	**d.d.f.**	**F pr**
Line	28.11	2	13.99	36.1	<0.001

Figure 2.5, FHBpt_CSterm_Poly_17					
Fixed term	**Wald statistic**	**n.d.f.**	**F statistic**	**d.d.f.**	**F pr**
Line	102.47	4	25.62	956	<0.001

Figure 2.7a, DON_CSterm_Poly_17					
Fixed term	**Wald statistic**	**n.d.f.**	**F statistic**	**d.d.f.**	**F pr**
Line	79.69	4	19.92	146.2	<0.001

Figure 2.7b, DON_CSterm_Poly_17					
Fixed term	**Wald statistic**	**n.d.f.**	**F statistic**	**d.d.f.**	**F pr**
Line	11.69	2	5.84	35	0.006

Figure 2.10, FHBsp_CSterm_Poly_18					
Fixed term	**Wald statistic**	**n.d.f.**	**F statistic**	**d.d.f.**	**F pr**
Tag_colour	7.84	1	7.84	307.4	0.005
Line	21.3	7	3.04	307.8	0.004

Figure 3.2, FHBpt_PG_CER_18					
Fixed term	**Wald statistic**	**n.d.f.**	**F statistic**	**d.d.f.**	**F pr**
Line	45.55	2	22.78	89.5	<0.001

Figure 3.3, FHBpt_PG_Poly_18					
Fixed term	**Wald statistic**	**n.d.f.**	**F statistic**	**d.d.f.**	**F pr**
Line	190.71	6	31.78	636.6	<0.001

Figure 3.9, FHBpt_PGkasp_CER_19					
Fixed term	**Wald statistic**	**n.d.f.**	**F statistic**	**d.d.f.**	**F pr**
Line	24.4	7	3.48	195.9	0.002

Figure 3.15b, FHBpt_PGskim_CER_19					
Fixed term	**Wald statistic**	**n.d.f.**	**F statistic**	**d.d.f.**	**F pr**
Line	55.85	5	11.17	241	<0.001

Figure 3.18, FHBpt_PGhom_Poly_19					
Fixed term	**Wald statistic**	**n.d.f.**	**F statistic**	**d.d.f.**	**F pr**
Line	28.06	9	3.12	399.4	0.001

Figure 4.1, DON_CZ_Poly_18					
Fixed term	**Wald statistic**	**n.d.f.**	**F statistic**	**d.d.f.**	**F pr**
Line	6.7	4	1.68	74.4	0.165

Figure 4.3a, DON_PG_CER_19					
Fixed term	**Wald statistic**	**n.d.f.**	**F statistic**	**d.d.f.**	**F pr**
Line	5.51	3	1.84	47.9	0.153

Figure 4.3b, DON_PG_CER_19					
Fixed term	**Wald statistic**	**n.d.f.**	**F statistic**	**d.d.f.**	**F pr**
Line	1.42	3	0.47	48.1	0.703